UCGE Reports
Number 20214

Department of Geomatics Engineering

Performance Evaluation of Multiple Reference Station GPS RTK for a Medium Scale Network

(URL: http://www.geomatics.ucalgary.ca/links/GradTheses.html)

by

Thi Hong Diep Dao

April 2005

UNIVERSITY OF CALGARY

Performance Evaluation of Multiple Reference Station GPS RTK for a Medium Scale Network

by

Thi Hong Diep Dao

A THESIS

SUBMITTED TO THE FACULTY OF GRADUATE STUDIES

IN PARTIAL FULFILMENT OF THE REQUIREMENTS FOR THE

DEGREE OF MASTER OF SCIENCE

DEPARTMENT OF GEOMATICS ENGINEERING

CALGARY, ALBERTA

APRIL, 2005

Abstract

Carrier phase-based single reference station (SRS) positioning is capable of providing decimetre to centimetre-level accuracy for static and kinematic positioning under normal atmospheric conditions where the inter-antenna distance is relatively short, namely below ten to twenty kilometres. However, under highly localized atmospheric activity, and/or with a longer inter-antenna distance, the residual differential error increases and the accuracy degrades. Carrier phase integer ambiguity resolution may be impossible.

Multiple reference station (MRS) approaches uses a network of GPS reference stations to predict the differential errors over a geographic region. The University of Calgary standard MRS approach uses a conditional least-squares adjustment technique. During the past few years, an MRS tightly-coupled approach, which used all available observables obtained at rover and network reference stations in one filter, was also developed; the objective of this approach was solely to estimate states such as ambiguities, rover position and ionospheric error, if specified.

This thesis focuses on an evaluation of the above-mentioned MRS approaches relative to the SRS approach in the observation, position and ambiguity domains under various ionospheric conditions, ranging from quiet to extremely active, using a medium scale reference network, with inter-reference station distances of 30 to 70 km. Long-term and short-term convergence accuracy tests are used to assess the effectiveness of each approach. The reference network used is located in Southern Alberta and consists of dual-

frequency receivers. The results show various levels of MRS performance compared to the equivalent SRS approach, ranging from unfavourable to significant, depending on many different parameters, chiefly ionospheric condition and carrier phase combination options. A major conclusion is that, under a highly disturbed ionosphere, the spatial correlation of the latter over distance of several tens of kilometres is weak, resulting in marginal improvements of MRS approaches.

Acknowledgements

I would like to express my sincere thanks to my supervisor, Dr. Gérard Lachapelle, for your excellent supervision and continuous support. I have gained knowledge and experience during my two years under his supervision that will guide me throughout my career.

Many thanks and appreciation are truly for my parents and sisters. Dad, thanks for your endless love and your knowledge that enriches my life. You are the one who understands me the most. Mum Tranh, thanks for bringing me to life and I know you are always up there, being with me on every step that I take in life. Mum Loan, thanks for your love and gentle care that you raise me each day with. Sisters, you perhaps do not really realize how wonderful you both are.

I deeply acknowledge many of my friends and colleagues, Heidi Kuusniemi, Scott Crawford, Oleg Mezentsev, Olivier Julien, Cecile Mongredien, Anastasia Salycheva, Paul Alves, Ning Luo, Mark Petovello, Glen MacGougan, Chaminda Basnayake and Batoul Maklad. Each of you is very special who makes my two years in Calgary becoming an unforgettable experience.

Table of Contents

Approval Page ii
Abstract iii
Acknowledgements v
Table of Contents vi
List of Tables viii
List of Figures and Illustrations xi
List of Symbols and Abbreviations and Nomenclature xvii
CHAPTER 1 1
INTRODUCTION 1
1.1 Background and Motivation 1
1.2 Literature Review and Contribution of the Thesis 5
1.3 Objectives 8
1.4 Thesis Outline 9
CHAPTER 2 11
CONCEPTS AND ALGORITHMS 11
2.1 Carrier Phase-Based Differential GPS Error Sources 11
2.1.1 Satellite Orbital Error 12
2.1.2 Ionospheric Error 13
2.1.3 Tropospheric Error 18
2.1.4 Multipath and Noise 20
2.2 Single Reference Station GPS RTK Algorithm 21
2.2.1 Kalman Filter 21
2.2.2 Phase Observations and Phase Combinations 27
2.2.3 Ambiguity Resolution 36
2.3 Multiple Reference Station GPS RTK Algorithms 38
2.3.1 Linear Interpolation Approach 39
2.3.2 Partial Derivative Approach (Low Order Surface Model) 41
2.3.3 Least-squares Collocation Approach 42

2.3.4 Tightly-coupled Approach 51
2.3.5 Least-squares Collocation versus Tightly Couple: Algorithm and Practical Implementation 53
2.4 MRS Standards and Issues 55
2.4.1 Virtual Reference Station Concept 55
2.4.2 Real-time RTCM Standards 55
CHAPTER 3 57
TEST NETWORK AND EVALUATION METHODOLOGY 57
3.1 Test Network 57
3.2 Testing Methodology 59
3.3 Evaluation Measures 63
CHAPTER 4 67
RESULTS AND ANALYSIS 67
4.1 Post-Mission Static Test 67
4.1.1 Normal Ionospheric Condition Results 69
4.1.2 Medium Ionospheric Condition Results 95
4.1.3 Ionospheric Storm Condition Results 119
4.1.4 Impact of MRS LSQC Network Initialization 148
4.2 Kinematic Test Results 149
4.3 Real-Time Static Test Results 158
CHAPTER 5 165
CONCLUSIONS AND RECOMMENDATIONS 165
REFERENCES 169

List of Tables

2.1 Different carrier phase combinations (Liu 2003) ……29

2.2 Phase combinations with their ionospheric and noise effects (Liu 2003)..... 30

3.1 WGS84 coordinates of the MSAN network..... 59

4.1 Local K values obtained at MEANOOK geomagnetic station located in Edmonton (approximately 300 km away from UOFC station) for the three test days 67

4.2 Weather conditions for the three test days 69

4.3 Statistics for double-difference observable misclosures for all satellite pairs - 24 May 2004 73

4.4 Statistics for position accuracy in L1 mode after a two-hour network initialization period - 24 May 2004..... 75

4.5 Statistics for position accuracy in IF mode after a two-hour network initialization period - 24 May 2004..... 77

4.6 Statistics for position accuracy in L1/L2 mode after a two-hour network initialization period - 24 May 2004..... 79

4.7 Percentage of fixed ambiguities using SRS, MRS LSQC and MRS TC approaches for 24 May 2004 using L1/L2 mode 80

4.8 Statistics for the average and maximum converging 3D position error in L1 mode - 24 May 2004 84

4.9 Statistics for the average and maximum converging 3D position error in IF mode - 24 May 2004 88

4.10 Statistics for the average and maximum converging 3D position error in L1/L2 with ionospheric modeling mode - 24 May 2004 92

4.11 Statistics for the average and maximum converging 3D position error in L1/L2 with ionospheric modeling mode for the first 15 segments, excluding segments 4, 5 and 12 - 24 May 2004 93

4.12 Stastics for double-difference observable misclosures for all satellite pairs - 6 April 2004 98

4.13 Statistics for position accuracy in L1 mode after a two-hour network initialization period - 6 April 2004 100
4.14 Statistics for position accuracy in IF mode after a two-hour network initialization period - 6 April 2004 102
4.15 Statistics for position accuracy in L1/L2 with stochastic ionosphere modeling after a two-hour network initialization period - 6 April 2004..... 104
4.16 Percentage of fixed ambiguities using SRS, MRS LSQC and MRS TC approaches for 6 April 2004 using L1/L2 mode 105
4.17 Statistics for the average and maximum converging 3D position error in L1 mode - 6 April 2004 108
4.18 Statistics for the average and maximum converging 3D position error in IF mode - 6 April 2004 112
4.19 Statistics for the average and maximum converging 3D position error in L1/L2 with ionospheric modeling mode – 6 April 2004..... 117
4.20 Statistics for the average and maximum converging 3D position error in L1/L2 with ionospheric modeling mode for the first 15 segments, excluding segments 6 and 8, - 6 April 2004 118
4.21 Statistics for double-difference observable misclosures for all satellite pairs – 8 November 2004..... 124
4.22 Statistics for position accuracy in L1 mode after a two-hour network initialization period - 8 November 2004 127
4.23 Statistics for position accuracy in IF mode after a two-hour network initialization period - 8 November 2004 131
4.24 Statistics for position accuracy in L1/L2 with stochastic ionosphere modeling mode after a two-hour network initialization period - 8 November 2004 134
4.25 Percentage of fixed ambiguities using SRS, MRS LSQC and MRS TC approaches for 8 November 2004 using L1/L2 mode..... 135
4.26 Statistics for the average and maximum converging 3D position error in L1 mode - 8 November 2004..... 139

4.27 Statistics for average and maximum converging 3D position error in IF mode - 8 November 2004 143
4.28 Statistics for average and maximum converging 3D position error in L1/L2 mode - 8 November 2004 147
4.29 Statistics for kinematic SRS and MRS position solution error 157
4.30 Statistics for real-time position accuracy in IF mode 163
4.31 Statistics for real-time position accuracy in L1 mode 164

List of Figures and Illustrations

1.1 Number of reference stations required in SRS concept 3
1.2 Number of reference stations required in MRS concept 3
2.1 Linearized Kalman filter loop (Brown & Hwang 1996) 22
2.2 Double differential carrier phase positioning procedure (Lachapelle 2003) ... 37
3.1 Minimal Southern Alberta Network (MSAN) 57
3.2 NovAtel receiver and antenna set-up for STRA reference station 58
3.3 Procedure of applying and evaluating MRS least-squares collocation approach in post-mission 62
3.4 Procedure of applying and evaluating MRS tightly-coupled approach in post-mission 63
4.1 Network configuration used with MRS LSQC - 24 May 2004 70
4.2 Network configuration used with MRS TC - 24 May 2004 70
4.3 Double-difference network corrections generated by MRS LSQC for all satellite pairs - 24 May 2004 (quiet ionospheric conditions) 72
4.4 Double-difference observable misclosures for all satellite pairs using raw measurements (red) and MRS LSQC corrected measurements (blue) - 24 May 2004 73
4.5 Position accuracy and ambiguity status in L1 mode after a two-hour network initialization period - 24 May 2004 75
4.6 Position accuracy and ambiguity status in IF mode after a two-hour network initialization period - 24 May 2004 76
4.7 Position accuracy and ambiguity status in L1/L2 with stochastic ionosphere modeling mode after a two-hour network initialization period - 24 May 200478
4.8 Converging 3D position accuracy and ambiguity status in L1 mode for 24 one-hour segments - 24 May 2004 82
4.9 Average absolute converging 3D position accuracy in L1 mode for 24 May 2004, separately for the first 15 hours (left) and for the last 9 hours (right) 83

4.10 Maximum absolute converging 3D position error in L1 mode for 24 May 2004, separately for the first 15 hours (left) and for the last 9 hours (right)..... 83
4.11 Average ambiguity status during convergence in L1 mode for 24 May 2004, separately for the first 15 hours (left) and for the last 9 hours (right)..... 84
4.12 Converging 3D position accuracy and ambiguity status in IF mode for 24 one-hour segments - 24 May 2004..... 86
4.13 Average absolute converging 3D position accuracy in IF mode for 24 May 2004, separately for the first 15 hours (left) and for the last 9 hours (right).... 87
4.14 Maximum absolute converging 3D position error in IF mode for 24 May 2004, separately for the first 15 hours (left) and for the last 9 hours (right)..... 87
4.15 Average ambiguity status during convergence in IF mode for 24 May 2004, separately for the first 15 hours (left) and for the last 9 hours (right)..... 88
4.16 Converging 3D position accuracy and ambiguity status in L1/L2 with ionospheric modeling mode for 24 one hour segments - 24 May 2004..... 90
4.17 Average absolute converging 3D position accuracy in L1 and L2 with ionospheric modeling mode for 24 May 2004, separately for the first 15 hours (left) and for the last 9 hours (right)..... 91
4.18 Maximum absolute converging 3D position error in L1/L2 with ionospheric modeling mode for 24 May 2004, separately for the first 15 hours (left) and for the last 9 hours (right)..... 91
4.19 Average absolute converging 3D position accuracy in L1 and L2 with ionospheric modeling mode for the first 15 segments, excluding segments 4, 5 and 12, - 24 May 2004..... 93
4.20 Average ambiguity status during convergence in L1/L2 with ionospheric modeling mode for 24 May 2004, separately for the first 15 hours (left) and for the last 9 hours (right)..... 94
4.21 Double difference network corrections generated by MRS LSQC for all satellite pairs - 6 April 2004 (medium ionospheric conditions)..... 96

4.22 Double-difference observable misclosures for all satellite pairs using raw measurements (red) and using MRS LSQC corrected measurements (blue) - 6 April 2004 98
4.23 Position accuracy and ambiguity status in L1 mode after a two-hour network initialization period - 6 April 2004 100
4.24 Position accuracy and ambiguity status in IF mode after a two-hour network initialization period - 6 April 2004 102
4.25 Position accuracy and ambiguity status in L1/L2 with stochastic ionosphere modeling after a two-hour network initialization period - 6 April 2004..... 103
4.26 Converging 3D position accuracy and ambiguity status in L1 mode for 24 one-hour segments - 6 April 2004..... 106
4.27 Average absolute converging 3D position accuracy in L1 mode for 6 April 2004, separately for the first 15 hours (left) and for the last 9 hours (right).. 107
4.28 Maximum absolute converging 3D position error in L1 mode for 6 April 2004, separately for the first 15 hours (left) and for the last 9 hours (right)..... 108
4.29 Average ambiguity status during convergence in L1 mode for 6 April 2004, separately for the first 15 hours (left) and for the last 9 hours (right)..... 109
4.30 Converging 3D position accuracy and ambiguity status in IF mode for 24 one-hour segments - 6 April 2004..... 110
4.31 Average absolute converging 3D position accuracy in IF mode for 6 April 2004, separately for the first 15 hours (left) and for the last 9 hours (right).. 111
4.32 Maximum absolute converging 3D position error in IF mode for 6 April 2004, separately for the first 15 hours (left) and for the last 9 hours (right)..... 111
4.33 Average ambiguity status during convergence in IF mode for 6 April 2004, separately for the first 15 hours (left) and for the last 9 hours (right)..... 113
4.34 Converging 3D position accuracy and ambiguity status in L1/L2 with ionospheric modeling mode for 24 one-hour segments – 6 April 2004..... 114
4.35 Average absolute converging 3D position accuracy in L1/L2 with ionospheric modeling mode for 6 April 2004, separately for the first 15 hours (left) and for the last 9 hours (right) 116

4.36 Maximum absolute converging 3D position error in L1 and L2 with ionospheric modeling mode for 6 April 2004, separately for the first 15 hours (left) and for the last 9 hours (right) 116
4.37 Average absolute converging 3D position accuracy in L1/L2 with ionospheric modeling mode for the first 15 segments, excluding segments 6 and 8, - 6 April 2004 118
4.38 Average ambiguity status during convergence in L1/L2 mode for 6 April 2004, separately for the first 15 hours (left) and for the last 9 hours (right) 119
4.39 Network configuration used with MRS LSQC - 8 November 2004 120
4.40 Network configuration used with MRS TC - 8 November 2004 121
4.41 Double-difference network corrections generated by MRS LSQC for all satellite pairs - 8 November 2004 (ionospheric storm conditions) 122
4.42 Double-difference observable misclosures for all satellite pairs using raw measurements (red) and using MRS LSQC corrected measurements (blue) - 8 November 2004 124
4.43 Position accuracy and ambiguity status in L1 mode after a two-hour network initialization period - 8 November 2004 126
4.44 One-second C/A code solutions (red), 100-second interval averages of C/A code solutions (yellow) and 1800-second interval averages of C/A code solutions (black) – 8 November 2004 128
4.45 One-second L1 carrier phase-based SRS solutions (red), one-second L1 carrier phase-based MRS LSQC solutions (blue) and 1800-second average L1 carrier phase-based SRS solutions (cyan) in comparison with 100-second average of C/A code solutions (yellow) and 1800-second average of C/A code solutions (black) – 8 November 2004 129
4.46 Position accuracy and ambiguity status in IF mode after a two-hour network initialization period - 8 November 2004 131
4.47 Detected cycle slips on raw L1 (left) and L2 (right) reference station AIRD observations – 8 November 2004 132

4.48 Detected cycle slips on corrected L1 (left) and L2 (right) reference station AIRD observations – 8 November 2004 132
4.49 Detected cycle slips on raw L1 (left) and L2 (right) UOFC rover observations – 8 November 2004 133
4.50 Position accuracy in L1/L2 with stochastic ionosphere modeling mode after a two-hour network initialization period - 8 November 2004 134
4.51 Converging 3D position accuracy and ambiguity status in L1 mode for 24 one-hour segments - 8 November 2004 137
4.52 Average absolute converging 3D position accuracy in L1 mode for 8 November 2004, separately for the first 15 hours (left) and for the last 9 hours (right) 138
4.53 Maximum absolute converging 3D position error in L1 mode for 8 November 2004, separately for the first 15 hours (left) and for the last 9 hours (right).. 139
4.54 Converging 3D position accuracy and ambiguity status in IF mode for 24 one-hour segments - 8 November 2004 140
4.55 Average absolute converging 3D position accuracy in IF mode for 8 November 2004, separately for the first 15 hours (left) and for the last 9 hours (right).. 142
4.56 Maximum absolute converging 3D position error in IF mode for 8 November 2004, separately for the first 15 hours (left) and for the last 9 hours (right).. 142
4.57 Converging 3D position accuracy and ambiguity status in L1/L2 mode for 24 one-hour segments - 8 November 2004 145
4.58 Average absolute converging 3D position accuracy in L1/L2 mode for 8 November 2004, separately for the first 15 hours (left) and for the last 9 hours (right) 146
4.59 Maximum absolute converging 3D position error in L1/L2 mode for 8 November 2004, separately for the first 15 hours (left) and for the last 9 hours (right) 146
4.60 Average ambiguity status during convergence in L1/L2 mode for 6 April 2004, separately for the first 15 hours (left) and for the last 9 hours (right)..... 148
4.61 Network configuration for kinematic test of the MRS LSQC approach..... 150

4.62 Kinematic test trajectory 151
4.63 Kinematic reference solutions: IF forward-backward averaged using GrafNav with UOFC reference station 152
4.64 Reported cycle slips on L1 measurements obtained at kinematic rover 153
4.65 Reported cycle slips on L2 measurements obtained at kinematic rover 153
4.66 Kinematic reference: forward and backward separation from the averaged solutions 154
4.67 Double difference network corrections generated by MRS LSQC for all satellite pairs for 22 October 2004 during the kinematic test 155
4.68 Kinematic position solution errors in L1 mode..... 156
4.69 Kinematic position solution errors in IF mode 157
4.70 Procedure for applying and evaluating the real-time (RT) MRS LSQC approach 160
4.71 Network configuration for real-time test of the MRS LSQC approach 161
4.72 Double-difference network corrections during the real-time test 161
4.73 Real-time MRS LSQC position solution accuracy in comparison with post-mission SRS solution accuracy using IF observations..... 162
4.74 MRS LSQC position solution accuracy using real-time corrected L1 observations and FLYKIN+™ (post mission) in comparison with post-mission SRS solution accuracy..... 163

List of Symbols and Abbreviations and Nomenclature

Symbols

$(\bullet)^z$ Zenith values

$\hat{(\bullet)}$ Correction values

$\tilde{(\bullet)}$ Unavailable measurements (which does exist, but is not available for use in the MRS algorithms)

$\dot{(\bullet)}$ Changing rate of values

$\bar{(\bullet)}$ Measurement-minus-true-range values

B Double-difference matrix

D_{trop} Total tropospheric error (m)

D_d Dry tropospheric error (m)

D_w Wet tropospheric error (m)

E Expectation

H Design matrix

I First-order slant ionospheric carrier phase error (m) or Identity matrix

I_1 Ionospheric error on L1 carrier phase observations (m)

I_2 Ionospheric error on L2 carrier phase observations (m)

N Ambiguity (cycles)

N_{w0} Wet refractivity

N_{d0} Dry refractivity

R Variance covariance matrix of the measurements in Kalman filter

R_h Relative humidity (%)

P_d Air pressure (millibars)

T Temperature (^oC/K) or Tropospheric delay (m)

T_0	Correlation time (s)
Q	System process noise matrix in Kalman filter
c	Speed of light (m/s)
d	Baseline length (m)
$d\rho$	Satellite orbital error (m)
e	Water vapour (millibars)
f_1	GPS carrier frequency L1 (=1575.42 MHz)
f_2	GPS carrier frequency L2 (=1227.60 MHz)
h	Height above the Geoid (m)
h_{user}	User height above the earth surface (m)
l	Measurement vector in least-squares collocation algorithm (m)
s	Interpolating signal vector in least-squares collocation algorithm (m)
sp	Spectral density (m^2/s^3)
ppm	Part per millions
v	Innovative sequence in Kalman filter
w	Processing noise
x	Estimation state vector in Kalman filter
z	Observation vector in Kalman filter
Δd	Error in length of a baseline (m)
$\Delta\rho$	Error in satellite position (m)
$\nabla\Delta$	Double-difference operation
α	Satellite elevation (degree)
δl	Measurement error vector (m)
δt	Transition time (s)
δt_r	Satellite clock error (s)
δT^s	Receiver clock error (s)
ε	Multipath and noise (m)
λ	Longitude (degrees)
λ_1	GPS carrier L1 wavelength (m)

λ_2	GPS carrier L2 wavelength (m)
μ	Mapping function
ϕ	Carrier phase observations (cycles) or Transition matrix in Kalman filter
φ	Latitude (degrees)
ρ	True satellite receiver geometric range (m)
σ	GPS measurement noise (m)

Abbreviations

C/A	Coarse Acquisition
DD	Double Difference
DGPS	Differential GPS technique
FTTF	First Time To Fixed
GF	Geometric-free observation combination
GPS	Global Positioning System
IF	Ionospheric-free observation combination
IP	Internet Protocol
LAMBDA	Least-squares AMBiguity Decorrelation Adjustment
L1	GPS frequency L1
L1/L2	L1 and L2 observation combination
L2	GPS frequency L2
MPC	Modulated Precision Clock
MRS	Multiple Reference Station
MRS LSQC	Multiple Reference Station Least-squares Collocation approach
MRS TC	Multiple Reference Station Tightly-Coupled approach
MSAN	Minimal Southern Alberta Network
NL	Narrow-lane observation combination
P	Code measurements
P_{L1}	L1 code measurements
P_{L2}	L2 code measurements
PRN	Pseudo-Random Noise
PRS	Primary Reference Station
RMS	Root mean squared
RTCM	Radio Technical Commission for Maritime Services
RTK	Real-time Kinematic
SAN	Southern Alberta Network
SRS	Single Reference Station
TCP	Transmission Control Protocol
TEC	Total Electronic Content
VRS	Virtual Reference Station

WGS84	World Geodetic System of 1984
WL	Wide-lane observation combination

Nomenclature

The Real-Time Kinematic (RTK) concept used herein refers to centimetre level accurate GNSS carrier phase-based positioning techniques, which can be applied in post-mission but assuming real-time. The rover can be static but the obtained data is processed in a kinematic mode.

CHAPTER 1

INTRODUCTION

1.1 Background and Motivation

Single reference station (SRS) differential GPS performs well under normal atmospheric conditions when the inter-antenna distances are less than ten kilometres, providing centimetre level accuracy under ideal conditions. However, under high atmospheric conditions or with longer inter-antenna distances, the position solution accuracy is degraded because of the decrease in the spatial correlation of errors - namely ionospheric, tropospheric and satellite orbit errors. This has led to the development of multiple reference station (MRS) differential GPS approaches, which attempt to model the spatially-correlated errors over a regional network and interpolate the corrections to rover positions (e.g. Lachapelle & Alves 2002). In order to do this, the inter-reference-station differential misclosures are estimated using highly accurate coordinates of the reference stations and assumed resolved ambiguities. These misclosures can be, then, spatially interpolated among the network region as corrections. This is done using different algorithms such as a linear combination (Han & Rizos 1996b), a low order surface-fitting function (Wübbena *et al* 1996) or a least-squares adjustment technique (Raquet 1998), to name a few. Because the corrections are explicitly generated in one separate step before

estimating the rover position, these algorithms are classified as correction-based. These network-generated corrections are used to correct the differential observables formed between the rover and one reference station, which is usually the closest one to the rover (the so-called primary reference station). These corrected observables are processed using conventional single reference station differential GPS algorithms. A recently developed Tightly-coupled (TC) MRS algorithm combines all observations obtained at reference stations and the rover into one filter to estimate the rover's position (Alves 2004, Alves & Lachapelle 2004). In this case, the rover becomes a part of the network. Summaries and discussions of the MRS algorithms are presented in Chapter 2.

In theory, MRS approaches offer a number of advantages over the SRS approach. First of all, the corrections are generated based on a network of reference stations placed around the rover. This yields more reduction of the low-frequency component of the spatially correlated differential errors compared to the equivalent SRS case. As a result, the overall position solution accuracy is improved. This, in addition, allows a differential GPS RTK service with a specific number of reference stations to cover a relatively large geographical region while maintaining standard accuracy requirements under quiet and normal atmospheric conditions. Moreover, the number of reference stations required to provide differential GPS service for a particular region is reduced. For instance, in order to cover an area of 200 km x 200 km, twenty-five reference stations are typically required with the use of an SRS approach, as shown in Figure 1.1, assuming the maximum inter-antenna distance necessary to maintain the service accuracy is 20 km. Using an MRS approach, only five reference stations may be needed, as shown in Figure 1.2. However, a

sparse GPS network under active ionospheric conditions performs poorly due to difficulties in fixing ambiguities and unreliable corrections. The MRS approach offers the use of fewer reference stations and produces superior reliability and availability in general. For instance, if a station fails in the network, the remaining stations may yet provide a better solution than with the use of a single reference station.

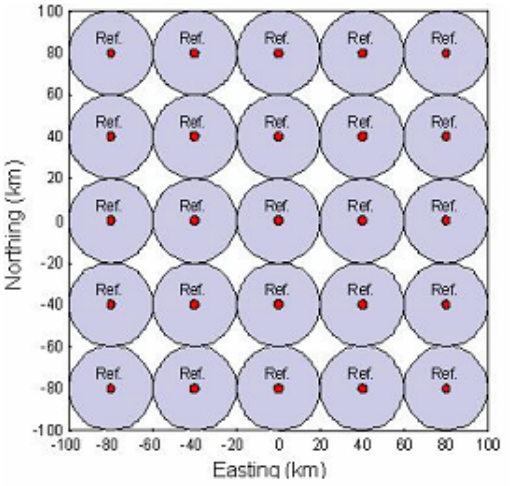

Figure 1.1: Number of reference stations required in SRS concept

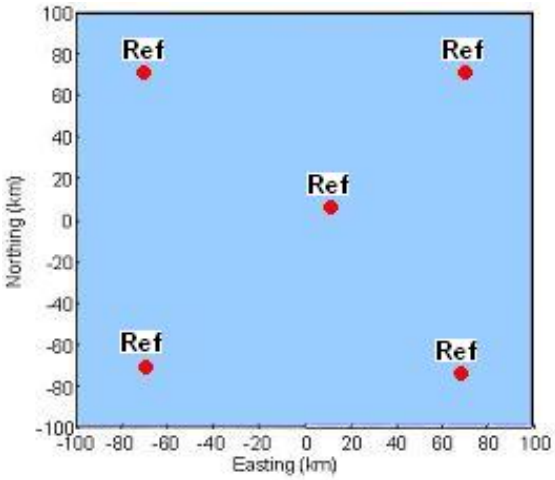

Figure 1.2: Number of reference stations required in MRS concept

However, there are some drawbacks and practical issues to be considered when applying MRS approaches, especially for real-time applications. Firstly, establishing a network of GPS reference stations is very expensive. Having an appropriate geometrical distribution of the reference stations is essential to attaining the highest efficiency of the MRS approach (Alves *et al* 2003). The antennas must be under open-sky tracking conditions, and in surroundings that are conducive to minimal multipath. Receivers designed specially for reference stations with narrow correlator and high quality antennas should

be used to obtain high quality data. After physical construction of the stations, estimating their coordinates is another challenging task. The accuracy of the network coordinates is an important consideration because it directly affects the network correction quality and, therefore, the effectiveness of MRS approaches. Collecting and storage of network data are very costly due to the requirement of high hard drive capacity and good data management. Moreover, in order to generate the network corrections, a significant amount of data transmission from all reference stations to the network processing centre is required. It is critical to have an effective communication link, especially for real-time applications to address the issue of time latency (Alves *et al* 2003).

A full evaluation of MRS approaches is a difficult task due to the numerous parameters that affect performance, the most important ones being network configuration, atmospheric activities, and processing options, even if one assumes the use of high performance receivers and unobstructed satellite availability as given initial conditions. Network characteristics, such as the number of reference stations and inter-receiver distances, directly affect the efficiency of the MRS approaches (e.g. Alves *et al* 2003). If the scale of the network is too large, it can be difficult to resolve network ambiguities over long baselines and, as a result, the corrections may be unreliable. It is also essential that the rover be located within the region of the network. Alves *et al* (2003) have shown that a network of four reference stations surrounding the rover is an effective configuration and the addition of additional reference stations does not substantially improve the performance of the MRS approaches. Different levels of atmospheric errors

result in correspondingly different levels of improvement. During quiet atmospheric conditions, the errors are fairly constant over the network area and the SRS approach can perform very well but the adoption of MRS approaches may not yield significant improvement. However, under fairly active ionospheric conditions, which allow the network ambiguities to be resolved correctly, MRS approaches are expected to offer significant improvements because the errors are better modeled using a network of reference stations. Very active atmospheric conditions associated with highly localized atmospheric activities, unfortunately, can cause difficulties when attempting to resolve ambiguities, resulting in small or no improvement offered by MRS approaches. The use of different processing options such as L1, dual frequency wide-lane (WL) and dual frequency ionospheric-free (IF) observables will lead to different results because of the specific advantages and disadvantages of each individual combination. Achieving an accurate and thorough evaluation for the least-squares collocation correction-based, and the tightly-coupled MRS algorithms in particular, is the motivation for this work.

1.2 Literature Review and Contribution of the Thesis

Extensive studies have been carried out to show the effectiveness of MRS approaches over the traditional SRS approach. Raquet (1998) introduced and evaluated the least-squares collocation algorithm using a network of eleven GPS reference stations located in Norway. The network covers an area of 400 km x 600 km with inter-reference-station baseline lengths ranging from 100 km to 300 km. Different network configurations were tested and compared to the equivalent SRS cases, which have baseline lengths of 0, 29,

67, 143, 164, 223 and 242 km. The results showed a significant improvement produced by the MRS approach in observation, position and ambiguity resolution domains using L1 and WL observables under a very low (1 - 2 ppm) level of ionospheric activity. Compared to the equivalent SRS case with a baseline of less than 100 km, the MRS approach offered an improvement of 17% for the L1 position solution and of 11% for the WL position solution. Compared to the equivalent SRS case with a baseline of more than 100 km, the MRS approach offered an improvement of 44% for the L1 position solution and of 43% for the WL position solution. However, analysis did not include the use of IF observables. Fortes (2002) introduced an optimization to the least-square collocation MRS approach with modifications made to the signal covariance function. However, it was concluded that the performance of MRS approaches is not very sensitive to the covariance function. The MRS approach therein was tested using both St. Lawrence network, which is a constricted seaway navigation channel from Québec City to the Great Lakes, and a Brazilian network. The inter-reference-station baseline lengths used for the St. Lawrence network ranged from 30 km to 83 km. Some improvement due to MRS was shown for both L1 and WL position solutions. The inter-reference-station baseline lengths used for the Brazilian network were in the range of a few hundred kilometres. The ionosphere was deemed to be fairly active as a solar eclipse occurred, with the degree of intensity at between 4 ppm and 6 ppm. Again, a 50% to 60% improvement was observed using the MRS approach in L1 and WL modes. A very minor improvement (a few millimetres) was observed in the IF mode. Pugliano (2002) presented a further evaluation of the least-squares collocation MRS approach using a network of GPS reference stations in Campania, Italy. Inter-reference-station distances ranged from 50 km

to 100 km, with a fairly active ionosphere at approximately 4 ppm due to the solar cycle. The equivalent SRS baseline lengths were from 30 km to 40 km. An analysis was carried out in the measurement, position and ambiguity resolution domains. A significant improvement of 30% to 60% was obtained with the MRS approach for the L1 and WL modes. However, the MRS approach offered no improvement (or, in some cases, minor negative effects) in IF mode. Alves (2004) introduced and tested the tightly-coupled algorithm against the least-squares collocation and SRS algorithms using two GPS networks located in Turkey and in Southern Alberta (Alves 2004; Alves and Lachapelle 2004). The inter-reference-station distances ranged from 25 to 74 km for the Turkish network. For the Southern Alberta network (SAN), network baseline lengths ranged from 30 km to 60 km. The ionospheric effect was normal during the tests. Compared to the least-squares collocation algorithm using the SAN network, the tightly-coupled approach performs quite similarly in some cases (Alves and Lachapelle 2004) and offered an improvement of 10% to 20% in other cases (Alves 2004).

Most of the above studies were done for the above medium to large scale networks with baseline lengths ranging from 50 to hundreds of kilometres, under quiet to medium ionospheric conditions. Alves (2004) used the Southern Alberta network, which is studied in this thesis, but considered only quiet to medium ionospheric conditions. Evaluating the effectiveness of MRS approaches under highly active ionospheric conditions is critical to determining availability under such conditions. Euler *et al* (2004b) discussed severe ionospheric effects that resulted in very poor network performance with a low percentage of ambiguity fixing, even over very short distances of

less than 15 km using a network in Hong Kong. A further performance measure introduced in this thesis is a comparison of MRS and SRS performance in the position accuracy convergence domain.

1.3 Objectives

Against this backdrop of current knowledge and research in this area, this thesis consists of further investigation and evaluation of the performance of the MultiRef^{TM} approaches. Data collected from a medium scale network (30 km to 60 km baseline lengths) for a long period of time (24-hour duration) under various atmospheric conditions are used for the evaluation. During this period of dramatic increase in the demand for high precision GPS applications, it is important to validate an accurate, continuous, and reliable differential system with high availability especially under challenging ionospheric conditions. Achieving this goal entails several associated sub-tasks, as outlined below:

(i) Evaluation of the performance of the two MRS algorithms (least-squares collocation and tightly-coupled) under ionospheric conditions varying from quiet (1 – 2 ppm) to extremely active (7 – 8 ppm).

(ii) Evaluation of the performance of the two algorithms in all domains; namely, the observation domain, long-term position domain, ambiguity resolution domain and position converging domain under the above ionospheric conditions. Different

measurement combinations are employed, including the L1, Ionospheric-free (IF) and L1/L2 with stochastic ionosphere modelling.

(iii) Evaluating the performance of the two MRS algorithms with a moving rover.

The above analyses are to be performed in the post-mission phase using software that can be used in real-time, making the analysis valid for a real-time network.

(iv) Evaluating the performance of the least-squares collocation algorithm in real-time.

1.4 Thesis Outline

Chapter 2 reviews differential error sources and their impacts on network GPS RTK. These include satellite orbital error, tropospheric error and ionospheric error. Various observation combinations, ambiguity resolution strategies and stochastic ionospheric modeling techniques are also discussed. A review of existing MRS algorithms follows, with a focus on the least-squares collocation and tightly-coupled algorithms. These two algorithms are evaluated in subsequent chapters. In addition, the Virtual Reference Station (VRS) concept and Radio Technical Commission for Maritime Services (RTCM) standards for DGPS are presented and discussed.

Chapter 3 presents the evaluation methodology, including data processing and analysis techniques of the results, oriented towards a comparison of MRS approaches and the SRS approach. A detailed description of the testing network and data sets is also given in this chapter.

Chapter 4 presents and analyzes the results obtained using the least-squares collocation and the tightly-coupled MRS algorithms. The analysis is divided into three parts corresponding to the static post-mission tests, the kinematic post-mission test and the static real-time test. For static post-mission tests, the algorithms are evaluated under various atmospheric conditions, especially under an ionospheric storm that occurred in November 2004. The kinematic post-mission and static real-time tests were carried out under normal ionospheric conditions.

Chapter 5 draws conclusions for this work and makes recommendations for further investigation.

CHAPTER 2

CONCEPTS AND ALGORITHMS

2.1 Carrier Phase-Based Differential GPS Error Sources

Differencing GPS measurements eliminates both receiver and satellite clock errors. These are, therefore, not discussed any further herein. The remaining GPS errors are classified into two groups: (i) spatially uncorrelated errors; and (ii) spatially correlated errors. The spatially uncorrelated errors - namely, receiver noise and multipath - depend on receiver types, antenna types and antenna environment. They are not reduced by operation in differential GPS (DGPS) mode. Employing a high quality receiver and antenna and antenna location in an open sky-tracking location with minimal multipath effects contribute to increasing data quality and reducing uncorrelated errors. The spatially correlated errors, including satellite orbital error, tropospheric and ionospheric errors - are a function of inter-antenna distance and atmospheric conditions. They, therefore, can be reduced in DGPS operation. As each error source has its own characteristics, they are described in the following sections.

2.1.1 Satellite Orbital Error

In order to estimate the unknown positioning states using GPS measurements, one must know the satellite positions, which are reported in an ephemeris. The satellite positions are predicted using a set of Keplerian orbit, perturbation, and satellite clock parameters (Kaplan *et al* 1996). Satellite orbital errors are caused by inaccurate estimations of satellite positions reported in the ephemeris. The most obvious way to reduce the satellite orbital error is by using a precise ephemeris, which allows the user to calculate the satellite positions within an accuracy of better than 5 cm (IGS 2004). The precise ephemeris is provided by various GPS agencies such as the International GPS Service (IGS), the US National Geodetic Survey (NGS) and the Geodetic Survey Division, Natural Resources Canada (GSD/NRCan). However, the precise ephemeris is available only in post-mission. For example, users must wait 12 days for a final precise ephemeris, 17 hours for a rapid ephemeris and 3 hours for an ultra-rapid ephemeris. For most real-time or near real-time applications, the broadcast ephemeris transmitted along with satellite navigation messages is used. The satellite positions calculated from the broadcast ephemeris have an RMS error of approximately 2 m (IGS 2004).

A satellite's orbital error is spatially correlated and is reduced using DGPS. According to Wells *et al* (1986), the relationship between a satellite orbital error and the resulting baseline error in DGPS is

$$\frac{\Delta d}{d} = \frac{\Delta \rho}{\rho} \qquad (2.\ 1)$$

where Δd is the total error in length of the baseline d (m), $\Delta\rho$ is the total error in the coordinates of a satellite position (m), and ρ is the mean distance from the stations to the satellite (m). Based on Equation (2.1), the baseline error caused by a satellite position error of 2 m is less than 1 cm for baseline lengths of up to 100 km, assuming an average satellite receiver distance of 20200 km. This effect is negligible for DGPS, typically at the centimetre level of accuracy.

2.1.2 Ionospheric Error

The ionosphere is a layer at approximately 50 km to 2000 km above the earth's surface and is a very important source of errors in GPS measurements. It is formed by the ionization of the neutral atmosphere by solar ultraviolet radiation (UV) and X-ray radiation coming from the corona of the Sun at low and middle altitudes and by energetic particles at high altitude (Skone 1998). The ionosphere itself is approximately a plasma, meaning that it is electrically neutral as a whole with equal numbers of electrons and ions. Within this sphere, the electrons gather around ions with a certain plasma frequency and spin along the magnetic field, resulting in collisions between electrons and ions (Skone 1998). GPS signals can travel through the ionosphere but may be attenuated, depending on the signal frequency, electron collisions and the electron density along the traveling path. The first-order slant ionospheric carrier phase error in units of metres, I, is (Leva *et al* 1996)

$$I = \left[1 - \frac{R_e \cos\alpha}{R_e + h_I}\right]^{-1/2} \frac{40.3\ \mathrm{VTEC}}{f^2} \qquad (2.2)$$

where R_e is the radius of the earth, α is satellite elevation, h_I is the height of the ionosphere above the earth's surface, f is the carrier frequency of the GPS signal, and VTEC stands for Vertical Total Electron Content in units of electrons/m^2. VTEC represents the electron density in a vertical column along the GPS signal trajectory, a quantity that varies with location and level of ionospheric activity. The electron number per unit of volume, moreover, changes with altitude: increasing from altitude of 50 km, reaching its peak of 10^{12} electrons/m^3 at an altitude of 300 to 350 km, and then decreasing significantly at higher altitudes. The ionosphere is also divided into different regions, namely D, E, F1, F2 and H based on their altitudes and characteristics (Klobuchar 1996). The D region (at altitude of 50 km -90 km) and the E region (at altitude of 90 km – 140 km) place negligible effects on GPS measurements (Klobuchar 1996). The F1 and F2 regions at altitude of 140 km – 210 km and 210 km – 1000 km, respectively, place the most significant impact on GPS measurements. The H region at altitude of larger than 1000 km and its impact on GPS measurements can be significant under storm conditions (Klobuchar 1996).

The magnitude of the ionospheric error varies depending on the process of ionization, which depends mainly on the nature of solar activities. It is, therefore, different from day to night, and from one season to another. Diurnally, the ionospheric error usually reaches its first peak at 14:00 local time, its secondary peak at 22:00 local time and drops to the

minimum before sunrise. This diurnal effect is the result of a variation in the electron number created and depleted through processes of ionization and recombination caused by the diurnal period of the Sun (Skone 2003). Seasonally, the ionospheric error is larger in winter (October to March for Calgary) versus summer (April to September for Calgary) due to the slower recombination process of free electrons caused by cold molecular nitrogen N_2 (Skone 2003). Another characteristic of the ionosphere is the equatorial anomaly. This is caused by the neutral wind motions pushing electrons to the two sides of the magnetic equator (± 10º magnetic latitude) resulting in a higher electron density in these regions (Skone 2003). The very complex interaction between the solar wind and the magnetosphere, which is formed outside the ionosphere due to the magnetic character of the earth itself, results in some ionospheric phenomena including sudden ionospheric disturbance (SID), polar cap absorption, aurora oval, magnetic storm and ionospheric storm (Skone 1998, Liu 2004). SID phenomena are caused by solar flares, which comprise transient brightening in a small active area on the solar surface leading to a sudden increase in TEC in the D, E and F regions of the ionosphere. The flares typically last from only a few minutes to several hours (Liu 2004). Large travelling solar flares produce many highly energetic protons, leading to intense ionization in some areas. This phenomenon is called polar cap absorption and is ordinarily observed at high latitudes of more than 75^{o} geomagnetic latitude (Skone 1998). This event usually lasts for long periods of time (a few days) but, fortunately, is rather rare. The auroral oval is a region of the ionosphere characterized by a high geomagnetic latitude of $65\text{-}67^{o}$ nightside and of $75\text{-}85^{o}$ dayside (Skone 1998). Enhanced conductivity and energetic electrons are formed in the auroral regions, especially under storms. The phenomenon is caused mostly by the

solar wind but its complexity is not fully explained in existing literature (Skone 1998). A magnetic storm is a global-scale event caused by a large sudden change in solar wind pressure on the magnetopause, resulting in disturbances of the geomagnetic field. An ionospheric storm is characterized by irregularities in electron density in the F region of the ionosphere. Ionospheric impact on GNSS signals is very significant under storm conditions due to highly localized electron density and scintillations. In addition to large measurement errors, loss of phase lock and cycle slips are the other most common impacts caused by a highly active ionosphere. Very fortunately, the ionospheric effect is dispersive to GPS frequencies and therefore can be modeled or eliminated using dual-frequency combinations. However, under extreme conditions, losing lock or cycle slips remain a problem even with the use of dual-frequency ionospheric-free combinations.

There are many techniques available to model the ionospheric error to a certain level of accuracy. One such model, the Klobuchar model, is based on the satellite broadcast ephemeris and is capable of modeling only 50% of the ionospheric error (Klobuchar 1996). Two-dimensional (2D) modeling techniques approximate the ionospheric error based on dual frequency measurements from a network of GPS stations, giving real-time or near real-time ionospheric corrections to users. These techniques consider the ionosphere as one unique layer at a fixed height above the earth (usually from 50 km to 500 km). There are two types of 2D models: function-based and grid-based. The function-based technique fits the zenith ionospheric delay observed at reference stations into a surface, which is usually described by a function of pierce points of the GPS signals on the ionosphere layer. The grid-based algorithm is more widely used than

function-based one. Using this technique, the GPS network geographical region is covered by a grid with precisely known coordinates and a certain degree of density depending on the size of the GPS network. The zenith ionospheric delay at each GPS reference station is estimated based on the GPS dual frequency observations. These estimations are then interpolated to the position of each grid point. The ionospheric delay at a given rover's position located inside the coverage area is estimated by interpolating the estimated delays at the four surrounding grid points.

For a DGPS user who has access to the dual frequency L1 and L2 GPS measurements, the most common method of significantly reducing the ionospheric effect on DGPS positioning is by using the GPS dual frequency measurements. The following equation represents the relationship between ionospheric error on GPS L1 and L2 measurements

$$I_2 = \left(\frac{\lambda_2}{\lambda_1}\right)^2 I_1 \qquad (2.3)$$

An ionospheric-free (IF) observation combination should be used when the inter-antenna distance is long or under unsettled ionospheric conditions. The ionospheric error can also be stochastically modeled using dual frequency observables. The above-mentioned technique using the dual GPS frequency observations, described in greater detail below, are used to produce position solutions in this thesis.

2.1.3 Tropospheric Error

The troposphere is neutral atmosphere, which means that it does not contain free electrons, and occupies the region from approximately 0 to 43 km above the earth's surface. The tropospheric error does not depend on solar activities. It is not GPS frequency-dependent and therefore cannot be eliminated by using a dual-frequency combination. The troposphere places two major delay effects on GPS measurements due to its dry component and its wet component (Skone 2003). The dry delay contributes approximately 90% of the total delay; however, the dry component is a function of local temperature and pressure, both of which vary relatively slowly. The dry delay is thus easily modeled. The wet delay is caused by a high concentration of water vapour at heights of between 0 and 15 km above the earth's surface. It constitutes only 10% of the total delay. However, this component is hard to predict and model due to the nature of the surface humidity variation. Being dependent on the humidity along the signal path, the troposphere also has a seasonal effect on GPS observations. In Calgary, it is generally more humid during summer than during winter, meaning that the tropospheric error on GPS measurements (mainly its wet component) is generally larger in summer than in winter (de Jong *et al* 2002). In winter, especially when it is very cold (-20 to -30^{o}C), the tropospheric error could drop to a negligible value (de Jong *et al* 2002). However, a large amount of wet snow or rain can change the situation, due to the increase in water vapour, increasing the tropospheric error considerably for high precision GPS techniques. Generally, tropospheric effects on GPS signals reach 2 to 5 metres for a satellite at zenith

and up to approximately 25 metres for a satellite at low elevation, for example, in the range of 5^{o} (Skone 2003).

In order to obtain the slant tropospheric effects, the effect at zenith is firstly modeled. A mapping function is then used to map the zenith delay to a certain angle of observation. The tropospheric model used in this thesis is the Hopfield model. The total tropospheric error at zenith, $D^{z}_{trop}(h_{user})$, is the sum of the dry error caused by the dry component, D^{z}_{d}, and the wet error caused by the wet component, D^{z}_{w}, and can be calculated as follows (Skone 2003)

$$D^{z}_{trop}(h_{user}) = D^{z}_{d} + D^{z}_{w} \tag{2. 4}$$

with the dry and wet components expressed as

$$D^{z}_{d} = \tfrac{10^{-6}}{5} N_{d0}(h_{d} - h_{user}) \qquad \text{for } h_{user} \le h_{d} = 43\,\text{km} \tag{2. 5}$$

$$D^{z}_{w} = \tfrac{10^{-6}}{5} N_{w0}(h_{w} - h_{user}) \qquad \text{for } h_{user} \le h_{w} = 12\,\text{km} \tag{2. 6}$$

$$N_{d0} = 77.604\left(\frac{P_{d}}{T}\right)\left(\frac{1}{1+P_{d}\left[57.97e^{-8}\left(1+0.52/T\right)-9.4611e^{-4}\,T_{c}/T^{2}\right]}\right) \tag{2. 7}$$

$$N_{w0} = \left(\frac{e}{T}\left(1+1650\frac{e}{T^{3}}\left[1-0.01317T_{c}+1.75e^{-4}T_{c}^{2}+1.44e^{-6}T_{c}^{3}\right]\right)\right)\left(64.79+\frac{377600}{T}\right)$$

where h_{user} is the height of the rover, h_{w} is the maximum height of the wet component, h_{d} is the maximum height of the dry components, N_{w0} represents the wet refractivity

and N_{d0} stands for the dry refractivity at the earth's surface. As shown in equation (2.7), the refractivity components are a function of temperature T (T_C is temperature in degrees Celsius and T_K is temperature in degrees Kelvin), dry air pressure P_d in millibars and partial pressure of the water vapour e in millibars. The partial pressure of the water vapour is estimated as a function of relative humidity R_h and temperature T. A mapping function is used to map the zenith value to the slant value, as follows

$$\mu = \frac{1}{\sin(\alpha)} \qquad (2.8)$$

where α is the satellite elevation of the measurement. This is the simplest form of mapping functions. However, it is adequate in this case due to the use of high elevation cut off angle, which is 15 degrees.

2.1.4 Multipath and Noise

Multipath, interference and noise have very short spatial correlation characteristics (Parkinson & Enge 1996). This means that the effect of these error sources obtained at a reference station can be very different from those obtained at a rover station when using the DGPS technique. Multipath occurs when the antenna receives both reflected and direct signals. Multipath depends highly on the reflector's properties, the antenna-reflector distance, the antenna gain pattern and the type of correlator used in a receiver (Ray 2000). The resulting impact on GPS carrier phase measurements is less than one-quarter of the carrier wavelength (Georgiadou & Kleusberg 1988, Ray 2000). Multipath

in static observations is typically non-Gaussian and follows a sinusoidal trend. In kinematic applications, multipath has a more random behaviour due to dynamic disturbances of the receiver. The effect of multipath is very short when correlated over the distance and therefore cannot be reduced using DGPS.

Receiver noise is due mainly to thermal noise, dynamic stress and oscillator stability in the tracking loop of the receiver (Lachapelle 2003). It has a very small effect (in the order of mm in magnitude) on carrier phase positioning. Differential GPS, in fact, approximately doubles the receiver noise, as compared to single point GPS. Similarly, using multiple reference stations result in more noise in the filter than using one reference station.

2.2 Single Reference Station GPS RTK Algorithm

2.2.1 Kalman Filter

In the carrier phase-based DGPS SRS approach examined in this thesis, Kalman filtering is the parameter estimation technique of choice. Kalman filtering combines the knowledge of system dynamics and the knowledge of the statistical nature of system errors to estimate the unknown states (Gao & Sideris 2002). The states at a time t_k are estimated using the measurements obtained at time t_k and the estimated states (at time t_{k-1}) immediately prior to the measurements. The procedure contains four steps: prediction, computation of the innovative sequence, computation of the Kalman gain, and

updating of the states (Brown & Hwang 1983), as shown in Figure 2.1, where x_k is the state vector estimated at epoch k, C_k is the variance covariance matrix of the state vector x_k at epoch k, z_k is the observation vector at epoch k, Q_k is the system process noise matrix at epoch k, R_k is the variance covariance matrix of the measurements z_k, ϕ is the transition matrix, K is the Kalman gain, v is the innovative sequence, I is an identity matrix, and H is the design matrix computed by taking the derivatives of the observables with respect to the estimated states. The '–' sign indicates the matrix or state vector prior to the update step and the '+' sign indicates the matrix or state vector after the update step.

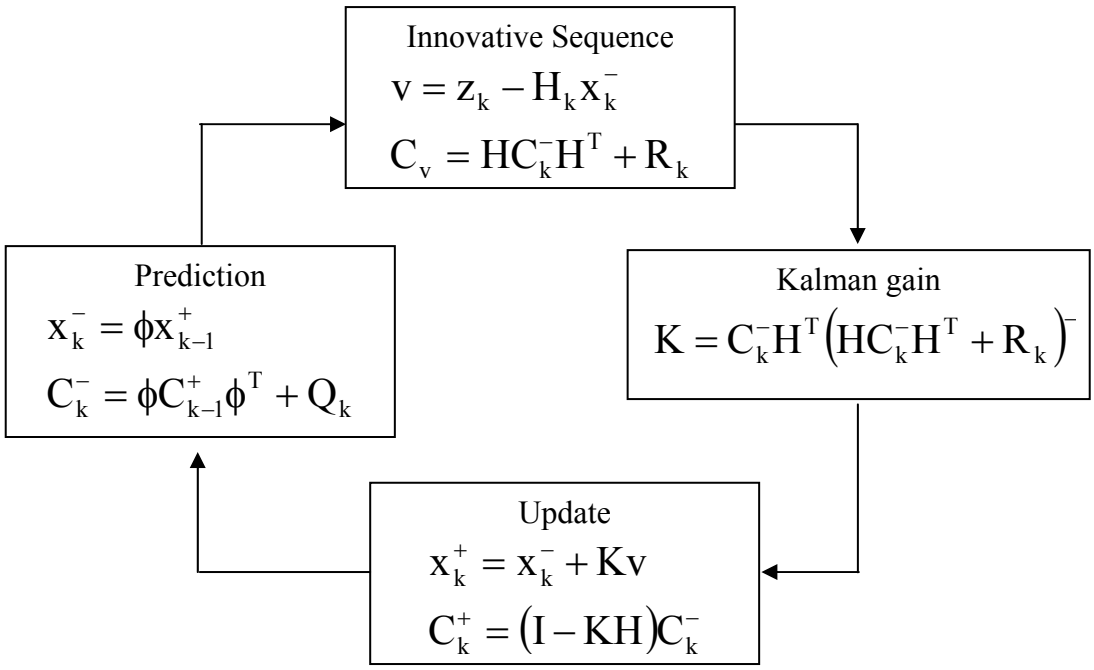

Figure 2.1: Linearized Kalman filter loop (Brown & Hwang 1996)

The state vector in GPS estimation, assuming that there is one rover and n satellite pairs available, usually contains the rover's position, its velocity and n double-difference ambiguities as follows

$$x = \left(\varphi, \lambda, h, \dot{\varphi}, \dot{\lambda}, \dot{h}, \nabla\Delta N_1, \nabla\Delta N_2, \cdots, \nabla\Delta N_{n-1}\right) \tag{2. 9}$$

where (φ, λ, h) represents the rover's latitude and longitude in radians and the rover's height in metres, respectively. $(\dot{\varphi}, \dot{\lambda}, \dot{h})$ represents the rover's latitude rate in radians per second, its longitude rate in radians per second and the rover's rate of change in height in metres per second. The term $\nabla\Delta N_i$ stands for the double-difference ambiguities for satellite pair i. In order to estimate the state vector, the Kalman filter uses two sets of models: the dynamic and measurement models. The dynamic model is based on knowledge of the system dynamics and describes how the state vector transforms from one epoch to the next via a transition matrix and also how the covariance of the state vector is used in this transition. As an operational assumption, the random-walk - or Gauss-Markov - model is considered the optimal dynamic model for most navigation processes, depending on the type of the estimating state. Herein, the random-walk process is used in position, velocity and float ambiguity estimations. The Gauss-Markov, however, is used in estimating the ionospheric error. Assuming a process with driving noise vector $\left(w_\varphi, w_\lambda, w_h\right)$ and velocity state vector $\left(\dot{\varphi}, \dot{\lambda}, \dot{h}\right) = \left(w_\varphi, w_\lambda, w_h\right)$, the transition matrix for position and velocity state vectors is defined as

$$\phi_1 = \begin{bmatrix} 1 & 0 & 0 & \delta t & 0 & 0 \\ 0 & 1 & 0 & 0 & \delta t & 0 \\ 0 & 0 & 1 & 0 & 0 & \delta t \\ 0 & 0 & 0 & 1 & 0 & 0 \\ 0 & 0 & 0 & 0 & 1 & 0 \\ 0 & 0 & 0 & 0 & 0 & 1 \end{bmatrix} \tag{2. 10}$$

where δt is the transition time. If the spectral density of the driving noise vector is $\left(sp_\varphi, sp_\lambda, sp_h\right)$ in units of m^2/s^3, the system noise matrix for position and velocity state vector is

$$Q_1 = \begin{bmatrix} \frac{sp_\varphi}{3}\delta t^3 & 0 & 0 & \frac{sp_\varphi}{2}\delta t^2 & 0 & 0 \\ 0 & \frac{sp_\lambda}{3}\delta t^3 & 0 & 0 & \frac{sp_\lambda}{2}\delta t^2 & 0 \\ 0 & 0 & \frac{sp_h}{3}\delta t^3 & 0 & 0 & \frac{sp_h}{2}\delta t^2 \\ \frac{sp_\varphi}{2}\delta t^2 & 0 & 0 & sp_\varphi \delta t & 0 & 0 \\ 0 & \frac{sp_\lambda}{2}\delta t^2 & 0 & 0 & sp_\lambda \delta t & 0 \\ 0 & 0 & \frac{sp_h}{2}\delta t^2 & 0 & 0 & sp_h \delta t \end{bmatrix} \tag{2. 11}$$

The ambiguities do not change unless there is a loss of phase lock, in which case they are modeled as random constants. The transition matrix for the n-1 ambiguities is

$$\phi_2 = \begin{bmatrix} 1 & 0 & \cdots & 0 \\ 0 & 1 & \cdots & 0 \\ \vdots & \vdots & \vdots & \vdots \\ 0 & 0 & 0 & 1 \end{bmatrix}_{(n \times n)} \tag{2. 12}$$

The system noise for ambiguities is a zero matrix

$$Q_2 = \begin{bmatrix} 0 & 0 & \cdots & 0 \\ 0 & 0 & \cdots & 0 \\ \vdots & \vdots & \vdots & \vdots \\ 0 & 0 & 0 & 0 \end{bmatrix}_{(n \times n)} \tag{2. 13}$$

The complete transition matrix for the state vector shown in equation (2.9) is

$$\phi = \begin{bmatrix} \phi_1 & 0 \\ 0 & \phi_2 \end{bmatrix} \tag{2. 14}$$

and the complete system noise matrix is

$$Q = \begin{bmatrix} Q_1 & 0 \\ 0 & Q_2 \end{bmatrix} \tag{2. 15}$$

If the ionosphere is stochastically estimated, the state vector shown in equation (2.9) is expanded to

$$x = \left(\varphi, \lambda, h, \dot{\varphi}, \dot{\lambda}, \dot{h}, \nabla\Delta N_1, \nabla\Delta N_2, \cdots, \nabla\Delta N_n, \nabla\Delta I_1, \nabla\Delta I_2, \cdots, \nabla\Delta I_n\right) \tag{2. 16}$$

where $\nabla\Delta I_i$ is the double-difference slant ionospheric error for satellite pair i. Assuming that the ionospheric state is temporally correlated with a correlation time T_0 and a driving noise w_i of spectral density sp_i, the relationship between the ionospheric errors obtained at times k+1 and k in discrete form is expressed as follows

$$\nabla\Delta I^{k+1} = e^{-\frac{\delta t}{T_0}} \nabla\Delta I^k + w_i^{k,k+1} \tag{2. 17}$$

where $\delta t = t^{k+1} - t^k$ is the transition time and $w_i^{k,k+1}$ is discrete white noise which is written as

$$w_i^{k,k+1} = \int_{t^k}^{t^{k+1}} e^{-\frac{1}{T_0}\left(t^{k+1}-\tau\right)} w(\tau) d\tau \tag{2. 18}$$

Its variance is $\frac{sp_i}{2} T_0 \left[1 - e^{-\frac{2}{T_0}\delta t} \right]$. Consequently, the transition matrix, θ_3, and the system noise matrix, Q_3, for double-difference ionospheric error state vectors are

$$\phi_3 = \begin{bmatrix} e^{-\frac{\delta t}{T_0}} & 0 & \cdots & 0 \\ 0 & e^{-\frac{\delta t}{T_0}} & \cdots & 0 \\ \vdots & \vdots & \vdots & \vdots \\ 0 & 0 & 0 & e^{-\frac{\delta t}{T_0}} \end{bmatrix}_{(n-1)\ x\ (n-1)} \tag{2. 19}$$

$$Q_3 = \begin{bmatrix} \frac{sp_i}{2} T_0 \left[1 - e^{-\frac{2}{T_0}\delta t} \right] & 0 & \cdots & 0 \\ 0 & \frac{sp_i}{2} T_0 \left[1 - e^{-\frac{2}{T_0}\delta t} \right] & \cdots & 0 \\ \vdots & \vdots & \vdots & \vdots \\ 0 & 0 & 0 & \frac{sp_i}{2} T_0 \left[1 - e^{-\frac{2}{T_0}\delta t} \right] \end{bmatrix}_{(n-1)\ x\ (n-1)} \tag{2. 20}$$

Finally, the completed transition matrix for the state vector presented in equation (2.16) is

$$\phi = \begin{bmatrix} \phi_1 & 0 & 0 \\ 0 & \phi_2 & 0 \\ 0 & 0 & \phi_3 \end{bmatrix} \tag{2. 21}$$

and the equivalent completed system noise matrix is

$$Q = \begin{bmatrix} Q_1 & 0 & 0 \\ 0 & Q_2 & 0 \\ 0 & 0 & Q_3 \end{bmatrix} \tag{2. 22}$$

The measurement model of a Kalman filter is based on the knowledge of the statistical nature of system errors and use of the variance covariance matrix of the measurements R. It also relates the measurements to the state vector by way of the design matrix H. The design matrix is derived by taking the derivatives of the measurements with respect to the state vector. The form of the design matrix varies depending on the measurement selection; this will be discussed further in the following section.

2.2.2 Phase Observations and Phase Combinations

Fundamentally, the GPS carrier phase measurement, in units of metres, can be expressed as follows (Lachapelle 2003)

$$\phi = \rho + d\rho + c(\delta t + \delta T) - I + T + \varepsilon_{multipath+noise} + \lambda N \qquad (2.\ 23)$$

where ρ is the true geometric range from satellite to receiver (m), $d\rho$ is orbital error (m), c is the speed of light (m/s), δt is satellite clock error (s), δT is receiver clock error (s), I is ionospheric delay (m), T is the tropospheric delay (m), ε is multipath and noise (m), and N is the integer carrier phase ambiguity (cycles). The carrier phase-based double-difference observable, in units of metres, is expressed as (Lachapelle 2003)

$$\nabla\Delta\phi = \nabla\Delta\rho + \nabla\Delta d\rho - \nabla\Delta I + \nabla\Delta T + \nabla\Delta\varepsilon_{multipath+noise} + \lambda\nabla\Delta N \qquad (2.\ 24)$$

where $\nabla\Delta\phi$ is the differenced carrier phase observable (m), $\nabla\Delta\rho$ is the differenced geometric range observable (m), $\nabla\Delta d\rho$ is the differenced orbital error (m), $\nabla\Delta I$ is the differenced ionospheric error (m), $\nabla\Delta T$ is the differenced tropospheric error (m), $\nabla\Delta\varepsilon$ is

the differenced multipath and noise error (m), $\nabla\Delta N$ is the differenced carrier phase ambiguity (cycles), and λ is the carrier wavelength (m). The satellite and receiver clock errors are eliminated when double differencing the measurements. When working with small to medium baseline lengths of less than 50 km (the focus in this thesis), it can be assumed that the tropospheric error is constant and mostly well modeled, resulting in a small differential tropospheric error residual. Over such a distance, the differential orbital error, multipath and noise are also small. The differential carrier phase observations L1 and L2, in units of cycles, are re-written as follows

$$\nabla\Delta\phi_1 = \frac{\nabla\Delta\rho}{\lambda_1} + \nabla\Delta N_1 - \frac{\nabla\Delta I_1}{\lambda_1} + \nabla\Delta\varepsilon_1 \tag{2. 25}$$

$$\begin{aligned}\nabla\Delta\phi_2 &= \frac{\nabla\Delta\rho}{\lambda_2} + \nabla\Delta N_2 - \frac{\nabla\Delta I_2}{\lambda_2} + \nabla\Delta\varepsilon_2 \\ &= \frac{\nabla\Delta\rho}{\lambda_2} + \nabla\Delta N_2 - \frac{\lambda_2}{\lambda_1^2}\nabla\Delta I_1 + \nabla\Delta\varepsilon_2\end{aligned} \tag{2. 26}$$

where $\nabla\Delta\varepsilon$ is the sum of differential satellite orbital errors, differential tropospheric residuals, differential multipath and noise. Various linear carrier phase combinations can be formed using GPS dual-frequency observations (Liu 2003)

$$\nabla\Delta\phi_{i.j} = i\nabla\Delta\phi_1 + j\nabla\Delta\phi_2 \tag{2. 27}$$

where i and j are combination coefficients. The wavelength $\lambda_{i,j}$ (m) and the differenced ambiguity $\nabla\Delta N_{i,j}$ (cycles) of the combination $\nabla\Delta\phi_{i,j}$ can be written as (Liu 2003)

$$\lambda_{i.j} = \left(\frac{i}{\lambda_1} + \frac{j}{\lambda_2}\right)^{-1} \tag{2. 28}$$

$$\nabla\Delta N_{i.j} = i\nabla\Delta N_1 + j\nabla\Delta N_2 \qquad (2.\ 29)$$

where λ_1 is the wavelength of GPS L1 carrier (m), λ_2 is the wavelength of GPS L2 carrier (m), $\nabla\Delta N_1$ is the differential carrier phase ambiguity on L1 (cycles), and $\nabla\Delta N_2$ is the differential carrier phase ambiguity on L2 (cycles). Expressed in terms of the error components, the combined observable in cycles is rewritten as follows

$$\nabla\Delta\phi_{i,j} = \frac{\nabla\Delta\rho}{\lambda_{i,j}} - \left(i + j\frac{\lambda_2}{\lambda_1}\right)\frac{\nabla\Delta I_1}{\lambda_1} + \nabla\Delta N_{i,j} + \nabla\Delta\varepsilon_{i,j} \qquad (2.\ 30)$$

In practice, many different carrier phase combinations can be formed. Their associated combination coefficients, wavelengths, ambiguities and observation equations are shown in Table 2.1.

Table 2.1: Different carrier phase combinations (Liu 2003)

Combinations	i	j	$\lambda_{i,j}$ (cm)	Combined phase observables $\nabla\Delta\phi_{i,j}$	$N_{i,j}$
L1	1	0	19.03	$\nabla\Delta\phi_{L1} = \frac{\nabla\Delta\rho}{\lambda_1} + \nabla\Delta N_1 - \frac{\nabla\Delta I_1}{\lambda_1} + \nabla\Delta\varepsilon_1$	N_1
L2	0	1	24.42	$\nabla\Delta\phi_{L2} = \frac{\nabla\Delta\rho}{\lambda_2} + \nabla\Delta N_2 - \frac{77}{60}\frac{\nabla\Delta I_1}{\lambda_1} + \nabla\Delta\varepsilon_2$	N_2
Wide-lane (WL)	1	-1	86.19	$\nabla\Delta\phi_{WL} = \frac{\nabla\Delta\rho}{\lambda_{WL}} + \nabla\Delta N_{WL} + \frac{17}{60}\frac{\nabla\Delta I_1}{\lambda_1} + \nabla\Delta\varepsilon_{WL}$	$N_1 - N_2$
Narrow-lane (NL)	1	1	10.70	$\nabla\Delta\phi_{NL} = \frac{\nabla\Delta\rho}{\lambda_{NL}} + \nabla\Delta N_{NL} - \frac{137}{60}\frac{\nabla\Delta I_1}{\lambda_1} + \nabla\Delta\varepsilon_{NL}$	$N_1 + N_2$
Ionospheric-free (IF)	1	$-\frac{\lambda_1}{\lambda_2}$	48.44	$\nabla\Delta\phi_{IF} = \frac{\nabla\Delta\rho}{\lambda_{IF}} + \nabla\Delta N_{IF} + \nabla\Delta\varepsilon_{IF}$	$N_1 - \frac{\lambda_1}{\lambda_2}N_2$

Table 2.2: Phase combinations with their ionospheric and noise effects (Liu 2003)

Combinations	Ionospheric Error		Noise	
	In cycles	In metres	In cycles	In metres
L1	$\frac{\nabla\Delta I_1}{\lambda_1}$	$\nabla\Delta I_1$	$\nabla\Delta\sigma_1$	$\nabla\Delta\sigma_1 \cdot \lambda_1 = 0.1903\nabla\Delta\sigma_1$
L2	$\frac{77}{60}\frac{\nabla\Delta I_1}{\lambda_1}$	$\frac{77}{60}\frac{\nabla\Delta I_1}{\lambda_1}\lambda_2 = \left(\frac{77}{60}\right)^2 \nabla\Delta I_1$	$\nabla\Delta\sigma_1$	$\nabla\Delta\sigma_1 \cdot \lambda_2 = 0.2442\nabla\Delta\sigma_1$
WL	$\frac{17}{60}\frac{\nabla\Delta I_1}{\lambda_1}$	$\frac{17}{60}\frac{\nabla\Delta I_1}{\lambda_1}\lambda_{WL} = \frac{77}{60}\nabla\Delta I_1$	$1.41\,\nabla\Delta\sigma_1$	$1.41\nabla\Delta\sigma_1 \cdot \lambda_{WL} = 1.21\nabla\Delta\sigma_1$
NL	$\frac{137}{60}\frac{\nabla\Delta I_1}{\lambda_1}$	$\frac{137}{60}\frac{\nabla\Delta I_1}{\lambda_1}\lambda_{NL} = \frac{77}{60}\nabla\Delta I_1$	$1.41\,\nabla\Delta\sigma_1$	$1.41\nabla\Delta\sigma_1 \cdot \lambda_{NL} = 0.15\nabla\Delta\sigma_1$
IF	0	0	$1.26\,\nabla\Delta\sigma_1$	$1.26\nabla\Delta\sigma_1 \cdot \lambda_{IF} = 0.60\nabla\Delta\sigma_1$

The Narrow-Lane (NL) combination has a very small wavelength of 10.7 cm. This makes resolution of the NL ambiguity very difficult. Therefore, the combination is not very practical unless a very short inter-receiver distance is used under quiet ionospheric conditions. The most popular phase combination strategies used for estimating GPS positioning states are single-frequency L1, dual-frequency wide-lane (WL), dual-frequency Ionospheric-free (IF) and dual-frequency L1 and L2 observations (or WL and L1) with ionospheric error modelling. The formulation for each strategy is presented in the following subsections.

2.2.2.1 Single-frequency L1

For users who do not have access to measurements on the L2 frequency, L1 carrier phase and C/A code measurements are used to estimate the state vector. The L1 double-difference carrier phase observations in cycles and C/A code observation in metres, respectively, are

$$\nabla\Delta\phi_{L1} = \frac{\nabla\Delta\rho}{\lambda_1} + \nabla\Delta N_1 + \nabla\Delta\varepsilon_{\phi_1} \tag{2. 31}$$

$$\nabla\Delta P = \nabla\Delta\rho + \nabla\Delta\varepsilon_P \tag{2. 32}$$

where $\nabla\Delta\rho$ is the differential true geometric range, $\nabla\Delta N_1$ represents the L1 differential ambiguities, and $\nabla\Delta\varepsilon$ is the sum of the double-difference ionospheric residuals, the double-difference tropospheric residuals, multipath and noise. This is the most basic and simplest strategy because no phase combination is formed. As shown in Table 2.2, the use of only the L1 observations produces the advantages of less ionospheric and noise effects, as compared to use of only the L2 observations. The ionospheric error can be either not parameterized, or partially modeled using: (i) the broadcast model or (ii) an ionospheric map from an external source. This strategy, therefore, does not work effectively in situations with long baseline lengths. The state vector in this case involves three rover position states, three rover velocity states and differential ambiguities as previously shown in equation (2.9). If there are n satellite pairs available, the design matrix is as follows, the mathematical expression of the derivatives being available in Cannon (1991).

$$H = \begin{bmatrix} \frac{\partial \nabla\Delta\phi_{L1}^{1}}{\partial\varphi} & \frac{\partial \nabla\Delta\phi_{L1}^{2}}{\partial\lambda} & \frac{\partial \nabla\Delta\phi_{L1}^{1}}{\partial h} & \frac{\partial \nabla\Delta\phi_{L1}^{1}}{\partial\dot{\varphi}} & \frac{\partial \nabla\Delta\phi_{L1}^{1}}{\partial\dot{\lambda}} & \frac{\partial \nabla\Delta\phi_{L1}^{1}}{\partial\dot{h}} & 1 & 0 & 0 \\ \cdots & & & \cdots & & & 0 & \ddots & 0 \\ \frac{\partial \nabla\Delta\phi_{L1}^{n}}{\partial\varphi} & \frac{\partial \nabla\Delta\phi_{L1}^{n}}{\partial\lambda} & \frac{\partial \nabla\Delta\phi_{L1}^{n}}{\partial h} & \frac{\partial \nabla\Delta\phi_{L1}^{n}}{\partial\dot{\varphi}} & \frac{\partial \nabla\Delta\phi_{L1}^{n}}{\partial\dot{\lambda}} & \frac{\partial \nabla\Delta\phi_{L1}^{n}}{\partial\dot{h}} & 0 & 0 & 1 \\ \frac{\partial \nabla\Delta P_{L1}^{1}}{\partial\varphi} & \frac{\partial \nabla\Delta P_{L1}^{1}}{\partial\lambda} & \frac{\partial \nabla\Delta P_{L1}^{1}}{\partial h} & \frac{\partial \nabla\Delta P_{L1}^{1}}{\partial\dot{\varphi}} & \frac{\partial \nabla\Delta P_{L1}^{1}}{\partial\dot{\lambda}} & \frac{\partial \nabla\Delta P_{L1}^{1}}{\partial\dot{h}} & 0 & 0 & 0 \\ \cdots & & & \cdots & & & 0 & \ddots & 0 \\ \frac{\partial \nabla\Delta P_{L1}^{n}}{\partial\varphi} & \frac{\partial \nabla\Delta P_{L1}^{n}}{\partial\lambda} & \frac{\partial \nabla\Delta P_{L1}^{n}}{\partial h} & \frac{\partial \nabla\Delta P_{L1}^{n}}{\partial\dot{\varphi}} & \frac{\partial \nabla\Delta P_{L1}^{n}}{\partial\dot{\lambda}} & \frac{\partial \nabla\Delta P_{L1}^{n}}{\partial\dot{h}} & 0 & 0 & 0 \end{bmatrix}_{(nx2,6+n)} \quad (2.\ 33)$$

where $\frac{\partial \nabla\Delta\phi_{L1}^{i}}{\partial j}$ is the derivative of the double-difference L1 carrier phase observation for satellite pair i with respect to state j, and $\frac{\partial \nabla\Delta P_{L1}^{i}}{\partial j}$ is the derivative of the double-difference L1 C/A code observation for satellite pair i with respect to state j.

2.2.2.2 Dual-frequency WL

This strategy employs WL observables and C/A code observations to estimate the sate vector containing the rover's position, velocity and ambiguities. The ionospheric error is again not parameterized, resulting in observation equations of the following form

$$\nabla\Delta\phi_{WL} = \frac{\nabla\Delta\rho}{\lambda_{WL}} + \nabla\Delta N_{WL} + \nabla\Delta\varepsilon_{\phi_{WL}} \quad (2.\ 34)$$

$$\nabla\Delta P = \nabla\Delta\rho + \nabla\Delta\varepsilon_{P} \quad (2.\ 35)$$

where $\nabla\Delta\rho$ is the true differential geometric range, $\nabla\Delta N_{WL}$ represents the WL ambiguities, and $\nabla\Delta\varepsilon$ is the sum of double-difference ionospheric residuals, double-difference tropospheric residuals, multipath and noise. The wide-lane (WL) combination is the most resistant to position error due to its long wavelength (86 cm) and, consequently, provides the most robust means of resolving ambiguities. In addition, the effect of the ionosphere in units of cycles is small using this combination (as compared to L1, L2 or NL), leading to a resistant ambiguity resolution when the ionosphere is active (Liu, 2003). However, the WL combination actually increases the effect of the ionosphere in the position domain. Moreover, the resolved WL ambiguities do not guarantee a high accuracy in the position domain because of its long wavelength. Therefore, the WL combination is usually employed in the first stage of an ambiguity estimation process (e.g. along with the IF strategy). The design matrix in this case is similar to the one presented in equation (2.33), except that the derivation is of WL observables, instead of L1 observations, with respect to the state vector. The measurement covariance matrix is also constructed with respect to the WL observable accuracy.

2.2.2.3 Dual-frequency IF

The ionospheric-free (IF) combination removes the ionospheric effect and is, therefore, very useful in practice. It is important to note that, although IF eliminates the ionospheric effect, it actually increases the noise effect, as shown in Table 2.2. The IF ambiguity itself is not an integer. From Table 2.1, the IF ambiguity is formulated as

$$\nabla\Delta N_{IF} = \nabla\Delta N_1 - \frac{\lambda_1}{\lambda_2}\nabla\Delta N_2 \qquad (2.\ 36)$$

where IF float ambiguities are used. The IF combined observables are used directly to estimate the state vector shown in equation 2.9. The observable equation is

$$\nabla\Delta\phi_{IF} = \nabla\Delta\phi_{L1} - \frac{\lambda_1}{\lambda_2}\nabla\Delta\phi_{L2} = \frac{\nabla\Delta\rho}{\lambda_{IF}} + \nabla\Delta N_{IF} + \nabla\Delta\varepsilon_{\phi_{IF}} \qquad (2.\ 37)$$

$$\nabla\Delta P = \nabla\Delta\rho + \nabla\Delta\varepsilon_P \qquad (2.\ 38)$$

where $\nabla\Delta\varepsilon$ is the sum of double-difference tropospheric residuals, multipath and noise. The corresponding design matrix and measurement covariance matrix have similar forms as in the case of a single frequency L1 strategy, but one constructed with respect to IF measurements. The "IF fixed" ambiguities can be formed using fixed L1 and fixed L2 ambiguities. In order to achieve this, the WL ambiguities are usually fixed first, the ease of which is aided by the long wavelength. This is followed by fixing the L1 ambiguities, when possible. The L2 ambiguities are then fixed as a result of differencing the fixed L1 and WL ambiguities. In this case, the observation equations for WL observables, L1 observations and C/A code observations have the following form

$$\nabla\Delta\phi_{WL} = \frac{\nabla\Delta\rho}{\lambda_{WL}} + \nabla\Delta N_{WL} + \nabla\Delta\varepsilon_{\phi_{WL}} \qquad (2.39)$$

$$\nabla\Delta\phi_{L1} = \frac{\nabla\Delta\rho}{\lambda_1} + \nabla\Delta N_1 + \nabla\Delta\varepsilon_{\phi_1} \qquad (2.40)$$

$$\nabla\Delta P = \nabla\Delta\rho + \nabla\Delta\varepsilon_P \qquad (2.41)$$

$$\nabla\Delta\phi_{IF} = \nabla\Delta\phi_1 - \frac{\lambda_2}{\lambda_1}\nabla\Delta\phi_2 = \frac{\nabla\Delta\rho}{\lambda_{IF}} + \nabla\Delta N_{IF} + \nabla\Delta\varepsilon_{\phi_{IF}} \qquad (2.42)$$

2.2.2.4 Dual-frequency observables with stochastic ionospheric error modeling

This strategy includes a first order Gauss-Markov model of the double-difference ionospheric error. With high quality input measurements, the ionospheric error is expected to be stochastically well modeled. Therefore, use of this strategy promises a comparable or even better performance, as compared to an IF combination. The observations used for this strategy herein are the L1 carrier phase, L2 carrier phase and C/A code observations. The respective equations have the following forms

$$\nabla\Delta\phi_{L1} = \frac{\nabla\Delta\rho}{\lambda_1} + \nabla\Delta N_1 - \frac{\nabla\Delta I_1}{\lambda_1} + \nabla\Delta\varepsilon_{\phi_1} \tag{2.43}$$

$$\nabla\Delta\phi_{L2} = \frac{\nabla\Delta\rho}{\lambda_2} + \nabla\Delta N_2 - \frac{77}{60}\frac{\nabla\Delta I_1}{\lambda_1} + \nabla\Delta\varepsilon_{\phi_2} \tag{2.44}$$

$$\nabla\Delta P = \nabla\Delta\rho + \nabla\Delta I_1 + \nabla\Delta\varepsilon_P \tag{2.45}$$

The state vector in this case includes the rover's position, velocity, ambiguities and the ionospheric error as shown in equation (2.16). The design matrix H in this case is

$$H=\begin{bmatrix}
\frac{\partial\nabla\Delta\phi_{L1}^{1}}{\partial\varphi} & \frac{\partial\nabla\Delta\phi_{L1}^{1}}{\partial\lambda} & \frac{\partial\nabla\Delta\phi_{L1}^{1}}{\partial h} & \frac{\partial\nabla\Delta\phi_{L1}^{1}}{\partial\dot{\varphi}} & \frac{\partial\nabla\Delta\phi_{L1}^{1}}{\partial\dot{\lambda}} & \frac{\partial\nabla\Delta\phi_{L1}^{1}}{\partial\dot{h}} & 1 & 0 & 0 & 0 & 0 & 0 & -\frac{1}{\lambda_1} & 0 & 0 \\
\cdots & & & \cdots & & & 0 & \ddots & 0 & 0 & \ddots & 0 & 0 & \ddots & 0 \\
\frac{\partial\nabla\Delta\phi_{L1}^{n}}{\partial\varphi} & \frac{\partial\nabla\Delta\phi_{L1}^{n}}{\partial\lambda} & \frac{\partial\nabla\Delta\phi_{L1}^{n}}{\partial h} & \frac{\partial\nabla\Delta\phi_{L1}^{n}}{\partial\dot{\varphi}} & \frac{\partial\nabla\Delta\phi_{L1}^{n}}{\partial\dot{\lambda}} & \frac{\partial\nabla\Delta\phi_{L1}^{n}}{\partial\dot{h}} & 0 & 0 & 1 & 0 & 0 & 0 & 0 & 0 & -\frac{1}{\lambda_1} \\
\frac{\partial\nabla\Delta\phi_{L2}^{1}}{\partial\varphi} & \frac{\partial\nabla\Delta\phi_{L2}^{1}}{\partial\lambda} & \frac{\partial\nabla\Delta\phi_{L2}^{1}}{\partial h} & \frac{\partial\nabla\Delta\phi_{L2}^{1}}{\partial\dot{\varphi}} & \frac{\partial\nabla\Delta\phi_{L2}^{1}}{\partial\dot{\lambda}} & \frac{\partial\nabla\Delta\phi_{L2}^{1}}{\partial\dot{h}} & 0 & 0 & 0 & 1 & 0 & 0 & \frac{-77}{60\lambda_1} & 0 & 0 \\
\cdots & & & \cdots & & & 0 & \ddots & 0 & 0 & \ddots & 0 & 0 & \ddots & 0 \\
\frac{\partial\nabla\Delta\phi_{L2}^{n}}{\partial\varphi} & \frac{\partial\nabla\Delta\phi_{L2}^{n}}{\partial\lambda} & \frac{\partial\nabla\Delta\phi_{L2}^{n}}{\partial h} & \frac{\partial\nabla\Delta\phi_{L2}^{n}}{\partial\dot{\varphi}} & \frac{\partial\nabla\Delta\phi_{L2}^{n}}{\partial\dot{\lambda}} & \frac{\partial\nabla\Delta\phi_{L2}^{n}}{\partial\dot{h}} & 0 & 0 & 0 & 0 & 0 & 1 & 0 & 0 & \frac{-77}{60\lambda_1} \\
\frac{\partial\nabla\Delta P_{L1}^{1}}{\partial\varphi} & \frac{\partial\nabla\Delta P_{L1}^{1}}{\partial\lambda} & \frac{\partial\nabla\Delta P_{L1}^{1}}{\partial h} & \frac{\partial\nabla\Delta P_{L1}^{1}}{\partial\dot{\varphi}} & \frac{\partial\nabla\Delta P_{L1}^{1}}{\partial\dot{\lambda}} & \frac{\partial\nabla\Delta P_{L1}^{1}}{\partial\dot{h}} & 0 & 0 & 0 & 0 & 0 & 0 & 1 & 0 & 0 \\
\cdots & & & \cdots & & & 0 & \ddots & 0 & 0 & \ddots & 0 & 0 & \ddots & 0 \\
\frac{\partial\nabla\Delta P_{L1}^{n}}{\partial\varphi} & \frac{\partial\nabla\Delta P_{L1}^{n}}{\partial\lambda} & \frac{\partial\nabla\Delta P_{L1}^{n}}{\partial h} & \frac{\partial\nabla\Delta P_{L1}^{n}}{\partial\dot{\varphi}} & \frac{\partial\nabla\Delta P_{L1}^{n}}{\partial\dot{\lambda}} & \frac{\partial\nabla\Delta P_{L1}^{n}}{\partial\dot{h}} & 0 & 0 & 0 & 0 & 0 & 0 & 0 & 0 & 1
\end{bmatrix} \tag{2.46}$$

where the first six columns are formulated with respect to the rover's position and velocity states, the next six columns are for L1 and L2 ambiguity states, and the last three columns are for the L1 ionospheric error.

2.2.3 Ambiguity Resolution

In order to take advantage of the precise carrier phase measurements, the unknown ambiguities must be correctly resolved to their integer values. This section reviews the ambiguity resolution approach used in this thesis - the Least-squares AMBiguity Decorrelation Adjustment (LAMBDA). Among the most popular ambiguity resolution techniques, LAMBDA was first introduced in Teunissen (1993). The procedure to estimate the fixed ambiguities and fixed positions contains three steps: (i) estimating float ambiguities and "float" position, (ii) resolving integer ambiguities, and (iii) estimating "fixed" positions using the resolved integer ambiguities. This procedure is demonstrated

in Figure 2.1. A Kalman filter is used to estimate the float ambiguities and "float' positions. After this step, the LAMBDA technique is used to resolve the ambiguities to their fixed values. The ambiguities are resolved so that (Teunissen 1993)

$$\left(\hat{N} - N\right) C_{\hat{N}}^{-1} \left(\hat{N} - N\right)^{T} \text{ is minimized} \qquad (2.47)$$

where N stands for the fixed ambiguities, $\hat{N}$ represents the estimated float ambiguities, and $C_{\hat{N}}^{-1}$ is the covariance matrix of the float ambiguities.

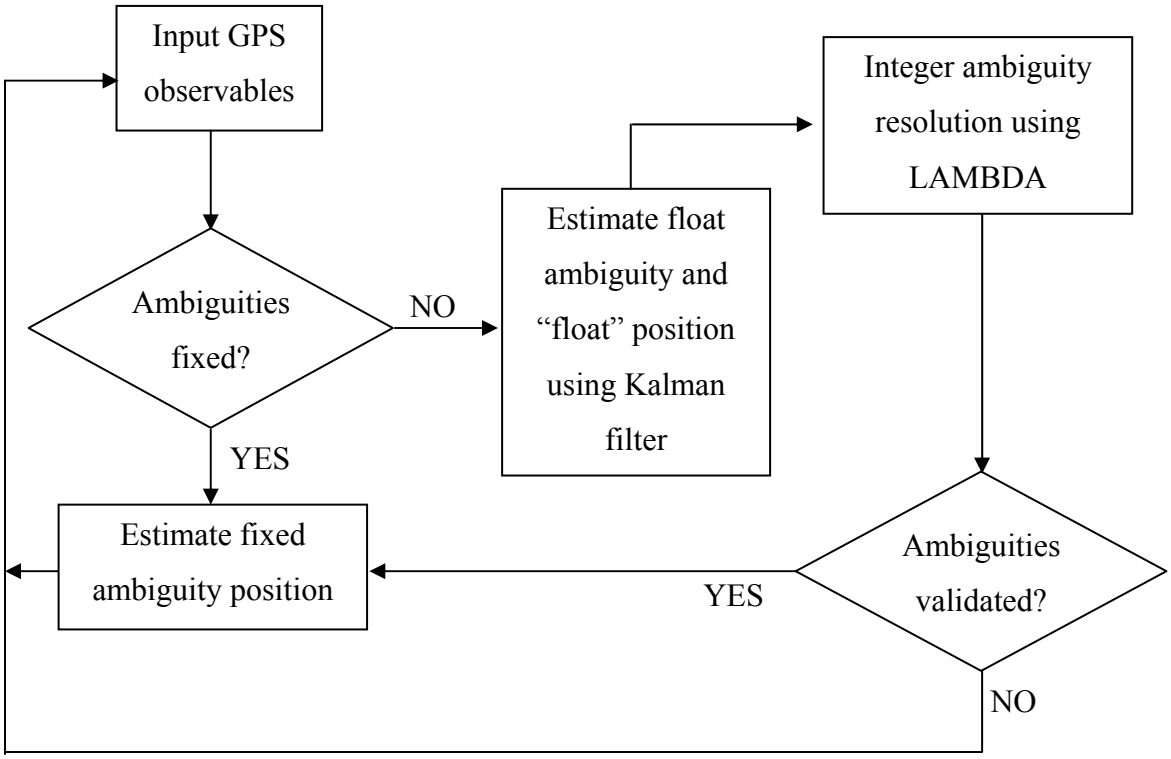

Figure 2.2: Double differential carrier phase positioning procedure (Lachapelle 2003)

There is a set of ambiguities that satisfy the above condition. In order to validate this best estimated ambiguities, a ratio test is used (Han & Rizos 1996a)

$$\text{ratio} = \frac{\left(\hat{\mathrm{N}} - \mathrm{N}_2\right)\mathrm{C}_{\hat{\mathrm{N}}}^{-1}\left(\hat{\mathrm{N}} - \mathrm{N}_2\right)^{\mathrm{T}}}{\left(\hat{\mathrm{N}} - \mathrm{N}_1\right)\mathrm{C}_{\hat{\mathrm{N}}}^{-1}\left(\hat{\mathrm{N}} - \mathrm{N}_1\right)^{\mathrm{T}}} \geq \delta \tag{2.48}$$

where N_1 is the ambiguity set that has the smallest sum of squared ambiguity residuals, and N_2 is the second-best ambiguity set by virtue of having the second smallest sum of squared ambiguity residuals. The threshold δ is defined based on the dimension of the ambiguity vector.

2.3 Multiple Reference Station GPS RTK Algorithms

MRS algorithms are divided into two main categories, namely correction-based and tightly-coupled approaches. The correction-based approach uses observations obtained at the reference stations to estimate the spatially correlated network errors and then interpolates these "corrections" to the rover position. Numerous correction-based algorithms have been developed using distinct means of interpolating the corrections to the rover. These include the linear interpolation algorithm (Han & Rizos 1996b, Gao *et al* 1997, Wanninger 1995), the partial derivative algorithm (Wübbena 1996) and the least-squares collocation algorithm (Raquet 1998). Dai *et al* (2004) compared the relative performance of these techniques, concluding that they are more or less equal. These algorithms are reviewed in depth herein, with a focus on the least-squares collocation and the tightly-coupled approaches, the latter as first presented by Alves *et al* (2004).

2.3.1 Linear Interpolation Approach

One type of approaches to linear interpolation is the linear combination first introduced by Han & Rizos (1996b). Assuming that a network of n reference stations is available, a set of parameters α_i is estimated satisfying the conditions presented in equations (2.49), (2.50) and (2.51)

$$\sum_{i=1}^{n} \alpha_i = 1 \tag{2.49}$$

$$\sum_{i=1}^{n} \alpha_i \left(\hat{X}_r - \hat{X}_i \right) = 1 \tag{2.50}$$

$$\sum_{i=1}^{n} \alpha_i^2 = \min \tag{2.51}$$

where $\hat{X}_r$ and $\hat{X}_i$ are the estimated horizontal coordinates of the user station (r) and the reference station (i), respectively. Assuming that the reference station coordinates and the ambiguities are known, the double-difference misclosure vectors $V_{i,n}$ for baselines formed between every reference station (i) and a primary reference station (n) in metres, is calculated as

$$V_{i,n} = \nabla\Delta\phi_{i,n} - \nabla\Delta\rho_{i,n} - \lambda\nabla\Delta N_{i,n} \tag{2.52}$$

where $\nabla\Delta\phi_{i,n}$ is the double-difference carrier phase measurement vector, $\nabla\Delta\rho_{i,n}$ is the double-difference geometric range vector, and $\nabla\Delta N_{i,n}$ is the double-difference ambiguity

vector. The double-difference observables formed between a rover (r) and the primary reference station (n) are corrected as follows

$$\begin{aligned}\nabla\Delta\phi_{r,n} - \left[\alpha_1 V_{l,n} + \cdots + \alpha_i V_{i,n} + \cdots \alpha_{n-l} V_{n-li,n}\right] \\ = \nabla\Delta\rho_{r,n} - \lambda\nabla\Delta N_{r,n} + \nabla\Delta\varepsilon \sum_{i=l}^{n-l} \alpha_i \nabla\Delta\phi_i\end{aligned} \tag{2.53}$$

Gao *et al* (1997) introduced a distance-based linear interpolation approach to interpolate ionospheric corrections to the rover's location; this is expressed mathematically as

$$\nabla\Delta\hat{I}_{r,n} = \sum_{i=l}^{n-l} \frac{s_i}{s} \nabla\Delta\hat{I}_{i,n} \tag{2.54}$$

where $\nabla\Delta\hat{I}_{r,n}$ is the double-difference ionospheric corrections vector for the baseline formed between the rover and the primary reference station n in the network, $\nabla\Delta\hat{I}_{i,n}$ is the double-difference ionospheric residual vector calculated for baselines formed between reference stations i and n using dual frequency L1 and L2 observables, and n is the number of reference stations. s_i and s are calculated using equations (2.55) and (2.56)

$$s = \sum_{i=l}^{n-l} s_{i,r} \tag{2.55}$$

$$s_{i,r} = \frac{1}{\sqrt{\left(x_i - x_r\right)^2 + \left(y_i - y_r\right)^2}} \tag{2.56}$$

where $\left(x_i, y_i\right)$ are the horizontal coordinates of the reference station i and $\left(x_r, y_r\right)$ are the horizontal coordinates of the rover. Gao & Li (1998) introduced some modifications to improve the performance of the distance-based linear interpolation algorithm. These

include the use of inter-reference station distances defined on the single ionospheric shell at an altitude of 350 km instead of using ground distances. The impact of the elevation angle of the ionospheric delay path on the ionosphere shell is also considered for the spatial correlation of the ionosphere.

2.3.2 Partial Derivative Approach (Low Order Surface Model)

The partial derivative algorithm (Wübbena *et al* 1996) uses a low order surface to model the spatial behaviour of the correlated error over the network coverage area. The following are some examples of the fitting function

$$V = a \cdot \Delta X + b \cdot \Delta Y + c \tag{2.57}$$

$$V = a \cdot \Delta X + b \cdot \Delta Y + c \cdot \Delta X^2 + d \cdot \Delta Y^2 + e \cdot \Delta X \Delta Y + f \tag{2.58}$$

$$V = a \cdot \Delta X + b \cdot \Delta Y + c \cdot \Delta H + d \tag{2.59}$$

$$V = a \cdot \Delta X + b \cdot \Delta Y + c \cdot \Delta H + d \cdot \Delta H^2 + e \tag{2.60}$$

where $(\Delta X, \Delta Y, \Delta Z)$ are the relative coordinates of reference stations with respect to a master point. The network coefficients of the surface are estimated using a least-squares adjustment procedure. Once the coefficients of the function are determined, they are sent to the user to estimate the corrections at the user location. This approach requires at least three reference stations.

2.3.3 Least-squares Collocation Approach

2.3.3.1 Fundamental Concept: Linear Minimum Error Variance Estimator

The most elementary concept of least-squares collocation is the linear minimum error variance estimator, also known as the optimal estimator. Consider a random variable l corresponding to the set of q measurements

$$\mathrm{l} = \left[\mathrm{l}_1, \mathrm{l}_2, \cdots, \mathrm{l}_q\right]^T \tag{2.61}$$

and a random variable s representing a set of m unknown "signals"

$$\mathrm{s} = \left[\mathrm{s}_1, \mathrm{s}_2, \cdots, \mathrm{s}_m\right]^T \tag{2.62}$$

It is assumed that each of the random variables has zero mean and follows a Gaussian distribution. This means that $\mathrm{E}\{\mathrm{l}\} = 0$ and $\mathrm{E}\{\mathrm{s}\} = 0$, where E denotes the expectation function. The relation between measurements l and signals s is known only through covariance matrices

$$\mathrm{C}_{\mathrm{ll}} = \mathrm{cov}(\mathrm{l},\mathrm{l}) = \mathrm{E}\{\mathrm{ll}^T\} \tag{2.63}$$

$$\mathrm{C}_{\mathrm{ss}} = \mathrm{cov}(\mathrm{s},\mathrm{s}) = \mathrm{E}\{\mathrm{ss}^T\} \tag{2.64}$$

$$\mathrm{C}_{\mathrm{sl}} = \mathrm{cov}(\mathrm{s},\mathrm{l}) = \mathrm{E}\{\mathrm{sl}^T\} \tag{2.65}$$

where C_{ll} is the covariance matrix of the measurements l, C_{ss} is the covariance of the interpolated signals s, and C_{sl} is the cross-covariance matrix between the measurements and the signals. A linear estimate of the signal s is

$$\hat{\mathrm{s}} = \mathrm{H}\,\mathrm{l} \tag{2.66}$$

where H is a matrix of size (q x m). This estimates each component of the signal s using a linear combination of the measurements l. After estimation, the error vector ε is formed as

$$\varepsilon = \hat{s} - s \tag{2.67}$$

where $\hat{s}$ is the estimated value and s is the true value. The error covariance matrix is formulated as

$$C_{\varepsilon\varepsilon} = \mathrm{cov}(\varepsilon, \varepsilon) = E\left\{ \varepsilon\varepsilon^T \right\} = E\left\{ (\hat{s} - s)(\hat{s} - s)^T \right\} \tag{2.68}$$

The error variances, σ_k^2, which are the diagonal terms of the error covariance matrix, are

$$\sigma_k^2 = E\left\{ \varepsilon_k^2 \right\} = E\left\{ (\hat{s}_k - s_k)^2 \right\} \tag{2.69}$$

The best linear estimate of the signal s based on the measurements l is that which minimizes the error variance. The matrix H in this case has the following form (Moritz 1980)

$$H = C_{sl} C_{ll}^{-1} \tag{2.70}$$

This optimal estimator is also known as least-squares collocation. Determination of the covariance matrix of the measurements, C_{ll}^{-1}, and the cross-covariance matrix between the measurements and the signals, C_{sl}, is essential for this estimation method. The components of these matrices are estimated using the same signal covariance function. In case of GPS signals, the signal covariance function, which for the spatially correlated errors, is dependent not only on the horizontal distance between two observation stations but also on, for example, the elevation of the satellites. This will be discussed further in the following sections.

2.3.3.2 Network Double-difference Error Observables

Assuming that a network of n GPS reference stations is available, the network single observable vector l is defined as follows

$$l_n = \left[\bar{\phi}_1^1, \cdots, \bar{\phi}_1^{n_{sv}}, \cdots, \bar{\phi}_{n_{rx}}^1, \cdots, \bar{\phi}_{n_{rx}}^{n_{sv}}\right]^T \tag{2.71}$$

where $\bar{\phi}_{rx}^{sv}$ is the phase measurement-minus-true-range observable from receiver rx to satellite sv in single form. The geometric ranges are calculated using precise coordinates of the reference stations. n_{rx} is the number of reference stations, and n_{sv} is the number of satellites observed at each station. The network double-difference observable vector is

$$\nabla\Delta l_n = \left[\nabla\Delta\bar{\phi}_{12}^{12}, \cdots, \nabla\Delta\bar{\phi}_{12}^{1n_{sv}}, \nabla\Delta\bar{\phi}_{13}^{12} \cdots, \nabla\Delta\bar{\phi}_{13}^{1n_{sv}}, \cdots, \nabla\Delta\bar{\phi}_{1n_{rx}}^{12}, \cdots, \nabla\Delta\bar{\phi}_{1n_{rx}}^{1n_{sv}}\right]^T \tag{2.72}$$

where $\nabla\Delta\bar{\phi}_{ab}^{xy}$ is the double-difference measurement-minus-true-range observable between receivers a, b and satellites x, y. Mathematically, a double-difference matrix B can be used to relate the network single observables and the network double-difference observables such that

$$\nabla\Delta l_n = B_n l_n \tag{2.73}$$

$$B_n = \frac{\partial\nabla\Delta l_n}{\partial l_n} \tag{2.74}$$

The dimension of the double-difference matrix is $(d_m \times m)$ where d_m is the number of network double-difference observables and m is the number of network single observations. For example, consider a network of 2 receivers a, b where each receiver

tracks 3 satellites 1, 2, 3. The network single observable vector is $\left[l_a^1\ l_a^2\ l_a^3\ l_b^1\ l_b^2\ l_b^3\right]$. Choosing satellite 1 to be the base satellite, the double-difference vector, then, is $\left[\nabla\Delta l_{ab}^{12}\ \nabla\Delta l_{ab}^{13}\right]=\left[\left(l_a^1-l_b^1\right)-\left(l_a^2-l_b^2\right)\ \ \left(l_a^1-l_b^1\right)-\left(l_a^3-l_b^3\right)\right]$. Performing the partial derivative as shown in equation (2.74), matrix B is

$$B_n=\begin{bmatrix}1 & -1 & 0 & -1 & 1 & 0\\ 1 & 0 & -1 & -1 & 0 & 1\end{bmatrix}$$

If the double-difference ambiguities of network baselines are correctly resolved, the network double-difference error vector is

$$\nabla\Delta\delta l_n=\nabla\Delta l_n-\lambda\nabla\Delta N_n=\nabla\Delta d_c\phi(p,p_0)+\nabla\Delta\delta_u\phi \qquad (2.75)$$

where $\nabla\Delta d_c\phi(p,p_0)$ is the network double-difference spatially correlated errors and $\nabla\Delta\delta_u\phi$ represents the network double-difference uncorrelated errors. A Kalman filter is used to estimate the float ambiguities using L1 observations, L2 observations and stochastic modeling of the ionospheric error. The ratio test is used to validate the fixed ambiguities. The network double-difference errors are also called the estimated network double-difference corrections. These will be used as input measurements for the linear minimum error variance estimator previously discussed in Section 2.3.3.1.

2.3.3.3 Optimal Estimation for Network GPS RTK Correction Generation

The objective of more precise GPS RTK is to reduce the error remaining after double differencing measurements obtained at the reference station and the rover. When

estimating the network corrections, the processing centre does not have access to the rover's measurements but merely an approximate coordinate of the rover. This point is referred to as "prediction point p_{pre}". If the rover's measurements were available, the double-difference observables among the network (including the rover) could be constructed as

$$\begin{aligned} \nabla\Delta\tilde{l} &= Bl \\ &= \begin{bmatrix} B_n & B_{pre} \end{bmatrix} \begin{bmatrix} l_n \\ \tilde{l}_{pre} \end{bmatrix} \end{aligned} \tag{2.76}$$

where B is the double-difference matrix for the network including the rover, and l represents the network (including the rover) single observables. The '~' is used to indicate an unavailable vector in practice due to the absence of measurements at the rover. As the network double-difference observable vector is the sum of network double-difference error and the ambiguities, equation (2.76) can be re-written as

$$\nabla\Delta\delta\tilde{l} + \lambda\nabla\Delta N = Bl \tag{2.77}$$

If single measurement-minus-true-range observables obtained at the reference stations and the rover were corrected as

$$\hat{l} = l + \delta\hat{l} \tag{2.78}$$

where $\delta\hat{l}$ is single observable corrections vector, the corrected double-difference observables could, then, be presented as

$$\nabla\Delta\hat{l} = B\hat{l} = B\left[l - \delta\hat{l}\right] \tag{2.79}$$

The corrections themselves could also be double-difference as

$$\nabla\Delta\delta\hat{l} = B\delta\hat{l} \tag{2.80}$$

Substituting (2.77), (2.78) and (2.80) into (2.79) , we have

$$\nabla\Delta\delta\tilde{l} + \lambda\nabla\Delta N - \nabla\Delta\delta\hat{l} = B\left[l - \delta\hat{l}\right] \tag{2.81}$$

which could be rewritten as

$$\nabla\Delta\delta\tilde{l} - \nabla\Delta\delta\hat{l} = B\left[l - \delta\hat{l}\right] - \lambda\nabla\Delta N \tag{2.82}$$

The left-hand side of the above equation presents the error in estimating the network (including the rover) double-difference corrections

$$\mathrm{err}\left(\Delta\nabla\delta l\right) = \nabla\Delta\delta\tilde{l} - \nabla\Delta\delta\hat{l} \tag{2.83}$$

Applying the described linear minimum error variance estimator, the network (including the rover) double-difference corrections, $\nabla\Delta\delta\hat{l}$, are the signals to be interpolated. The optimal estimator will minimize the error variances which comprise the trace of the covariance matrix $C_{\mathrm{err}(\Delta\nabla\delta l)}$. Although the double-difference corrections, $\nabla\Delta\delta\hat{l}$, are indeed needed, the corrections to single measurements obtained at the reference stations and at the rover, $\delta\hat{l}$, are generated in order to be easily applied by the rover (Raquet 1998)

$$\delta\hat{l}_n = C_{\delta l_n} B_n^T \left(B_n C_{\delta l_n} B_n^T\right)^{-1} \left(B_n l_n - \lambda\nabla\Delta N_n\right) \tag{2.84}$$

$$\delta\hat{l}_{pre} = C_{\delta l_{pre},\delta l_n} B_n^T \left(B_n C_{\delta l_n} B_n^T\right)^{-1} \left(B_n l_n - \lambda\nabla\Delta N_n\right) \tag{2.85}$$

where $\delta\hat{l}_n$ is the single correction vector at each reference station, $\delta\hat{l}_{pre}$ is the single correction vector at the approximated rover position, $C_{\delta l_n}$ is the covariance matrix of the reference station observation errors, $C_{\delta l_{pre},\delta l_n}$ is the cross-covariance matrix between the rover observation errors and the reference station observation errors, B is the double-difference matrix, l_n is the vector of double-difference measurement-minus-true-range

observables form between reference stations, λ is the carrier wavelength, and $\nabla\Delta N_n$ is the vector of double-difference ambiguities between reference stations. Double differencing the above corrected single measurements between a reference station and the rover will result in the most optimal scheme of estimated double differential errors with minimum error variance (Raquet 1998).

In order to estimate the corrections, the covariance matrix of reference station measurement errors $C_{\delta l_n}$ and the cross-covariance matrix between rover measurement errors and the reference station measurement errors $C_{\delta l_{pre},\delta l_n}$ need to be determined. Each component of these matrices is the variance or cross-covariance of the two measurement errors, δl_a^x (for a measurement from receiver a to satellite x) and δl_b^y (for a measurement from receiver b to satellite y). The slant variance or cross-covariance of the two measurement errors, C_{ab}^{xy}, can be derived from its zenith component using a mapping function $\mu^2(\alpha)$

$$\begin{aligned} C_{ab}^{xy} &= \mu^2(\alpha) C_{ab_z}^{xy} \\ &= \mu^2(\alpha)\left[f_{zc}(p_a, p_b, p_0) + f_{zu}(rx_a, rx_b)\right] \end{aligned} \tag{2.86}$$

$$\mu(\alpha) = \frac{1}{\sin\alpha} + c_\mu\left(0.53 - \frac{\alpha}{180}\right)^3 \tag{2.87}$$

where α is the satellite elevation and c_μ is determined with the use of function-fitting. The zenith component of the cross-covariance is the sum of the zenith-correlated error component and the zenith uncorrelated error component. The uncorrelated error is

constant, depending only on particulars related to the receiver type. The zenith-correlated errors between two points p_a and p_b relative to a point p_0 can be described using a functional form (Raquet 1998)

$$f_{zc}(p_a, p_b, p_0) = \frac{\sigma_{cz}^2(p_a, p_0) + \sigma_{cz}^2(p_b, p_0) - \sigma_{cz}^2(p_a, p_b)}{2} \qquad (2.88)$$

where $\sigma_{cz}^2(p_m, p_n)$ is a variance of the differential error between two points, m and n, which can be described by a function of the distance between two points, m and n (the inter-receiver distance). This function is known as the signal covariance function. Raquet (1998) introduced a signal covariance function using a second order polynomial of the inter-receiver distance d

$$\sigma_{cz}^2(p_m, p_n) = c_1 d + c_2 d^2 \qquad (2.89)$$

The fit coefficients, c_1 and c_2 can be determined by fitting the function to a data set.

The signal covariance function used to define the covariance matrices represents the stochastic behaviour of the correlated errors that affect the measurements. It, therefore, theoretically plays an important role on the effectiveness of the MRS approach. Ideally, the covariance function coefficients should be estimated adaptively using real-time data, however, previous results have shown that the MultiRef™ corrections are not very sensitive to the covariance function itself under an intermediate level of ionospheric activity (Fortes 2002). Alves (2004) presented an adaptive signal covariance function taking into account separately the impact of the troposphere and the ionosphere. It is not only a function of the inter-antenna distance but also of the great circle angle between the

observations and the pierce point distance (on the ionosphere shell) between the observations

$$C_{ab}^{xy} = f(d, \alpha, d_I) = e^{\left(-\frac{d}{\beta_d}\right)} e^{\left(-\frac{\alpha}{\beta_\alpha}\right)} \sigma_T^2 + e^{\left(-\frac{d_I}{\beta_{d_I}}\right)} \sigma_I^2 \qquad (2.90)$$

where d is the inter-antenna distance between the station a and b, β_d is the correlation length for the inter-antenna distance between the station for the troposphere, α is the great circle angle between observations to the satellites x and y, β_T is the correlation angle for the great circle angle of the troposphere, σ_T^2 is the tropospheric error variance, d_I is the distance between the pierce points on the ionosphere shell, β_{dI} is the correlation length for the pierce point distance for the ionosphere, and σ_I^2 is the ionospheric error variance. Due to the ability to take into account the correlation of the ionospheric error and the tropospheric error in isolation, this signal covariance function appears to be a more promising means of providing superior results under active atmospheric conditions. This signal covariance function is, therefore, used to generate the results in this thesis.

The corrections are applied to the observations of one reference station (referred to as the primary reference station) in the form of single differencing between the reference station and the rover. These corrected observations are then used at the rover in single reference station mode. A more detailed description of the processing procedure for this approach can be found in Chapter 3 of this thesis.

2.3.4 Tightly-coupled Approach

The major advantage of the correction-based approach is that, once the corrections are generated and applied to the carrier phase observables, existing standard single reference station algorithms and software can be used to process the corrected carrier phase observables. However, if this constraint is removed, a tightly-coupled approach that uses all observations obtained both at the reference stations and at the rover in one Bayesian filter can yield superior results (Alves *et al* 2004). The Bayesian filter is an alternative form of Kalman filter. By using the inversion of the covariance matrix of the *a priori* state vector instead of the measurement vector, this filter is more useful when there is a significant amount of input measurements. The Bayesian filter estimation is expressed in the following form

$$\hat{x} = x^0 + \left(H^T\left(BC_{ll}B^T\right)^{-1}H + C_{x^0x^0}^{-1}\right)^{-1}H^T\left(BC_{ll}B^T\right)^{-1}\left(Hx^0 - Bl\right) \qquad (2.91)$$

where l represents the measurements comprised by single GPS measurements, C_{ll} is the covariance matrix of the measurements, $\hat{x}$ is the state vector or estimated parameters, x^0 is the vector of the parameters *a priori* to the adjustment, $C_{x^0x^0}$ is the covariance matrix of the *a priori* vector representing the approximate accuracy of these values with respect to the true values, B is the double-difference matrix, and H is the design matrix. L1 and L2 observations are used as measurements for the filter. The estimated state vector includes the rover's position, double-difference ambiguities and double-difference ionospheric errors. Assuming a network of n baselines connected to the rover and m

baselines not connected to the rover, the design matrix, H, is formed from the sub-matrices as follows

$$H = \begin{bmatrix} H_{(n,n)} & H_{(n,r)} \\ H_{(r,n)} & H_{(r,r)} \end{bmatrix} \tag{2.92}$$

where the first row refers to baselines connected to the rover and the second row refers to baselines not connected to the rover. There is no common estimated parameter between the use of these two types of baselines; therefore,

$$H_{(n,r)} = H_{(r,n)} = 0$$

$H_{(n,n)}$ has the following form

$$H_{(n,n)} = \begin{bmatrix} \frac{\partial \nabla \Delta \phi_{L1}}{\partial \varphi} & \frac{\partial \nabla \Delta \phi_{L1}}{\partial \lambda} & \frac{\partial \nabla \Delta \phi_{L1}}{\partial h} & \lambda_1 & 0 & -1 \\ \frac{\partial \nabla \Delta \phi_{L2}}{\partial \varphi} & \frac{\partial \nabla \Delta \phi_{L2}}{\partial \lambda} & \frac{\partial \nabla \Delta \phi_{L2}}{\partial h} & 0 & \lambda_2 & -\left(\frac{f_2}{f_1}\right)^2 \\ \frac{\partial \nabla \Delta P_{L1}}{\partial \varphi} & \frac{\partial \nabla \Delta P_{L1}}{\partial \lambda} & \frac{\partial \nabla \Delta P_{L1}}{\partial h} & 0 & 0 & 1 \\ \frac{\partial \nabla \Delta P_{L2}}{\partial \varphi} & \frac{\partial \nabla \Delta P_{L2}}{\partial \lambda} & \frac{\partial \nabla \Delta P_{L2}}{\partial h} & 0 & 0 & \left(\frac{f_2}{f_1}\right)^2 \end{bmatrix} \tag{2.93}.$$

The first row constitutes the L1 observations, the second row presents L2 observations, and the last two rows contain L1 and L2 code observations. The first three columns correspond to the derivatives of measurements with respect to three position states of the rover, the fourth and the fifth columns are for L1 and L2 ambiguities, respectively. The last column contains L1 ionospheric errors in metres. The design matrix for baselines not connected to the rover, $H_{(r,n)}$, is

$$H_{(r,r)} = \begin{bmatrix} 0 & 0 & 0 & \lambda_1 & 0 & -1 \\ 0 & 0 & 0 & 0 & \lambda_2 & -\left(\frac{f_2}{f_1}\right)^2 \\ 0 & 0 & 0 & 0 & 0 & 1 \\ 0 & 0 & 0 & 0 & 0 & \left(\frac{f_2}{f_1}\right)^2 \end{bmatrix} \tag{2.94}$$

where the rows contain L1 carrier phase, L2 carrier phase, L1 code and L2 code observations, respectively. By contrast to the design matrix for baselines connected to the rover, the first three columns are derivatives with respect to the rover's position; in this case, they are all 0. The last three columns are for L1 ambiguities, L2 ambiguities and L1 ionospheric errors, respectively.

2.3.5 Least-squares Collocation versus Tightly Couple: Algorithm and Practical Implementation

The least-squares collocation approach has some limitations, as compared to the tightly-coupled approach. Firstly, it generates corrections based on the assumption that correctly fixed ambiguities are used; however, this assumption does not always hold, especially with long network baselines or under disturbed ionospheric conditions. Upon generation of the corrections, errors in network ambiguities are transferred into the corrections, in at least two respects: (i) incorrectly fixed ambiguities cause a long-term bias impact on the corrections, and (ii) float ambiguities result in corrections that have a lower accuracy and that may be biased. One solution for this problem is to use only fixed ambiguities to

generate the corrections. Unfortunately, this reduces the availability of the valid corrected measurements. Because single corrections are valid only when used in their double-difference form, one cannot assign zero corrections for satellite measurements with float ambiguities; to do so will generate an incorrect double-difference correction when double differencing the zero correction with a valid correction. It is also impossible to create a non-zero correction for a satellite with float ambiguities such that its double-difference correction with all other valid corrections will be zero. The second disadvantage of the least-squares collocation approach is typically the use of longer network baselines, as compared to an equivalent single reference station approach where the rover is usually located in the middle of the network region. This leads to difficulties in estimating the parameters, such as ambiguities and ionospheric errors, which are essential for correction generation.

The tightly-coupled approach, on the other hand, has the advantage of having access to the rover's measurements. This requires a two-way communication link if real-time is required, so that the user can send its observations and its approximate position to the processing centre, whence the processing centre will return the rover's estimated position. In case an effective communication link exists allowing the rover to receive all network measurements, it can estimate an MRS solution without the processing centre. Including the rover in the network improves the configuration by shortening baseline lengths. The ambiguities are, therefore, possibly better resolved and the ionospheric errors are more effectively modeled and, as a result, the unknown states are more accurately estimated.

2.4 MRS Standards and Issues

2.4.1 Virtual Reference Station Concept

Currently there are no off-the-shelf receivers that are capable of accepting network RTK corrections; therefore, the corrections are usually generated and applied to measurements obtained at the primary reference station. These corrected reference observations are then used to process single baseline data from the primary reference station to the rover using existing single baseline processing software. Unfortunately, these software packages usually weight the corrections obtained from the reference station based on the inter-antenna distance. In order to avoid this, a Virtual Reference Station (VRS) is created at a closer position to the rover so that the receiver will not heavily weight the corrected observations (Lachapelle & Alves 2002). In order to generate the VRS measurements, the primary reference station measurements are transferred to the VRS location. These transferred measurements are then corrected by interpolating the network corrections from three surrounding grid points. This step of generating a VRS can be eliminated if an interoperability data transmission standard for network corrections is developed.

2.4.2 Real-time RTCM Standards

The existing Radio Technical Commission for Maritime Services (RTCM) version 2.3 is a well known series of messages allowing one to transmit the reference station raw

observations (Messages 18, 19) or the reference station corrections (message 20, 21) to users for real-time DGPS applications. However, this standard allows only the transmission of one reference station's information for the single reference station RTK approach. In order to support network RTK positioning, the latest version of RTCM with proposed network RTK messages was only recently released, while an industry-wide data transmission standard is anticipated (Euler *et al* 2004a). The proposed messages utilize the RTCM, version 2.3, based on a Master-Auxiliary concept, which uses two types of messages. The first one is the standard single reference station information of a reference station in the network. This station is referred to as the master station. The second message contains the correction differences of other reference stations in the network with respect to the master station. These correction differences allow users to directly interpolate the corrections spatially (Euler 2001). This could possibly result in generating corrections for a VRS or reconstructing the standard correction messages for each reference station with respect to the master station (Euler 2001).

CHAPTER 3

TEST NETWORK AND EVALUATION METHODOLOGY

3.1 Test Network

A portion of the GPS RTK network located in Southern Alberta, Canada, the so called the Minimal Southern Alberta Network (MSAN), is used herein to test the MRS approaches. The network of interest has six GPS reference stations as shown in Figure 3.1, and covers a geographical region of 80 km x 80 km. This is a medium scale network with inter-station distances of 30 km to 70 km.

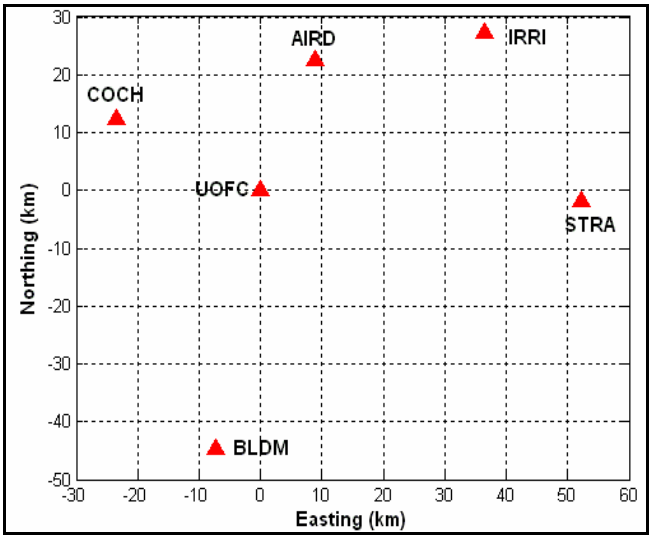

Figure 3.1: Minimal Southern Alberta Network (MSAN)

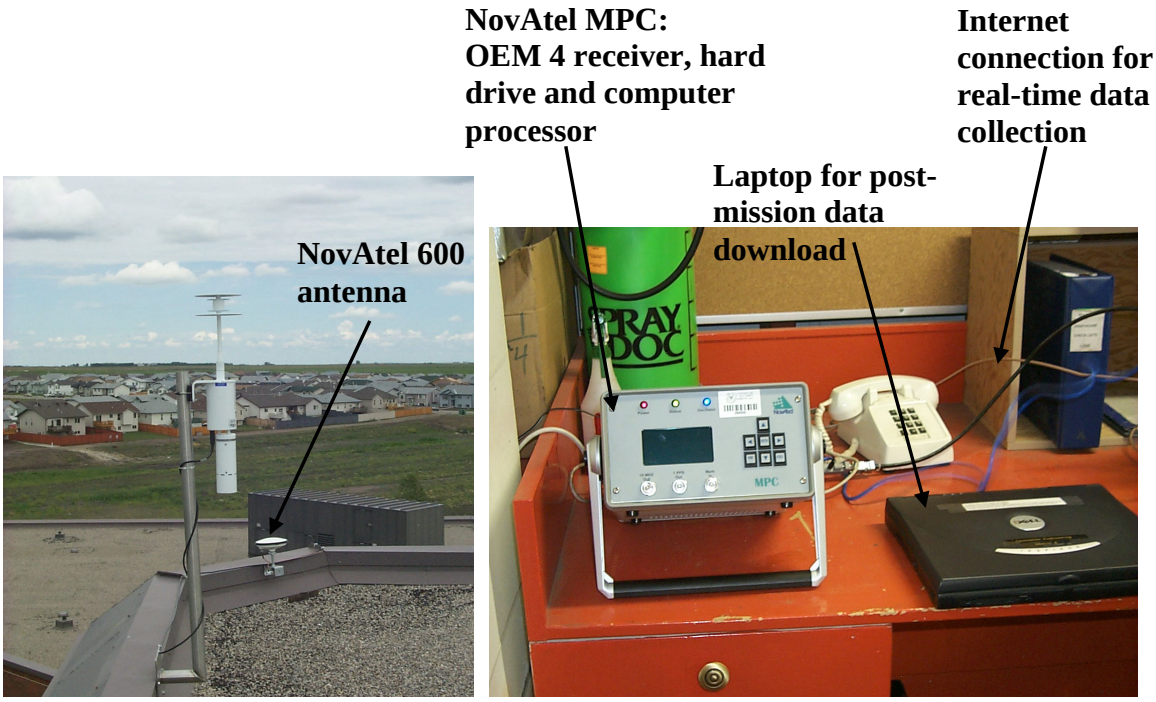

Figure 3.2: NovAtel receiver and antenna set-up for STRA reference station

Each reference station is equipped with a high performance NovAtel 600 antenna and a NovAtel Modulated Precision Clock (MPC) receiver. As an example, Figure 3.2 shows the antenna-receiver set-up for the STRA reference station. The antennas are usually mounted atop stable buildings to ensure open sky-tracking conditions. The MPC receiver is a NovAtel OEM4-receiver-based unit in combination with a low end computer and hard disk for data logging. The MPC receivers allow tracking of the dual GPS L1 and L2 frequency signals of up to 12 satellites. A high tracking bandwidth of 10 Hz is used which might cause a higher level of noise as compared to the use of a lower bandwidths (0.01 – 0.1 Hz). At each station of the network, an internet connection is installed, allowing real-time data collection.

The coordinates of the reference stations were estimated in February 2004 using the Bernese GPS software version 4.0 developed by the Astronomical Institute, University of Bern, Switzerland (Astronomical Institute, University of Bern 2004). The process involved four 24-hour-duration data sets having a 30-second data interval. The network coordinates were constrained to the well known coordinates of an IGS station (PRDS) that is located approximately 20 km away from the UOFC station. The coordinates were re-estimated in July 2004 to account for station movements, changes which are negligible in this case. The final coordinates of the stations used in this thesis are listed in Table 3.1.

Table 3.1: WGS84 coordinates of the MSAN network

	X (m)	Y (m)	Z (m)
PRDS	-1659602.844	-3676725.756	4925493.611
AIRD	-1626487.912	-3652431.048	4954122.770
COCH	-1659446.602	-3646495.350	4947682.596
IRRI	-1599842.090	-3660288.830	4956774.018
STRA	-1594672.090	-3687317.008	4938566.873
BLDM (before and after June 18, 2004)	-1662679.956	-3693557.148	4911862.448
	-1662393.508	-3692754.260	4912525.740
UOFC	-1641889.753	-3664879.425	4939969.731

3.2 Testing Methodology

Both the MRS least-squares collocation, and the MRS tightly-coupled, algorithms were evaluated in post-mission, but assuming real-time operation with the use of data collected

with five stations of the MSAN. Not all six stations can be used due to the inconsistent availability of one station. In the tests presented in this thesis, the UOFC station located in the middle of the network acted as rover and therefore was not used in the reference network. The AIRD station, located 24 kilometres away from UOFC, is the closest reference station to the rover and was chosen as the primary reference station. Three dual-frequency 24-hour data sets with a one-second data rate (collected on 24 May 2004, 6 April 2004 and 8 November 2004) were used for testing. The ionosphere was normal, medium and extremely active during these three days, respectively. The ionospheric double difference effect reaches 7 ppm on an active day over an inter-antenna distance of 24 km. A kinematic test and a real-time test were also carried out to test the MRS LSQC approach, as detailed in the following section.

The MRS least-squares collocation (MRS LSQC) approach entails two processing steps. The first step involves running the MultiRef^{TM} software using observations collected from reference stations to generate network corrections. Both L1 and L2 observations are used in this process and their ambiguities are resolved separately. The approximate rover position is used as the prediction point. As a result, single difference corrections between the primary reference station and the rover are estimated using equations (2.84) and (2.85). Using these corrections, the observations made at the primary reference station are then corrected using the double-difference corrections. In the second step, the corrected primary reference observations, along with the raw rover observations, are used in a single baseline processing routine to estimate the rover positioning solutions. These findings are referred to as the MRS LSQC solutions. It is assumed that a certain time, e.g.

2 hours in these tests, is required for network initialization. The uncorrected primary reference station observations are also used in parallel to obtain the equivalent SRS positioning solutions for comparison. An external commercial software package, GrafNav™ Version 7.01, developed by Waypoint Consulting Inc., is used for the single baseline processing herein to provide independence from the University of Calgary software. The software is capable of epoch-by-epoch carrier phase-based differential processing using single and dual frequency observations. An ionospheric-free (IF) model is used with dual frequency measurements. In order to obtain the IF ambiguities in GrafNav™, the Wide-lane (WL) ambiguities are resolved first, followed by the L1 and then L2 ambiguities. GrafNav™ position solutions based on the use of L1 and L2 observations, without combination and stochastic estimation of the ionospheric error, is also presented. The software processing options were designed to attempt to resolve ambiguities after 11.6 minutes using single frequency L1 observations and after 4.6 minutes using dual frequency observations with a baseline length of 24 km. A 15 degree elevation cut-off was used. Figure 3.3 demonstrates the procedure for applying the least-squares collocation approach in GPS RTK positioning.

In contrast to the LSQC approach, the tightly-coupled approach neither requires a separate step to generate the corrections nor a step for estimating the rover position solution using an independent single baseline processor. All observations obtained at the reference stations and at the rover are input into a single filter, as shown in Figure 3.4, in

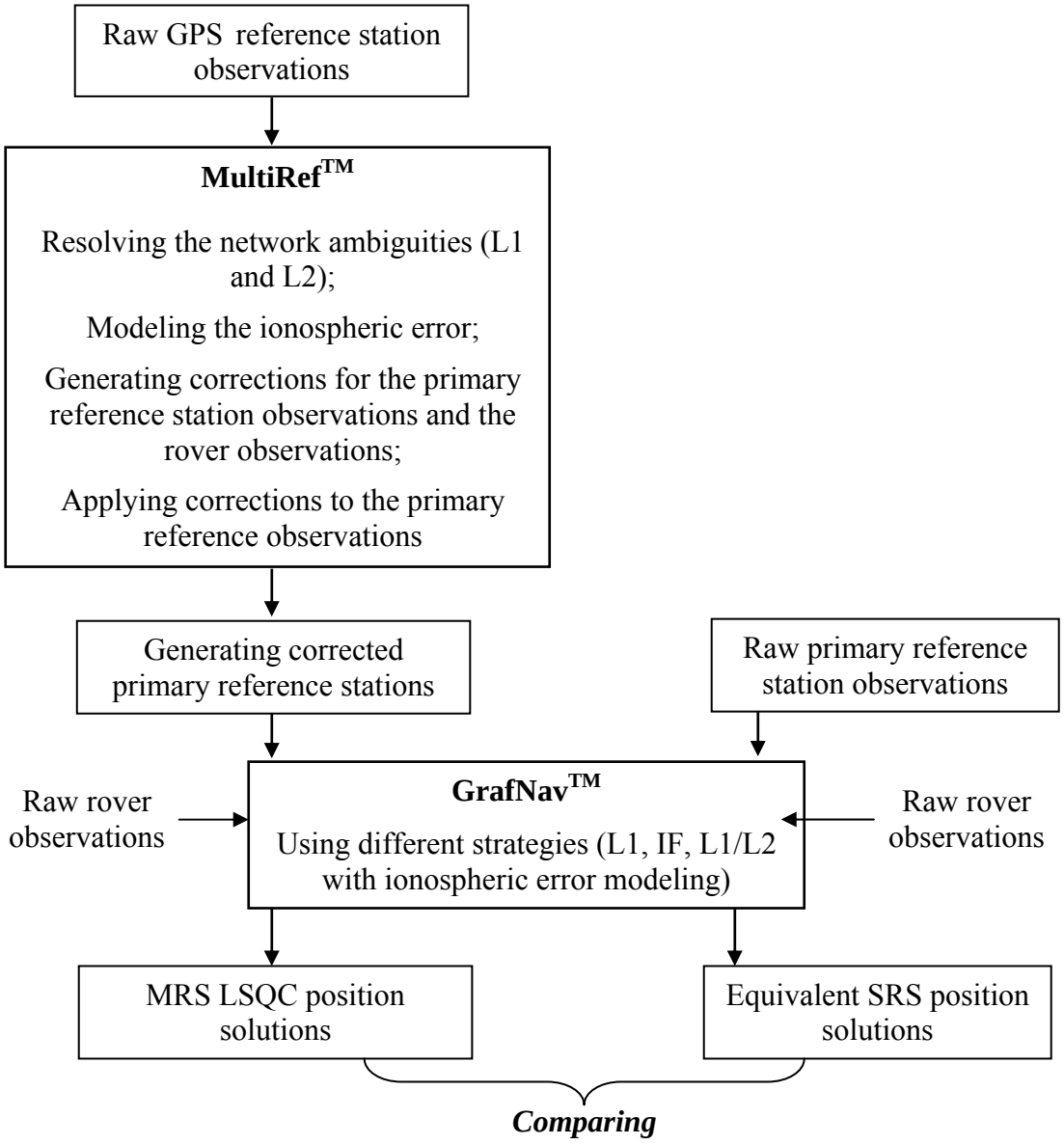

Figure 3.3: Procedure of applying and evaluating MRS least-squares collocation approach in post-mission

which the estimation of all states (including rover position, ambiguities and ionospheric error) is the sole objective. A software package called MRS TC developed by the PLAN group at the University of Calgary was used for processing. Four reference stations were used, depending on their availability for each data set, while the UOFC station still acted

as rover in the test. Under quiet to medium ionospheric conditions, the rover is connected in every baseline. Under active ionospheric conditions, the shortest baselines are formed. Consequently, not every baseline involving the rover is necessarily used. The reference stations that are not connected to the rover contribute to rover position estimation via the covariance of their measurements.

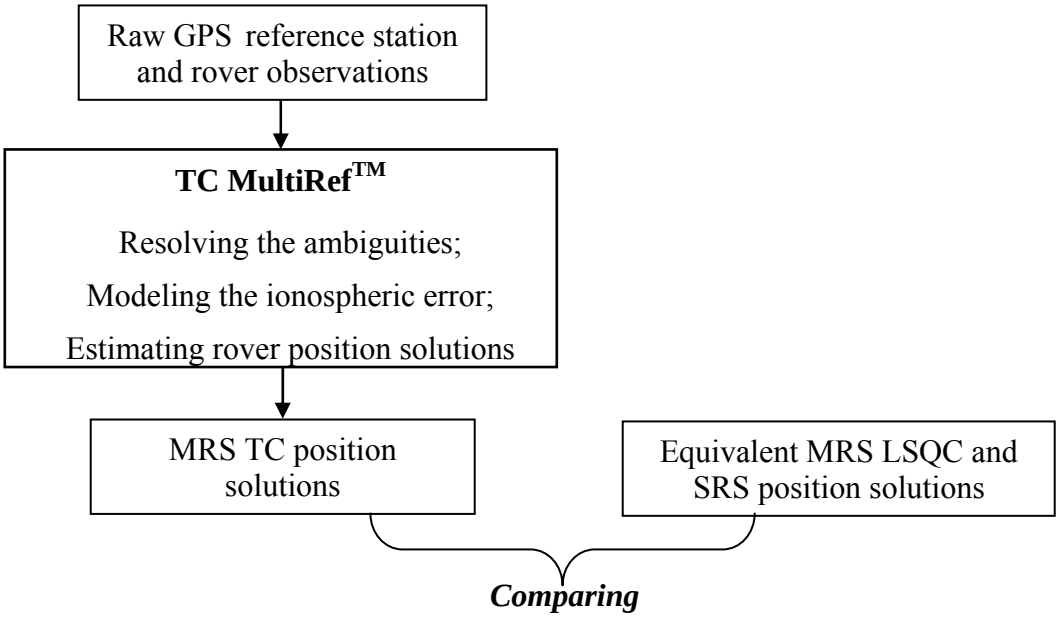

Figure 3.4: Procedure of applying and evaluating MRS tightly-coupled approach in post-mission

3.3 Evaluation Measures

The MRS LSQC approach is evaluated against the equivalent SRS approach based on a certain number of measures - namely, the double-difference correction values, the performance in the measurement domain, the ambiguity resolution domain, the long-term

position domain, and the short-term converging position domain. First of all, it is important to examine the network-generated double-difference corrections. These are the estimated double-difference errors between the primary reference station and the rover, based on the known station coordinates and network ambiguities. These corrections should be reasonable with respect to the approximately known inter-antenna distances and the level of ionospheric error. As previously mentioned, the *a priori* assumption for generating valid corrections is expressed as correctly resolved network ambiguities. The use of float ambiguities in this process results in double difference corrections between the primary reference station and the prediction point (approximated rover position) that have a lower accuracy and that may be biased. Thus, a high performance in resolving the network ambiguities likely suggests that the corrections are reliable. The corrections of most interest are the ones associated with the L1 or L2 observations, the IF and Geometric-Free (GF) derived observables. The corrections on the L1 or L2 observations show the corrected total errors on L1 and L2 measurements, respectively. The corrections on the IF observables are mainly for tropospheric residuals and uncorrelated errors while those on the GF observables are mainly for ionospheric errors and uncorrelated errors. The two latter corrections, thus, give an approximate estimation of the network-estimated tropospheric and ionospheric errors. Secondly, if coordinates of both the primary reference station and the rover are well known, it is expected that the measurement misclosures can be calculated by subtracting the geometric ranges from the measured ranges between the satellites and the antennas. Considering the use of corrected primary reference station observations provided by the MRS LSQC technique, the double-difference measurement misclosures should be smaller than those derived using the raw

primary reference station observations. The reduction in double-difference measurement misclosures represents an improvement in the measurement domain offered by the MRS LSQC approach by comparison to the SRS approach. Most importantly in the positioning domain is the accuracy of the rover position. The analysis herein applies to both long-term steady position accuracy and short-term converging position accuracy. The long-term steady positions are defined as the solutions estimated after the single baseline processing filter has converged and maintained non-reset during a long period of time, which is 21 hours herein. The converging positions are the ones estimated during the time necessary for the single baseline processing filter to converge, which is assumed to be one hour. Position accuracy is estimated using the previously established accurate (sub-cm level) coordinates of the UOFC station. In order to evaluate the short-term converging position accuracy, the filter is reset every one hour, resulting in 24 segments of one-hour duration for each data set. The statistics reported herein for the position solution errors are Root Mean Squared (RMS), usually for individual coordinate components (east, north, height) and for 3D position solution errors. The associated probability levels of these are 68.3% for one dimension and 60.8% for the 3D position (Mikhail & Ackermann 1976). In order to generate a 95% 3D position accuracy, one needs to multiply the values by 1.56 (Mikhail & Ackermann 1976). Along with the position domain, the performance of the approaches in resolving the ambiguities is also very important as it directly relates to the accuracy of the position solutions. A better performance in ambiguity resolution is represented by a faster First Time To Fixed (FTTF) ambiguities and a higher percentage of ambiguities correctly fixed. The fixed ambiguity status flagged as one from GrafNav results indicates that over 80% of the

ambiguities are fixed. The float ambiguity status flagged as zero from GrafNav results indicates that less 80% of the ambiguities are fixed. These indicators will be examined for each and all approaches during the estimation of not only long-term steady position solutions but also converging position solutions. Given that the corrections are valid (meaning that the network ambiguities are successfully resolved), the MRS LQSC approach yields smaller measurement errors, as compared to the SRS approach and, thus, can be considered as aiding the ambiguity resolution process.

In comparison to the MRS LSQC approach, the MRS TC approach does not explicitly generate the double-difference corrections for the primary reference station observations with respect to the rover's position. Consequently, the double-difference network corrections and double-difference measurement misclosures cannot be evaluated directly. Moreover, the ambiguity resolution process, in this case, does not resolve ambiguities of the primary reference station - rover baseline in one discrete step, but only as an addition to those of all other baselines in one filter. There might be more than one baseline connected to the rover. For a rigorous comparison to the equivalent MRS LSQC and SRS cases, an assessment of the ambiguity performance on the same baseline formed from the station (which is the primary reference station in the MRS LSQC case) to the rover is needed. Because there are a large number of solution states to be estimated in this filter as compared to those of the other two approaches, it is expected that a longer time is required to fix the ambiguities.

CHAPTER 4

RESULTS AND ANALYSIS

4.1 Post-Mission Static Test

Three days corresponding to three different levels of ionospheric activities ranging from quiet to very active were chosen to evaluate the MRS approaches in post-mission. Given the availability of software capable of real-time processing, the test results presented herein are valid for a real-time network and associated applications.

Table 4.1: Local K values obtained at MEANOOK geomagnetic station located in Edmonton (approximately 300 km away from UOFC station) for the three test days

Hour of UTC day	0-3	3-6	6-9	9-12	12-15	15-18	18-21	21-24
Local time	17-20	20-23	23-2	2-5	5-8	8-11	11-14	14-17
24 May 2004	3	1	4	3	4	2	2	2
6 April 2004	6	4	5	5	5	2	2	3
7 November 2004	0	2	0	2	2	4	4	7
8 November 2004	8	8	7	8	7	2	3	5
9 November 2004	6	7	7	8	8	7	7	5
10 November 2004	6	8	9	8	9	6	5	3
11 November 2004	4	5	4	4	2	3	2	4
12 November 2004	2	2	4	2	2	2	1	1

In order to obtain an approximate measure of the ionospheric activity in the region on these days, local ionospheric K values are shown in Table 4.1 for three-hour intervals throughout the 24-hour data sets. These values are calculated based on observations of the magnetic field fluctuations obtained at the MEANOOK magnetometer station, which is located in Edmonton, which is approximately 300 kilometres north of the UOFC station. In theory, local K values range from 0 (quiet) to 9 (extreme). A more active ionosphere was observed during the night-time, from 17:00 to 08:00 local time (00:00 - 15:00 UTC) than during the daytime, from 08:00 to 17:00 local time (15:00 – 24:00 UTC) on all three days. This does not follow the usual ionospheric diurnal trend wherein the first and second peaks occur at 14:00 and 22:00 local time, respectively. This is likely due to the aurora effects discussed earlier in chapter 2, which responds to approximately 58º geomagnetic latitude in the Calgary region. On 24 May 2004, the ionosphere was normal during night-time, and local K values of 3 to 4 were observed. On 6 April 2004, local K values of 5 to 6 were observed, indicating a more active ionosphere. A quiet ionospheric condition was experienced during daytime on both days with local K values of 2 to 3. An ionospheric storm was observed on a global scale during the first two weeks of November 2004. In Southern Alberta, a storm was observed from 7 November to 12 November 2004, during which period the local K indices increased to values of 8 and 9 at the peak, as shown in Table 4.1. One day, 8 November 2004, was chosen for the testing reported herein; on this date, local K values of 7 to 8 were observed during the night-time while, during the day time, local K values decreased to 3. Although this indicates lower ionospheric activities during the daytime, this range is still considered unsettled.

The differential tropospheric error on GPS position solutions is mainly caused by the residual wet component, as discussed earlier. Humidity and precipitation values were analyzed in order to approximately estimate the magnitude of the tropospheric error on these three days, as shown in Table 4.2. These values are provided by the Canadian National Climate Data and Information Archive website (Environment Canada 2003). Neither snow nor rain occurred on all three days. The humidity values are less than 70%, indicating a low tropospheric effect on GPS observations during the three days.

Table 4.2: Weather conditions for the three test days

	Temperature (^{o}C)	Average Humidity (%)	Precipitation (mm)
24 May 2004	Low -1, High 14	68	0.4
6 April 2004	Low 0, High 11	39	0.0
8 November 2004	-1 to 18	63	0.0

4.1.1 Normal Ionospheric Condition Results

4.1.1.1 Network Configuration

The network configuration used for testing with the data set obtained on 24 May 2004 is shown in Figure 4.1 and Figure 4.2 for MRS LQSC and MRS TC approaches, respectively. Red triangle markers are used to represent the reference stations while red round markers symbolize the rover station. The AIRD station is the closest reference

station to the UOFC station (rover) and was chosen to be the primary reference station using the MRS LQSC approach, forming a 24 km SRS baseline.

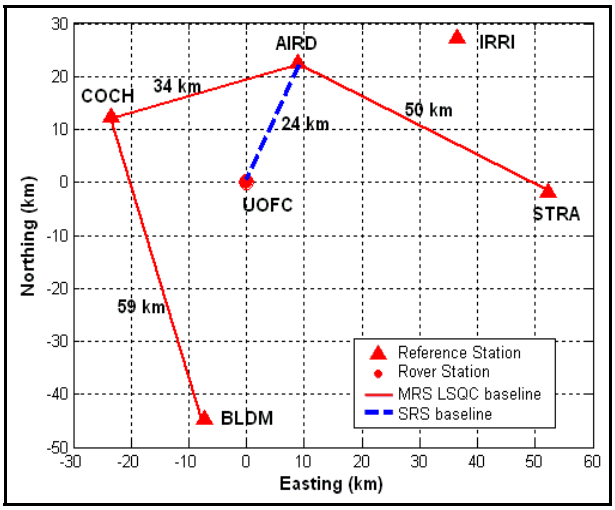

Figure 4.1: Network configuration used with MRS LSQC - 24 May 2004

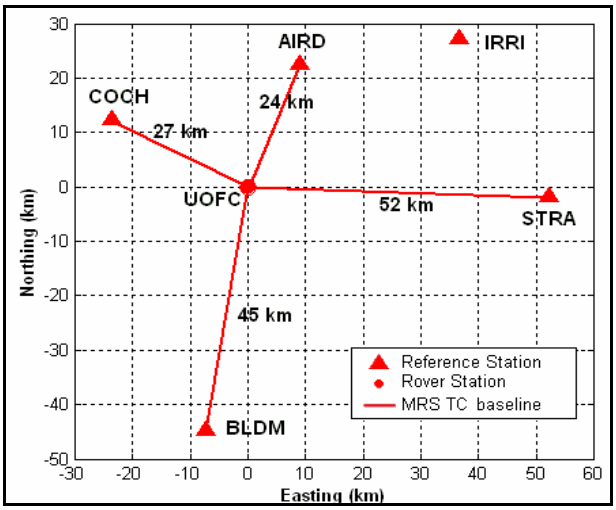

Figure 4.2: Network configuration used with MRS TC - 24 May 2004

As discussed previously, the MRS TC approach benefits the shorter baseline lengths due to the involvement of the rover in network processing. In this case, the baseline lengths

are reduced from a range of 34 km to 59 km using the MRS LSQC approach to 24 km to 52 km using the MRS TC approach.

4.1.1.2 Network Double-Difference Corrections

Network double-difference corrections for different combined observables obtained on 24 May 2004 are shown in Figure 4.3. These are the estimated double-difference correctable errors between the primary reference station, AIRD, and the rover, UOFC. The RMS values are shown in red separately for the active ionospheric period, comprising the first 15 hours of the data set, and for the quiet ionospheric period, which is the last 9 hours of the data set. The RMS double-difference corrections on L1, L2 and WL observables during the active ionosphere period are 3.7 cm (1.5 ppm), 6.1 cm (2.5 ppm) and 5.3 cm (2.2 ppm), respectively. Over a baseline length of 24 km, these values are considered reasonable under normal ionospheric error conditions. The GF (Geometric-Free) corrections are 2.6 cm, representing ionospheric errors of approximately 1.1 ppm. These corrections are smaller during the quiet ionosphere period with an RMS of 1.4 cm (approximately 0.6 ppm). The IF (Ionospheric-Free) corrections are small and constant throughout the day, with a magnitude of 1 cm (0.4 ppm). These corrections are mainly due to the tropospheric residuals, noise and carrier phase multipath.

The network ambiguities were resolved with a high percentage of ambiguities being fixed for all three baselines; specifically, they are 94%, 89% and 87% for AIRD-COCH (34

km), AIRD-STRA (50 km) and COCH-BLDM (59 km), respectively. The network corrections can be considered reliable with such a high percentage of ambiguities fixed.

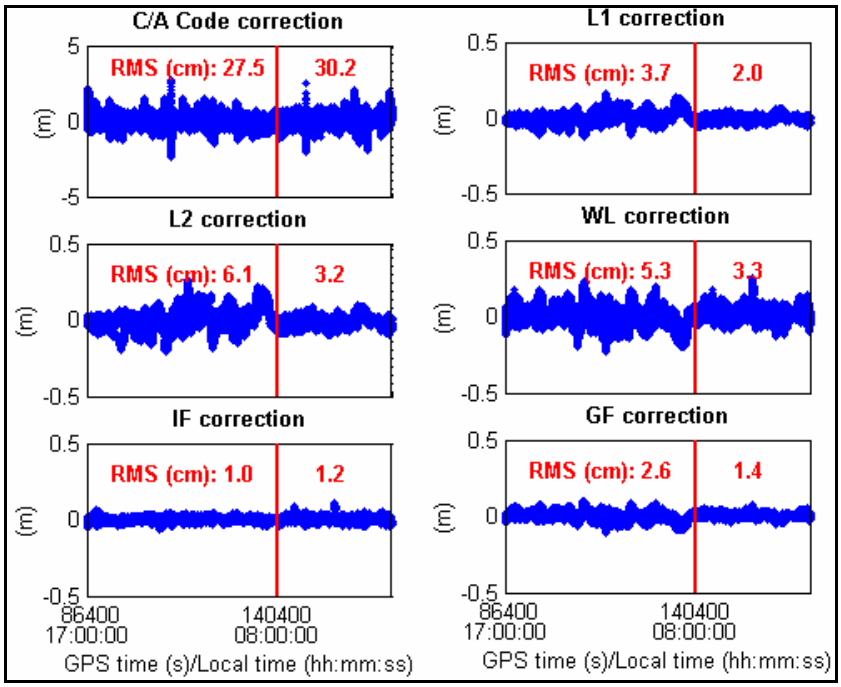

Figure 4.3: Double-difference network corrections generated by MRS LSQC for all satellite pairs - 24 May 2004 (quiet ionospheric conditions)

4.1.1.3 MRS Improvement in Observation Domain

Figure 4.4 shows the AIRD-UOFC double-difference misclosures for 24 May 2004. Both the AIRD and UOFC stations were fixed to their true coordinates for this analysis. The misclosures calculated using the raw uncorrected AIRD observations (SRS) are shown in red, while those using the corrected AIRD observations (MRS LSQC) are shown in blue. Statistics are provided in Table 4.3.

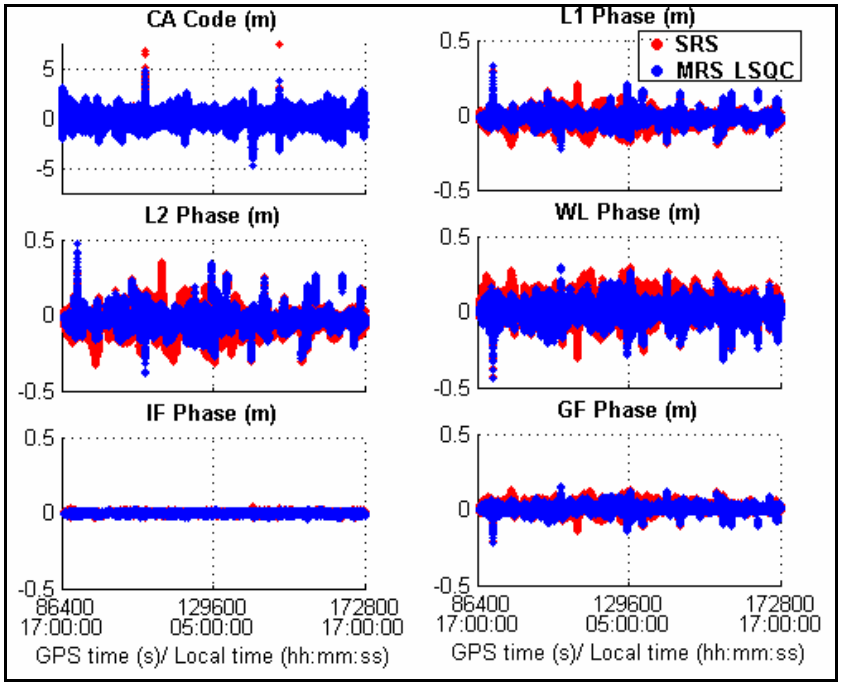

Figure 4.4: Double-difference observable misclosures for all satellite pairs using raw measurements (red) and MRS LSQC corrected measurements (blue) - 24 May 2004

Table 4.3: Statistics for double-difference observable misclosures for all satellite pairs - 24 May 2004

RMS (cm)	SRS	MRS	Improvement (%)
C/A Code	44.8	44.7	0
L1 Phase	3.5	2.4	31
L2 Phase	5.7	3.8	33
WL	4.5	2.9	36
IF	0.4	0.4	0
GF	2.2	1.4	36

The MRS approach yields approximately 30% to 35% improvement relative to the SRS approach with the use of L1, L2, WL and GF observables. However, no improvement is realized for IF observables, as anticipated; this is because the largest error source (ionospheric error) is eliminated in this case while the double-difference troposphere

residuals and satellite orbit errors are small over the 24 km distance. No corrections are applied herein for C/A code observations.

4.1.1.4 Long-term Position Domain Improvement with MRS

The single baseline AIRD-UOFC was processed to estimate epoch-by-epoch MRS LSQC and SRS UOFC position solutions using the corrected and uncorrected AIRD observations, respectively. The UOFC position errors and the ambiguity status using L1 observations for 24 May 2004 are shown in Figure 4.5, where SRS solutions are shown in red and MRS solutions in blue. Statistics are given in Table 4.4 for both the active and quiet ionospheric periods. The first two hours, which were used for network initialization and the following hour for single baseline filter convergence, were not included in the statistics.

The L1 position solutions are affected by the ionospheric errors for both MRS LSQC and SRS cases. Compared to the SRS approach, the MRS approach yields a significant 8 cm improvement (equivalent to 44 %) in the 3D RMS position accuracy during the active ionospheric period of this data set. During the second half of the data set, however, the improvement is not significant with magnitude of a few millimetres. The MRS LSQC achieves a 17% and 20% improvement in the east and height components, respectively, but none in 3D position accuracy. This shows that the MRS approach effectively reduces the differential ionospheric errors compared to the SRS approach under normal atmospheric conditions during the first half of the data set. Under quiet conditions, the

SRS approach performs as well as the MRS LSQC approach. The L1 ambiguities are resolved faster in the MRS LSQC case.

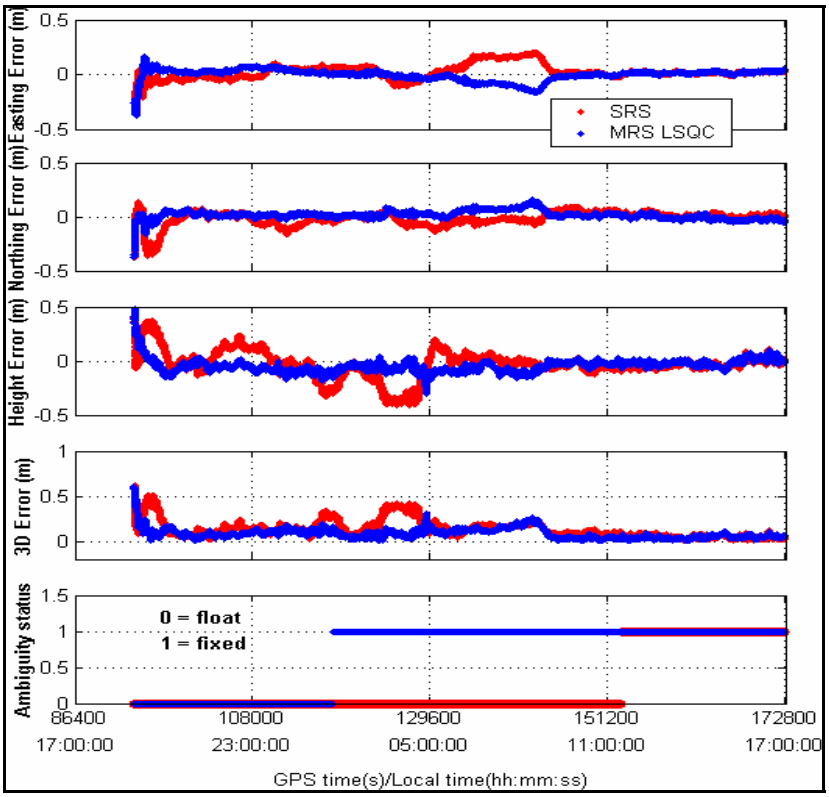

Figure 4.5: Position accuracy and ambiguity status in L1 mode after a two-hour network initialization period - 24 May 2004

Table 4.4: Statistics for position accuracy in L1 mode after a two-hour network initialization period - 24 May 2004

	First 12 hours, after 2 hours of network and 1 hour of single baseline filter convergence				Last 9 hours (Low ionospheric activities)			
	RMS (cm)				RMS (cm)			
	E	N	H	3D	E	N	H	3D
SRS	8	5	16	18	6	4	5	8
MRS LSQC	5	4	8	10	5	4	4	8
Improvement (%)	38	20	50	44	17	0	20	0

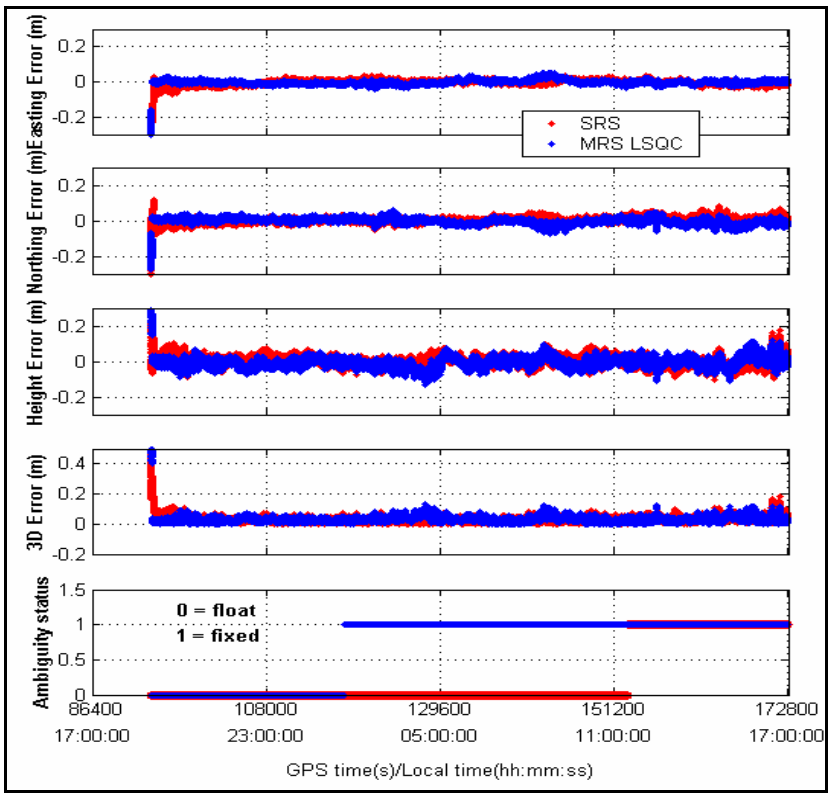

Figure 4.6: Position accuracy and ambiguity status in IF mode after a two-hour network initialization period - 24 May 2004

The ionospheric-free (IF) position solutions derived from L1 and L2 fixed ambiguities shown in Figure 4.6 are affected only by the tropospheric residuals, multipath and noise. The satellite orbital error is negligible over a baseline length of 24 km. The IF ambiguities are, therefore, resolved very well in this case for both approaches. The associated statistics are shown in Table 4.5. Both approaches offer a similar RMS 3D position accuracy of a few centimetres for both halves of the data set. This shows that, under quiet or normal atmospheric conditions, the MRS and SRS approaches yield more or less the same accuracy using IF observables, at least for this medium scale network. This is not surprising because there is no ionospheric impact while the tropospheric error residuals are small, as in this case.

Table 4.5: Statistics for position accuracy in IF mode after a two-hour network initialization period - 24 May 2004

	First 12 hours, after 2 hours of network and 1 hour of single baseline filter convergence				Last 9 hours (Low ionospheric activities)			
	RMS (cm)				RMS (cm)			
	E	N	H	3D	E	N	H	3D
SRS	1	1	2	3	1	2	3	4
MRS LSQC	1	1	3	3	1	2	3	4
Improvement (%)	No improvement				No improvement			

The performance of the MRS TC approach in comparison with the corresponding SRS and MRS LSQC approaches is shown in Figure 4.7. The statistics are provided in Table 4.6. In contrast to the above IF results, the results presented in this figure are produced by using L1 and L2 observations and modeling the ionospheric error stochastically, to produce herein the so-called L1/L2 position solutions. Depending on the effectiveness in modeling the ionospheric error, the L1/L2 solutions could be very similar to the IF solutions. For example, the MRS LSQC position solutions for both cases are the same in this case. However, the SRS IF position solutions are a few centimetres more accurate than the SRS L1/L2 position solutions, especially during the data set's active ionospheric period. During this period, for this particular data set, both MRS approaches offer an improvement of 5 cm in RMS 3D position accuracy, equivalent to 60% compared to the SRS approach. When the ionospheric error is small during the second half of the day, the three approaches provide very similar solutions. Although the MRS TC approach provides some improvement compared to the others, the magnitude is only 1 cm. The

ambiguities status shown in Figure 4.7 is for SRS approach (red) and MRS LSQC approach (blue). The percentages of ambiguities fixed associated with the MRS TC solutions are shown in Table 4.7. Using this approach, 88% of the ambiguities are fixed for the AIRD-UOFC baseline. This is further discussed in the next sub-section.

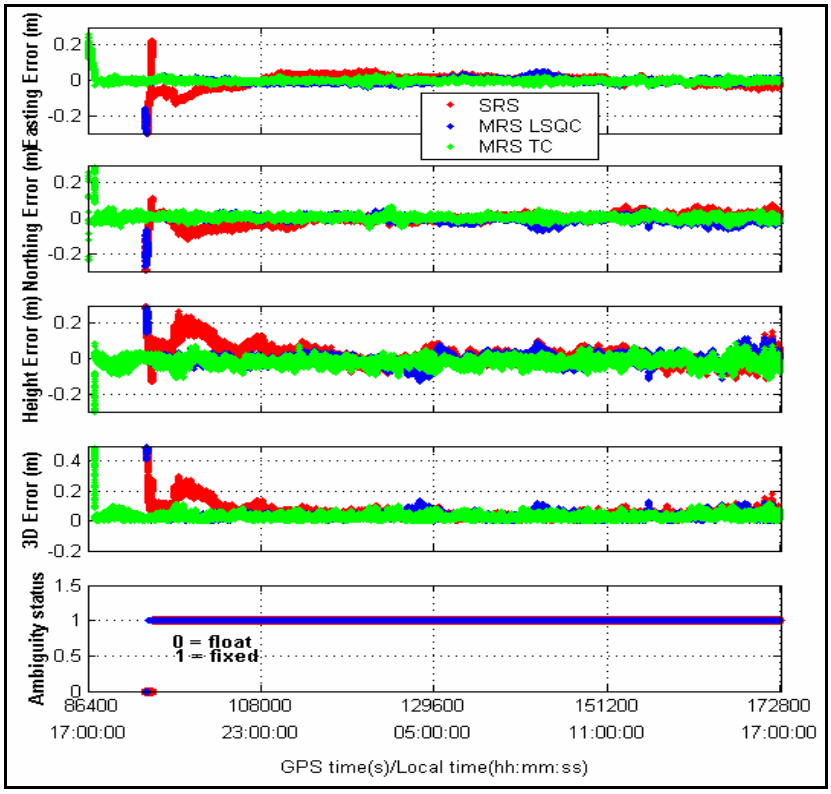

Figure 4.7: Position accuracy and ambiguity status in L1/L2 with stochastic ionosphere modeling mode after a two-hour network initialization period - 24 May 2004

Table 4.6: Statistics for position accuracy in L1/L2 mode after a two-hour network initialization period - 24 May 2004

	First 12 hours, after 2 hours of network and 1 hour of single baseline filter convergence				Last 9 hours (Low ionosphere activities)			
	RMS (cm)				RMS (cm)			
	E	N	H	3D	E	N	H	3D
SRS	3	3	7	8	2	2	3	4
MRS LSC	1	1	3	3	1	2	3	4
Improvement (%) relative to SRS	67	67	57	63	50	0	0	0
MRS TC	1	1	3	3	1	1	3	3
Improvement (%) relative to SRS	67	67	57	63	50	50	0	25

4.1.1.5 Network Ambiguity Performance

A comparison between the SRS and MRS approaches in ambiguity resolution domain is shown in Table 4.7. To produce a fair comparison, only the performances in L1/L2 mode are of interest as both MRS approaches use this technique to generate corrections and to estimate the rover position solutions. One common baseline between all three approaches is between the primary reference station and the rover (AIRD-UOFC). Both SRS and MRS LSQC approaches resolve the ambiguities very well, leading to levels of 99% and 100% fixed, respectively. This is because of the low ionospheric error that is associated with this data set. The MRS TC approach, however, results in a lower percentage of fixed ambiguities (88%). Although the MRS TC approach deals with shorter baselines, their percentages of ambiguities fixed are still lower in comparison to the MRS LSQC

approach. This is due to the comparatively longer time required for the MRS TC filter to estimate many more states, especially when the rover is integrated into every baseline. Also, the use of additional data results in more noise in this case, without any benefit of reducing atmospheric biases as these are near 0 in this case.

Table 4.7: Percentage of fixed ambiguities using SRS, MRS LSQC and MRS TC approaches for 24 May 2004 using L1/L2 mode

	AIRD COCH	AIRD STRA	COCH BLDM	COCH UOFC	STRA UOFC	BLDM UOFC	AIRD UOFC
Distance (km)	34	50	59	27	52	45	24
% of fixed							
SRS	n/a	n/a	n/a	n/a	n/a	n/a	99
MRS LSQC	94	89	87	n/a	n/a	n/a	100
MRS TC	n/a	n/a	n/a	95	64	76	88

4.1.1.6 MRS Improvement in Solution Convergence

The 24-hour data set was divided into 24 one-hour segments, which were processed independently with GrafNav™ using only L1 observations and IF observables for both SRS and MRS LSQC approaches. MultiRef™ was configured to generate network corrections from the beginning to the end of the 24-hour data set without being reset. A similar processing procedure for SRS and MRS LSQC approaches, albeit using L1/L2 mode, was implemented for comparison with the MRS TC approach. For the MRS TC approach, the filter is entirely reset at every hour.

The 3D UOFC position errors for the 24 segments on 24 May 2004 in L1 mode are presented in Figure 4.8. The float and fixed SRS solutions are in pink and red, respectively, while the float and fixed MRS LQSC solutions are in light blue and blue, respectively. For most of the segments, the MRS approach converges faster and provides a more accurate converging position solution accuracy. The improvement is noticeable during the period of high ionospheric activity (the first 15 segments). Under quiet ionospheric conditions, there is an inconsistency in the MRS improvement. For example, during the periods of 11:00-12:00 and 12:00-13:00 (Hours 19 and 20), the MRS approach performs worse than the SRS approach. However, the differences are not very significant with magnitude of approximately 10 centimetres. Moreover, the low level of ionospheric errors makes the ambiguities relatively easy to resolve when using the SRS approach.

Figure 4.9 shows the average position errors separately for the first 15 segments and the last 9 segments while the corresponding maximum position errors are shown in Figure 4.10. The associated statistics are shown in Table 4.8. During the active ionospheric activity of the data set, the MRS LSQC approach offers a significant improvement of 30% on average for the L1 position solution accuracy during convergence. Improvement is also observed in reducing the maximum converging position solution errors during this period of the day when the MRS LSQC approach is used. During the quiet ionospheric period, however, no improvement is offered by the MRS LSQC approach. This is due to the SRS performing very well with low ionospheric error. Apart from this, the MRS approach suffers a higher level of noise.

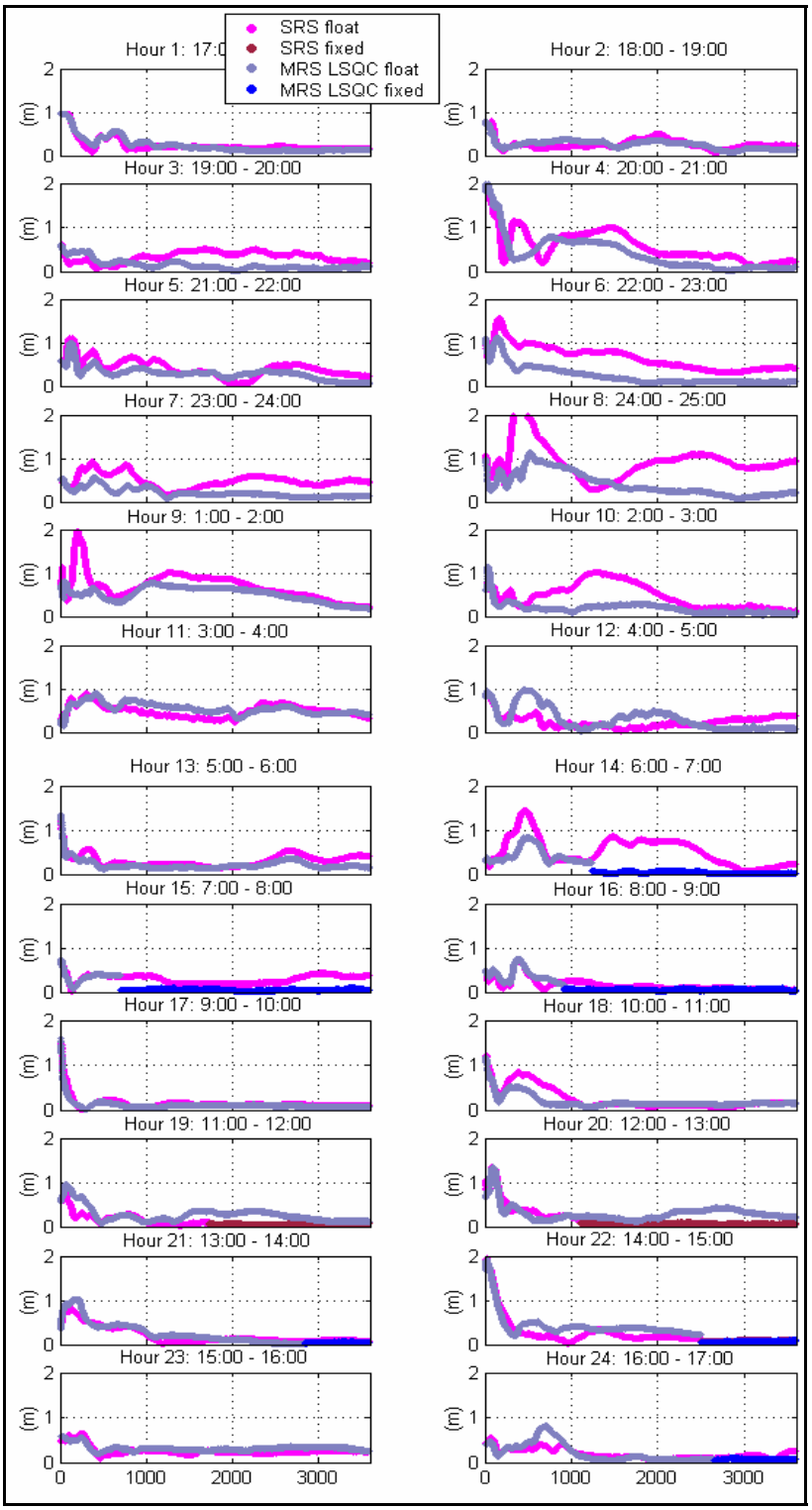

Figure 4.8: Converging 3D position accuracy and ambiguity status in L1 mode for 24 one-hour segments - 24 May 2004

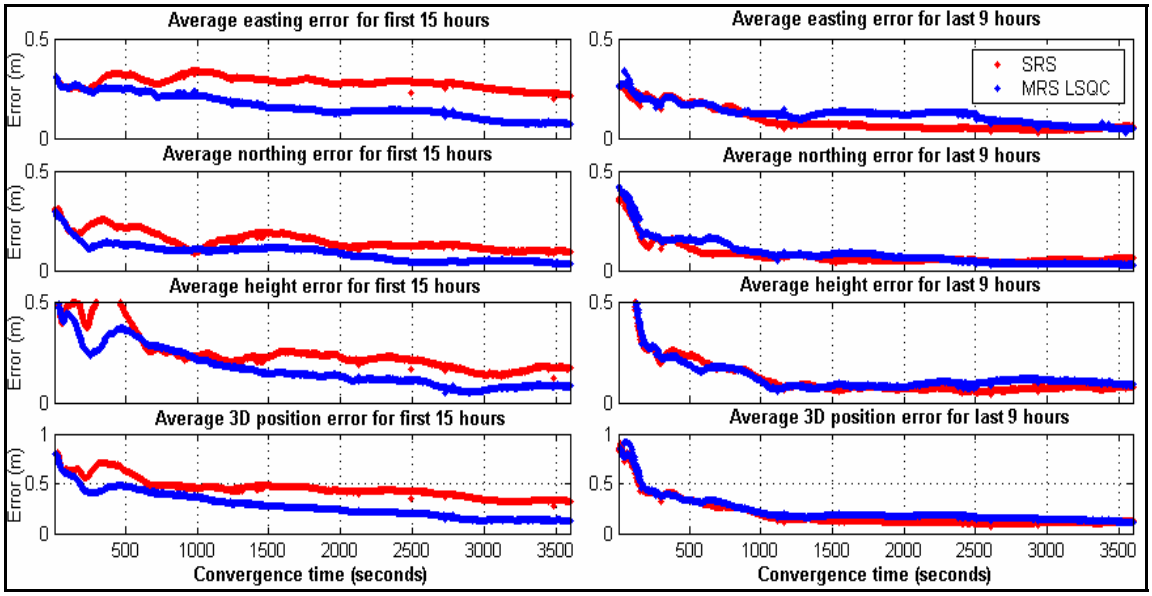

Figure 4.9: Average absolute converging 3D position accuracy in L1 mode for 24 May 2004, separately for the first 15 hours (left) and for the last 9 hours (right)

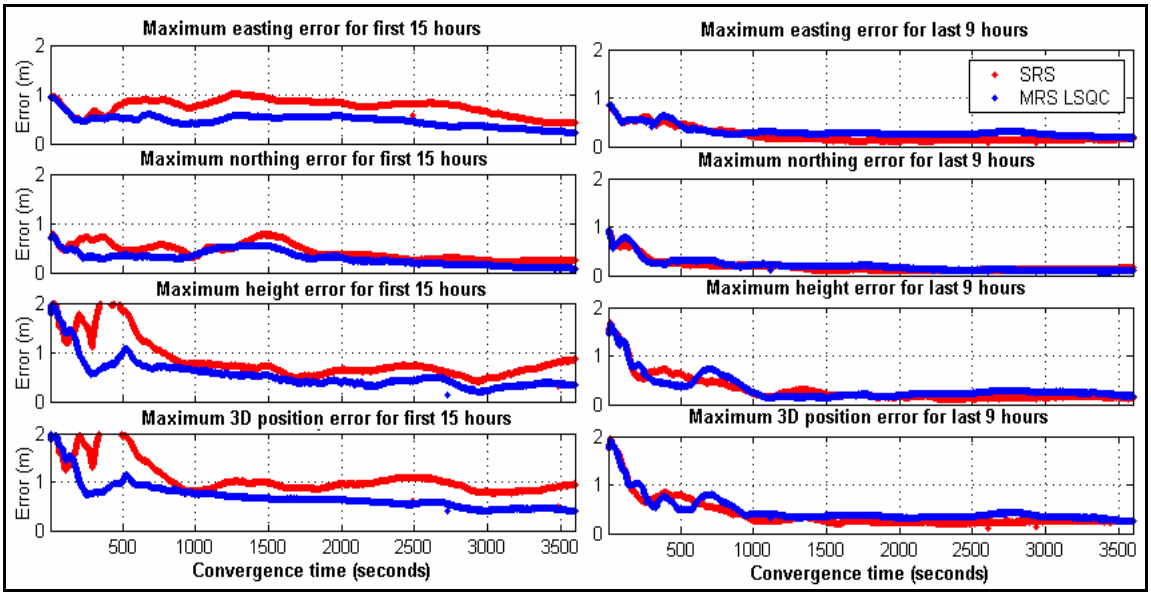

Figure 4.10: Maximum absolute converging 3D position error in L1 mode for 24 May 2004, separately for the first 15 hours (left) and for the last 9 hours (right)

Table 4.8: Statistics for the average and maximum converging 3D position error in L1 mode - 24 May 2004

	Average				Maximum			
	RMS (cm)				RMS (cm)			
	E	N	H	3D	E	N	H	3D
SRS first 15	28	16	27	47	77	236	406	704
MRS LSQC first 15	17	10	20	31	256	150	300	468
Improvement (%) first 15	39	38	26	34	-233	36	26	34
SRS last 9	11	10	17	24	27	86	149	218
MRS LSQC last 9	13	11	17	27	117	100	153	240
Improvement (%) last 9	No improvement				No improvement			

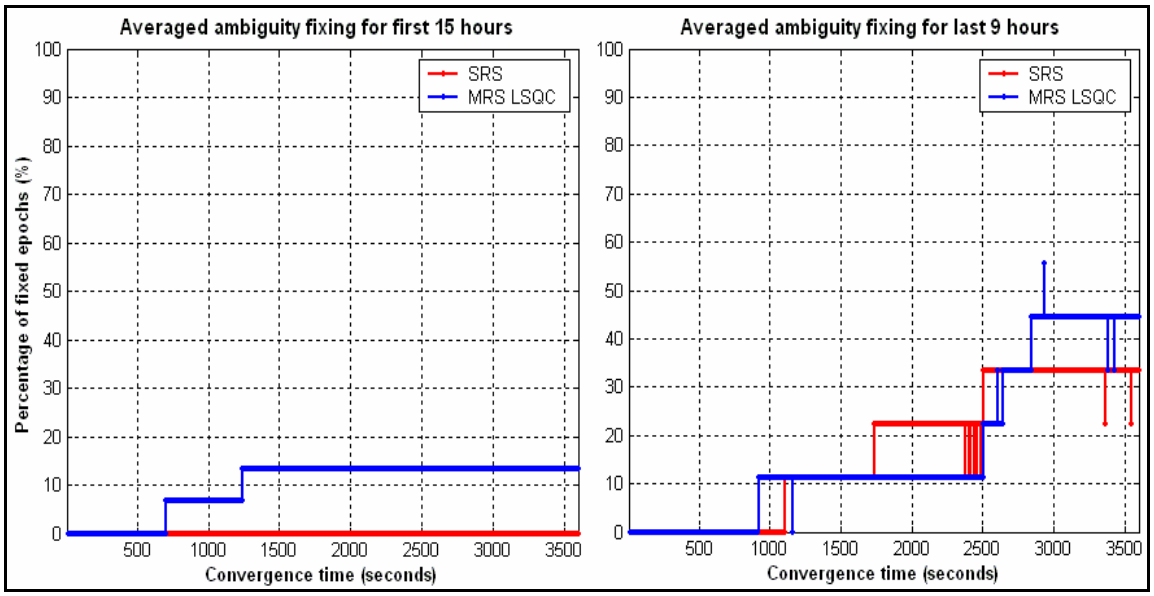

Figure 4.11: Average ambiguity status during convergence in L1 mode for 24 May 2004, separately for the first 15 hours (left) and for the last 9 hours (right)

The average percentage of ambiguity fixing for the first 15 segments and the last 9 segments are shown in Figure 4.11. Overall, the performance of both approaches in this domain is very poor due to the use of only L1 observations, resulting in a full impact of

the ionospheric error. However, a slight improvement is offered by the MRS LSQC approach during both periods of the data set.

The short-term converging solutions using IF observables of this data set for both SRS and MRS LSQC approaches are shown in Figure 4.12. The same colour assignment as previously presented for L1 converging solutions is used herein. Achievement of convergence using IF observables is generally faster, and more accurate position solutions are obtained because the ionospheric error is eliminated in comparison with using L1 observations alone. For most of the segments, the MRS LSQ approach yields more accurate 3D position solutions and also faster First Time To Fix (FTTF) values in resolving the ambiguities. During segment 12, some of the ambiguities are fixed to wrong values, producing biased solutions when using the SRS approach. The average 3D position errors and the maximum 3D position errors are shown (separately for the first 15 segments and the last 9 segments) in Figures 4.13 and Figure 4.14, respectively, with the associated statistics shown in Table 4.9. The MRS LSQC approach yields an improvement of 20% and 10% in the position solution accuracy on average for the first 15-hour period and the last 9-hour period, respectively. Use of the MRS LSQC approach also produces a reduction in the maximum errors.

Figure 4.15 shows the average percentage of IF ambiguities fixed during convergence time for the two periods of the day. A lower average percentage of ambiguities fixed is observed using the SRS approach throughout the entire data set.

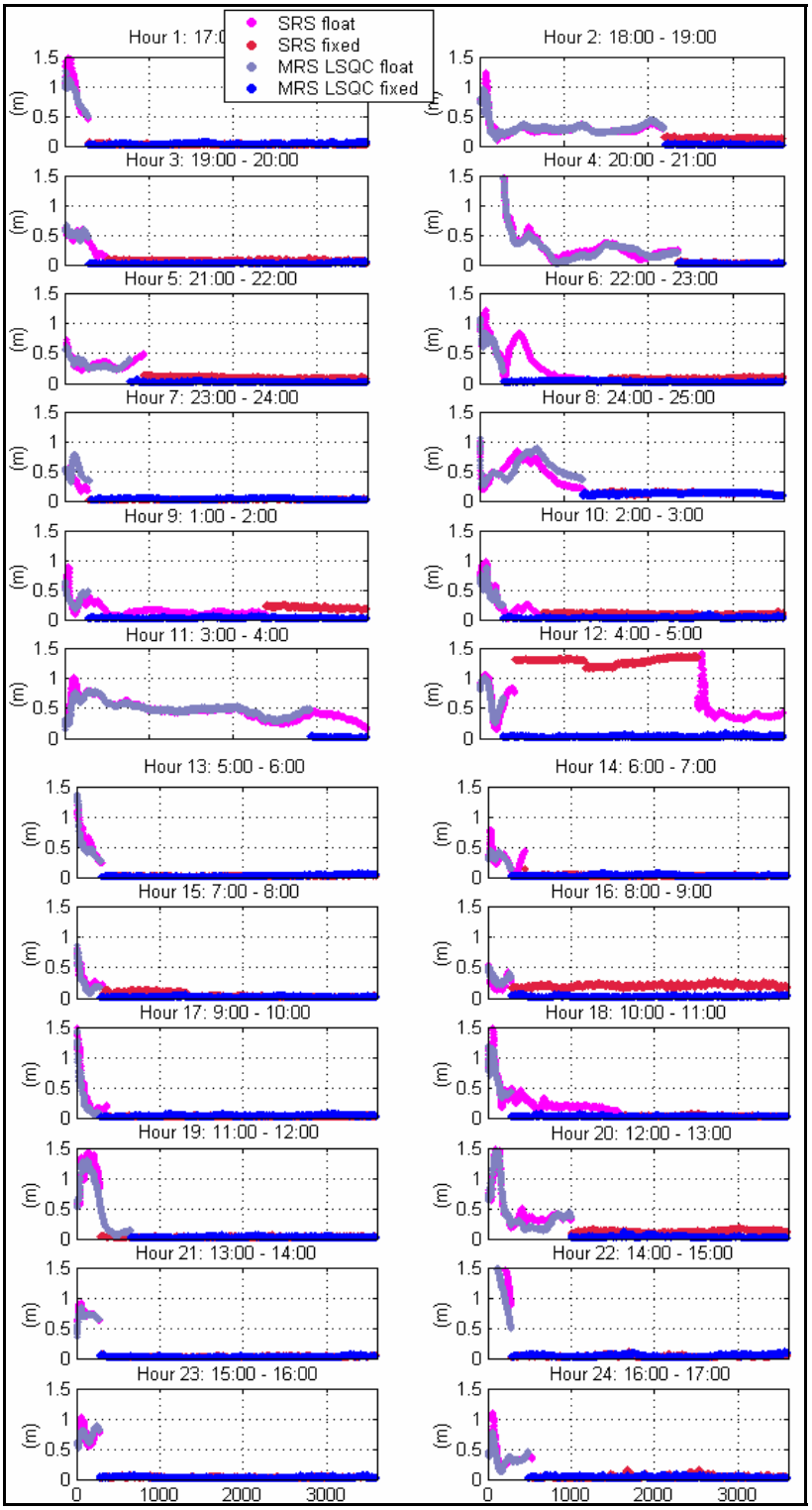

Figure 4.12: Converging 3D position accuracy and ambiguity status in IF mode for 24 one-hour segments - 24 May 2004

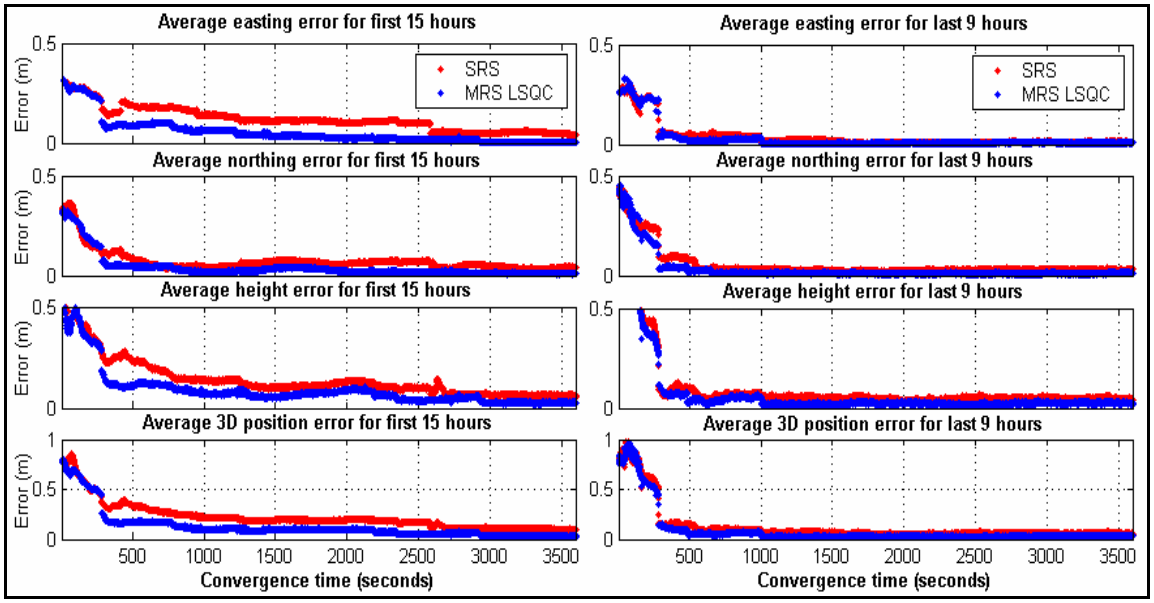

Figure 4.13: Average absolute converging 3D position accuracy in IF mode for 24 May 2004, separately for the first 15 hours (left) and for the last 9 hours (right)

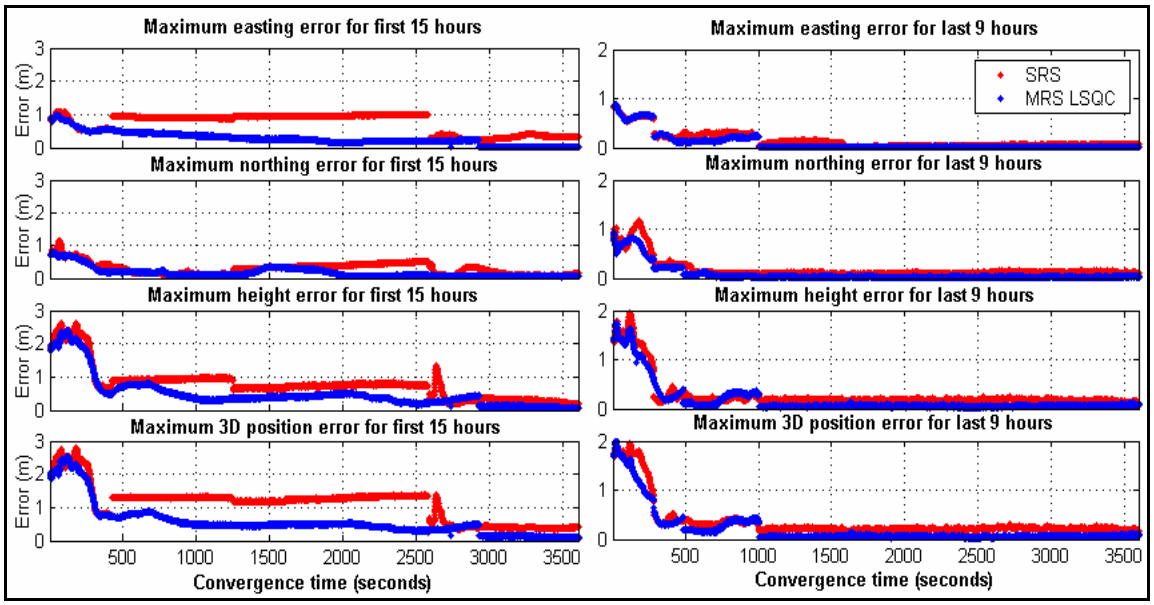

Figure 4.14: Maximum absolute converging 3D position error in IF mode for 24 May 2004, separately for the first 15 hours (left) and for the last 9 hours (right)

Table 4.9: Statistics for the average and maximum converging 3D position error in IF mode - 24 May 2004

	Average				Maximum			
	RMS (cm)				RMS (cm)			
	E	N	H	3D	E	N	H	3D
SRS first 15	13	9	17	26	79	136	264	396
MRS LSQC first 15	9	7	13	20	130	109	195	293
Improvement (%) first 15	31	22	28	23	-63	20	26	26
SRS last 9	7	9	17	23	23	82	151	203
MRS LSQC last 9	7	8	15	20	63	70	134	182
Improvement (%) last 9	0	11	12	9	-174	15	11	10

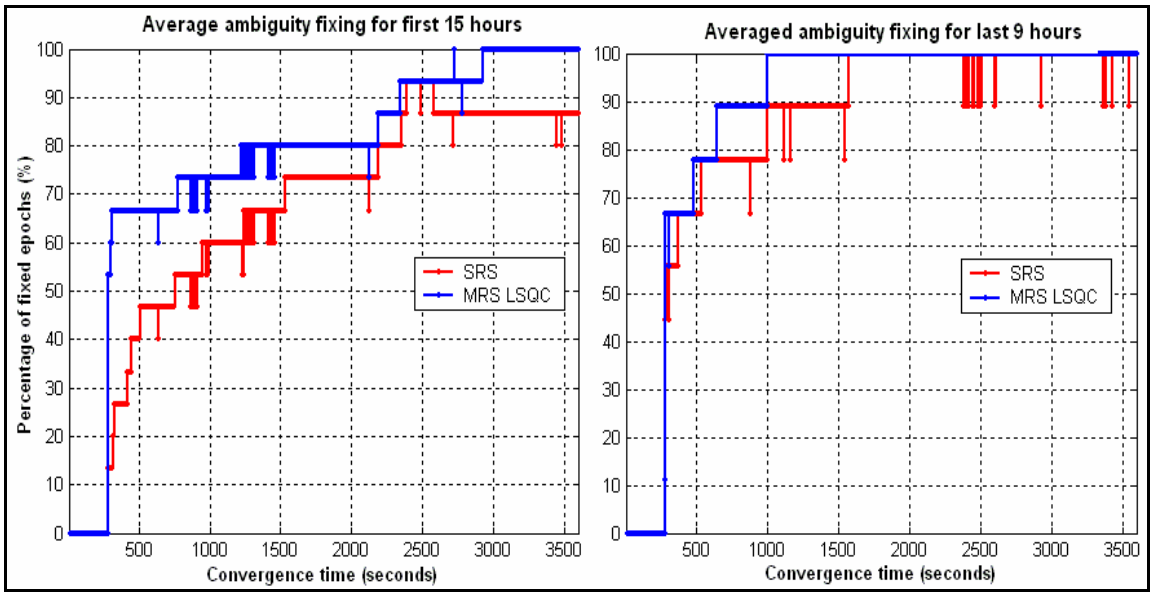

Figure 4.15: Average ambiguity status during convergence in IF mode for 24 May 2004, separately for the first 15 hours (left) and for the last 9 hours (right)

The converging 3D position accuracy using L1 and L2 observations with the SRS approach and the two MSR approaches are shown in Figure 4.16. The pink and red colors

are used to present the SRS float and fixed solutions, respectively. The light blue and blue colors represent MRS LSQC solutions, while the green and dark green colors symbolize MRS TC solutions. It is observed that the MRS approaches perform better during various segments, as compared to the SRS approach. For the fist 12 segments, there are some inconsistent results obtained using the MRS TC approach (e.g. in segments 2 and 4). Some of the ambiguities were resolved to wrong values, leading to long-term biased solutions. The same phenomenon is also observed for SRS solutions (e.g. in segments 5 and 12). The average 3D position errors and the maximum position errors for the first 15 hours are shown on the left sides of Figure 4.17 and Figure 4.18, respectively. Both MRS approaches offer an improvement of approximately 30% over the SRS approach, as shown in Table 4.10. Due to the dominance of the bias results obtained in the afore-mentioned segments, the MRS TC offers less improvement than the MRS LSQC approach by a few centimetres in RMS 3D position solution accuracy. However, when excluding these segments (e.g. segments 4, 5 and 12), the MRS TC approach offers significant improvement in converging solutions as compared to the MRS LSQC approach during the first 15 hours of the data set. This is demonstrated in Figure 4.19 and the related statistics are given in Table 4.11. The MRS LSQC technique, in this case, yields 3 cm, which is equivalent to a 15% improvement, more accurate than the SRS technique. By comparison, the MRS TC solutions result in a value of 6 cm, which is equivalent to a 30% improvement.

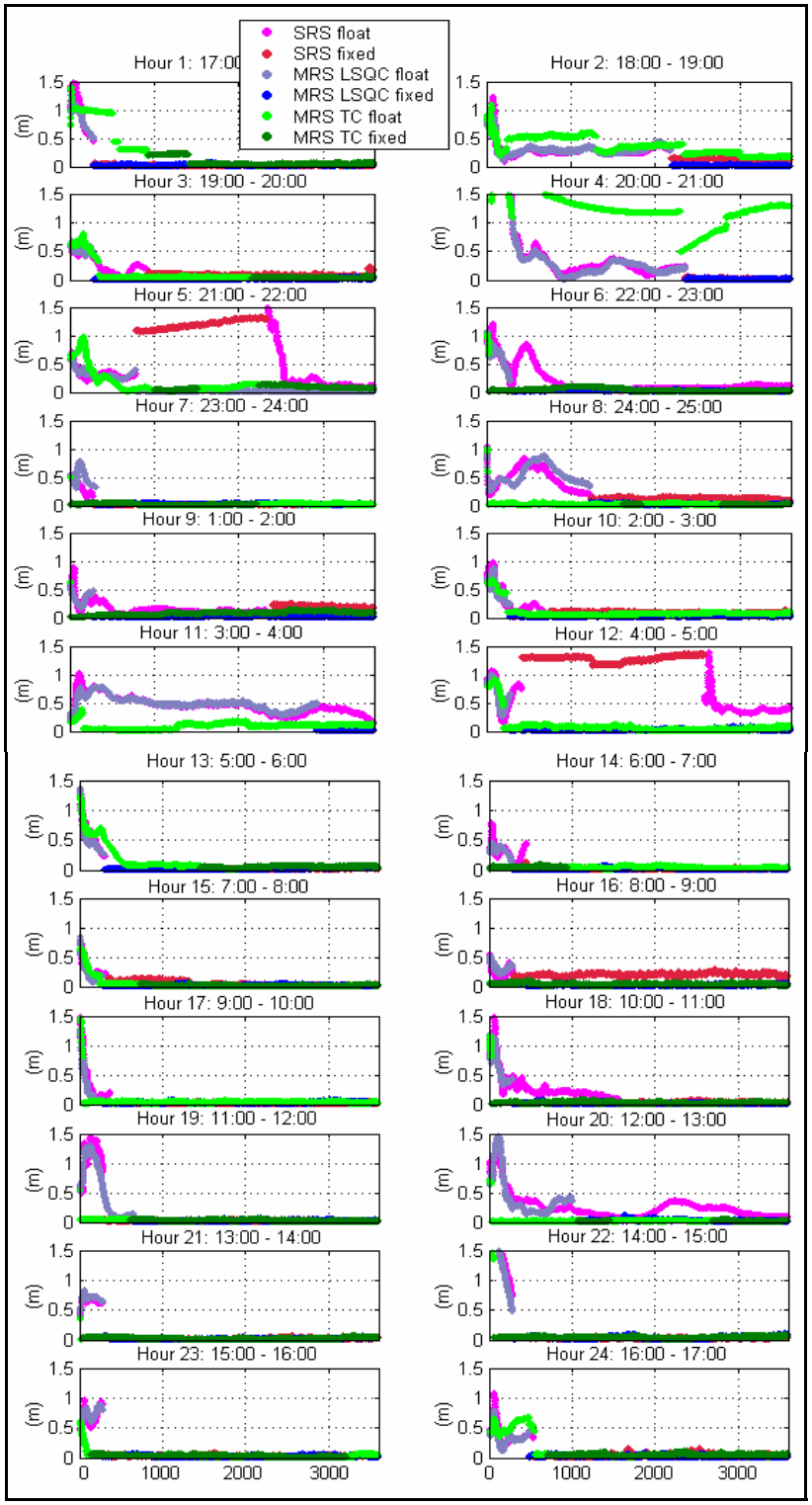

Figure 4.16: Converging 3D position accuracy and ambiguity status in L1/L2 with ionospheric modeling mode for 24 one hour segments - 24 May 2004

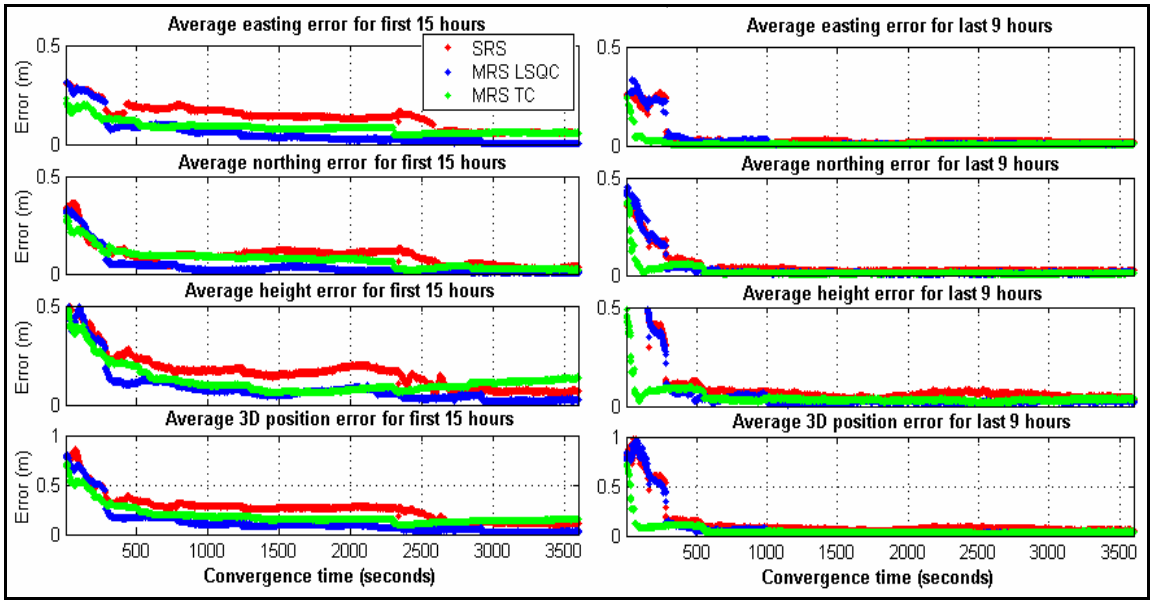

Figure 4.17: Average absolute converging 3D position accuracy in L1 and L2 with ionospheric modeling mode for 24 May 2004, separately for the first 15 hours (left) and for the last 9 hours (right)

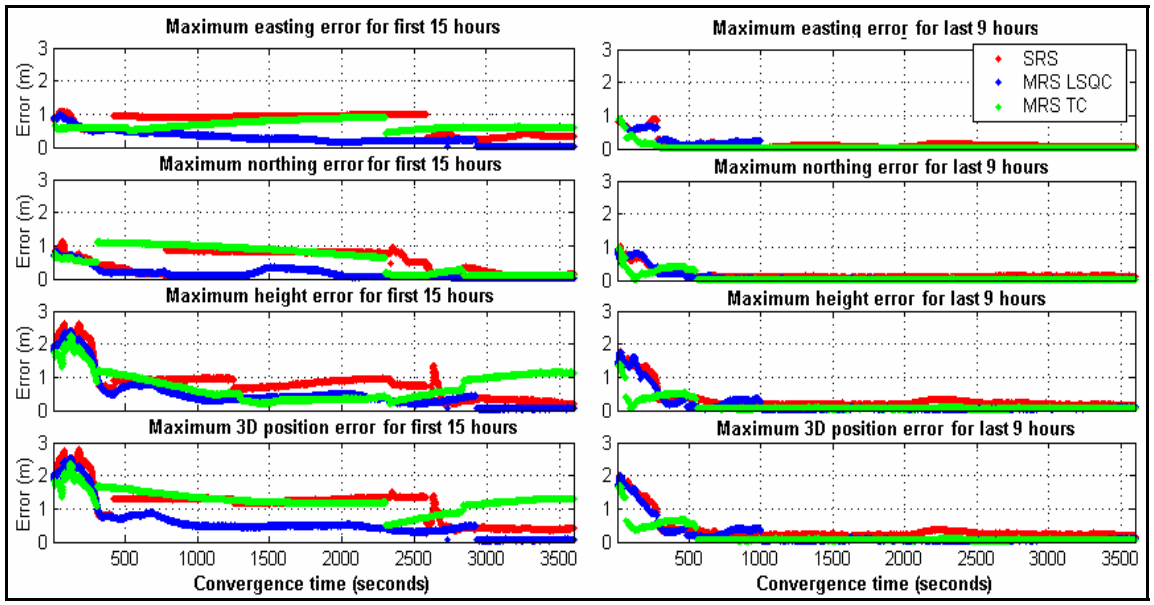

Figure 4.18: Maximum absolute converging 3D position error in L1/L2 with ionospheric modeling mode for 24 May 2004, separately for the first 15 hours (left) and for the last 9 hours (right)

Table 4.10: Statistics for the average and maximum converging 3D position error in L1/L2 with ionospheric modeling mode - 24 May 2004

	Average				Maximum			
	RMS (cm)				RMS (cm)			
	E	N	H	3D	E	N	H	3D
SRS first 15	15	11	20	29	79	162	292	441
MRS LSQC first 15	9	7	13	19	130	108	193	291
LSQC Improvement (%) first 15	40	36	32	35	-65	33	34	34
MRS TC first 15	9	9	15	21	135	130	220	318
TC Improvement (%) first 15	40	18	21	28	-71	20	25	28
SRS last 9	7	8	17	22	22	70	149	197
MRS LSQC last 9	7	8	15	20	63	70	134	182
LSQC Improvement (%) last 9	0	0	12	9	-186	0	10	8
MRS TC last 9	3	4	6	8	22	37	54	76
TC Improvement (%) last 9	57	50	65	64	0	48	64	61

During the last 9 hours of the data set, which is associated with a ‘quiet’ level of ionospheric activity, both MRS approaches offer an improvement over the SRS approach. There is a gain of 2 cm, equivalent to 9%, on average 3D position solution accuracy produced with the use of MRS LSQC techniques. The 14 cm improvement offered by the MRS TC approach is very significant, equivalent to 64% over the SRS approach during this period.

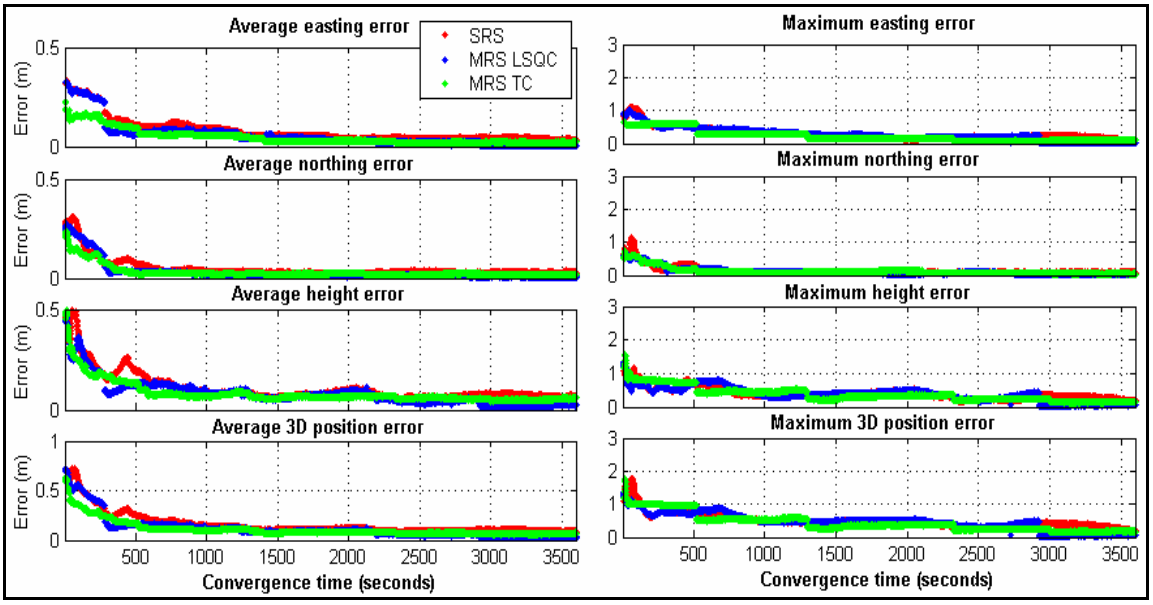

Figure 4.19: Average absolute converging 3D position accuracy in L1 and L2 with ionospheric modeling mode for the first 15 segments, excluding segments 4, 5 and 12, - 24 May 2004

Table 4.11: Statistics for the average and maximum converging 3D position error in L1/L2 with ionospheric modeling mode for the first 15 segments, excluding segments 4, 5 and 12 - 24 May 2004

	Average				Maximum			
	RMS (cm)				RMS (cm)			
	E	N	H	3D	E	N	H	3D
SRS for first 15 hrs.	10	7	13	20	36	80	158	237
MRS LSQC for first 15	9	6	11	17	104	69	126	198
Improvement (%) for first 15	10	14	15	15	-189	14	20	17
MRS TC for first 15	6	5	10	14	74	54	120	165
Improvement (%) for first 15	40	43	23	30	-106	33	24	30

The average percentage of ambiguities fixed in L1/L2 mode for the segments is presented in Figure 4.20. Overall, the MRS LSQC has the highest number of fixed ambiguities, followed by the SRS and the MRS TC approaches. This relationship has been previously explained in reference to the tightly-coupled approach's requirement for more time to fix the ambiguities due to a large number of unknown states. The MRS TC ambiguities presented in this comparison apply to the equivalent primary reference station-rover baseline only.

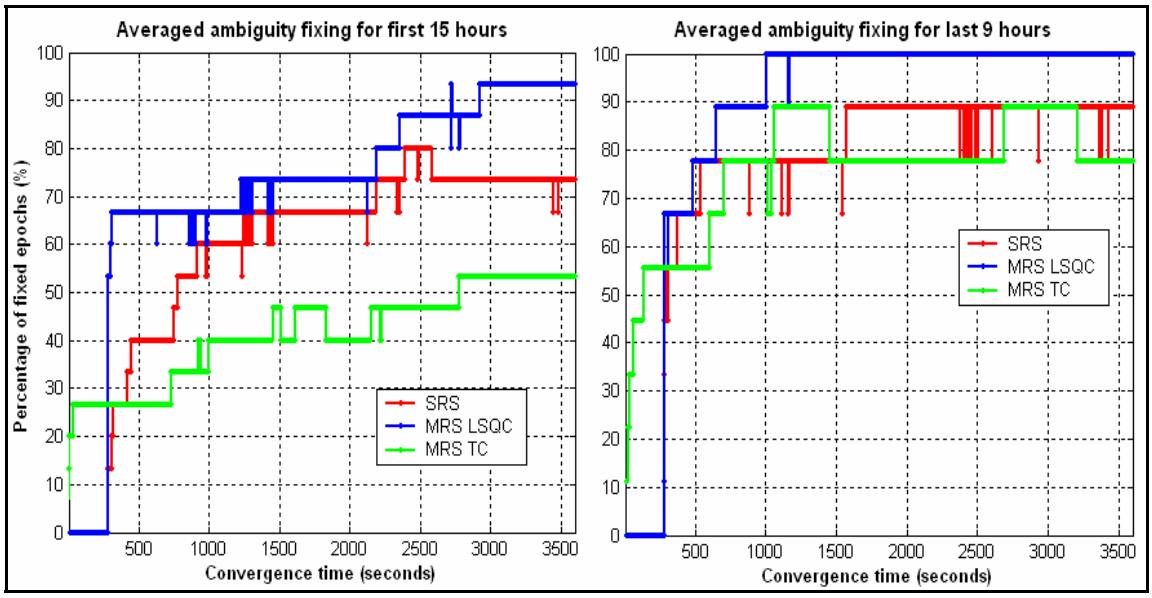

Figure 4.20: Average ambiguity status during convergence in L1/L2 with ionospheric modeling mode for 24 May 2004, separately for the first 15 hours (left) and for the last 9 hours (right)

4.1.2 Medium Ionospheric Condition Results

A second data set associated with a slightly more active ionosphere, on 6 April 2004, is chosen to evaluate the MRS approaches referred to above. Details of the local index K and the tropospheric error parameters for this data set were presented previously at the beginning of this chapter, in Tables 4.1 and 4.2.

4.1.2.1 Network Configuration

The same network configurations used for the previous data set (24 May 2004) are used for this data set. They are presented in Figure 4.1 and Figure 4.2 for the least-squares collocation and the tightly-coupled approaches, respectively. To recall, the UOFC station is the rover and the AIRD station, located 24 km away from UOFC, is the primary reference station. The network baseline lengths for the MRS LSQC approach range from 34 km to 59 km, while those for the MRS TC approach range from 24 km to 52 km. Using the tightly-coupled approach, the UOFC station is the rover and is connected to the other four reference stations to form baselines with lengths ranging from 24 km to 52 km.

4.1.2.2 Network Double Difference Corrections

Figure 4.21 shows the network double-difference corrections generated for this data set by the MRS LSQC approach. They are generally larger than the ones obtained for 24 May 2004, especially during the first 15 hours – the usual active ionosphere period of the

day. During the first 15 hours of the day, the estimated RMS double-difference correction on L1 observations is 5.7 cm. This is equivalent to 2.4 ppm over the 24 km baseline. The errors on L2 and WL are higher than on L1, with values of 9.4 cm (3.9 ppm) and 7.7 cm (3.2 ppm), respectively. The GF corrections are 3.9 cm (1.6 ppm) and are mainly caused by the ionospheric error. This is considered a medium ionospheric condition. During the last 9 hours of the day (quiet ionosphere), the corrections are smaller than those obtained during night-time. The correction variation correlates very well with the variation in the local K indices. The IF corrections, with a magnitude of approximately 1.1 cm for the entire day, constitute a measure of the relative consistency of tropospheric residuals over the region.

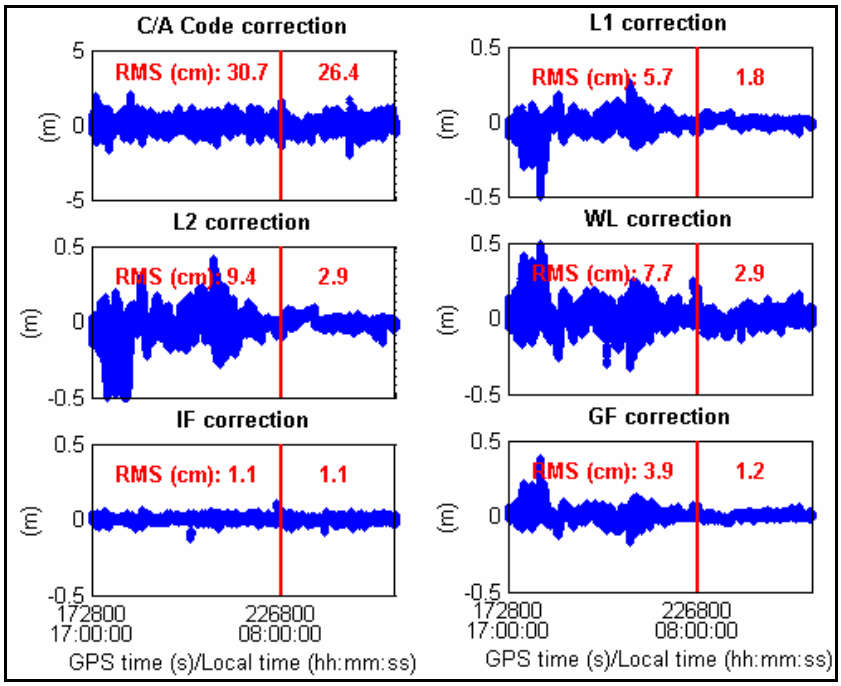

Figure 4.21: Double difference network corrections generated by MRS LSQC for all satellite pairs - 6 April 2004 (medium ionospheric conditions)

The MRS LSQC approach, in this case, also performs very well in resolving ambiguities, as compared to the previous data set, although the ionospheric activity was slightly greater. The actual percentages of ambiguities fixed are 94 %, 91 % and 87% for AIRD-COCH (34 km), AIRD-STRA (50 km) and COCH-BLDM (59 km), respectively. This suggests that the stochastic ionospheric model used in the MRS LSQC approach was effective in estimating the double difference slant ionospheric error under the prevailing conditions. Again, the network corrections can be considered reliable based on such a high percentage of fixed ambiguities.

4.1.2.3 MRS Improvement in Observation Domain

The double-difference misclosures in the measurement domain for this data set are presented in Figure 4.22 for all satellite pairs between the primary reference station AIRD and the rover UOFC. The misclosures obtained in this case are generally larger than those of 24 May 2004 due to a higher ionospheric error. The associated statistics are provided in Table 4.12. Similarly to the previous data set, the MRS approach yields smaller misclosures on L1, L2, WL and GF observables as compared to the SRS approach. A higher level of improvement is observed. In this case, the MRS approach reduces the RMS misclosures by 45%, instead of 35% as in the previous data set of 24 May 2004. This reflects that the MRS LSQC technique is relatively effective under the medium ionospheric condition. The MRS LSQC approach again does not yield any improvement for IF observables, and this is well expected as explained in the previous section by the

elimination of the ionospheric error and the existence of very small tropospheric residuals.

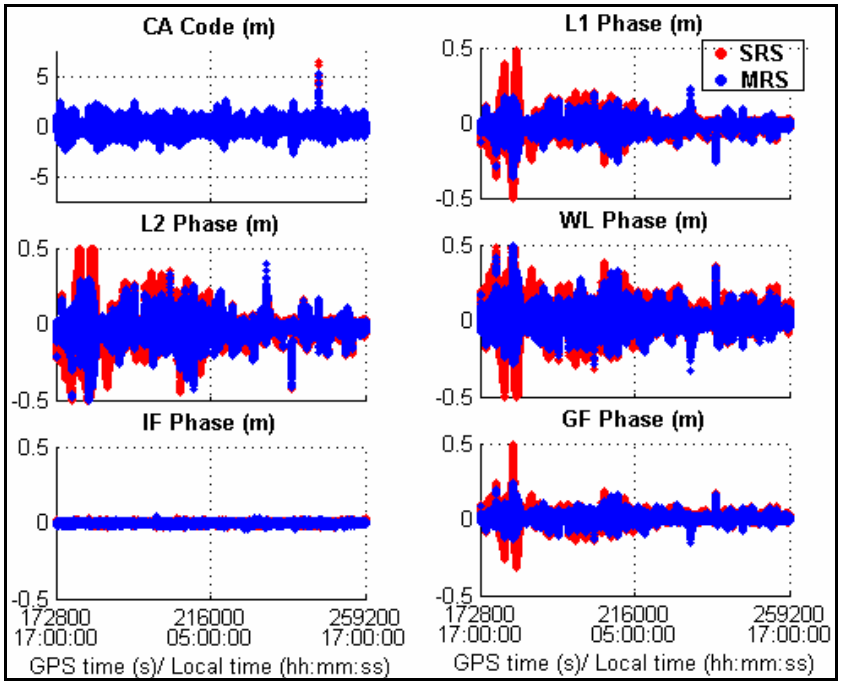

Figure 4.22: Double-difference observable misclosures for all satellite pairs using raw measurements (red) and using MRS LSQC corrected measurements (blue) - 6 April 2004

Table 4.12: Stastics for double-difference observable misclosures for all satellite pairs - 6 April 2004

RMS (cm)	SRS	MRS	Improvement (%)
C/A Code	43.4	43.3	0
L1 Phase	4.2	2.5	40
L2 Phase	6.9	3.8	45
WL	5.5	3.0	45
IF	0.3	0.4	0
GF	2.7	1.5	44

4.1.2.4 Long-term Position Domain Improvement with MRS

This data set was also used for analysis to evaluate the performance of the MRS and SRS approaches in the long-term position solution domain. The very first two hours of the data set are used for network initialization; the rover position solutions are not estimated during this time to ensure validity in the application of corrections. The UOFC 3D position errors and the associated ambiguity status in L1 mode are shown in Figure 4.23. Statistics are provided in Table 4.13 for the first 12 hours of the day, during which the ionosphere was active; and for the last nine hours of the day, during which the ionosphere was quiet. The converging solutions estimated during the first hour are not included in the calculation of these statistics because the focus of this analysis is only on long-term position solutions. The medium scale ionospheric error degrades the SRS L1 3D position solution accuracy to 49 cm and the MRS LSQC L1 3D position solution accuracy to 14 cm. An improvement of 70% results from the use of the MRS approach. However, by having a limited RMS MRS position accuracy of 14 cm, it shows that, during a period of relatively medium level ionospheric activity, the spatial decorrelation of the ionospheric effect is relatively rapid; consequently, the use of a medium scale multiple reference network can improve the SRS method only by a certain amount. The ambiguities during this period cannot be resolved for either case and the position solutions are estimated using the float ambiguities. During the last 9 hours of the day (quiet ionospheric conditions), very accurate position solutions of better than 6 cm are obtained with both SRS and MRS approaches. Although it does not produce any improvement in the position domain during this period, the MRS LSQC offers a faster FFTF in the ambiguity domain.

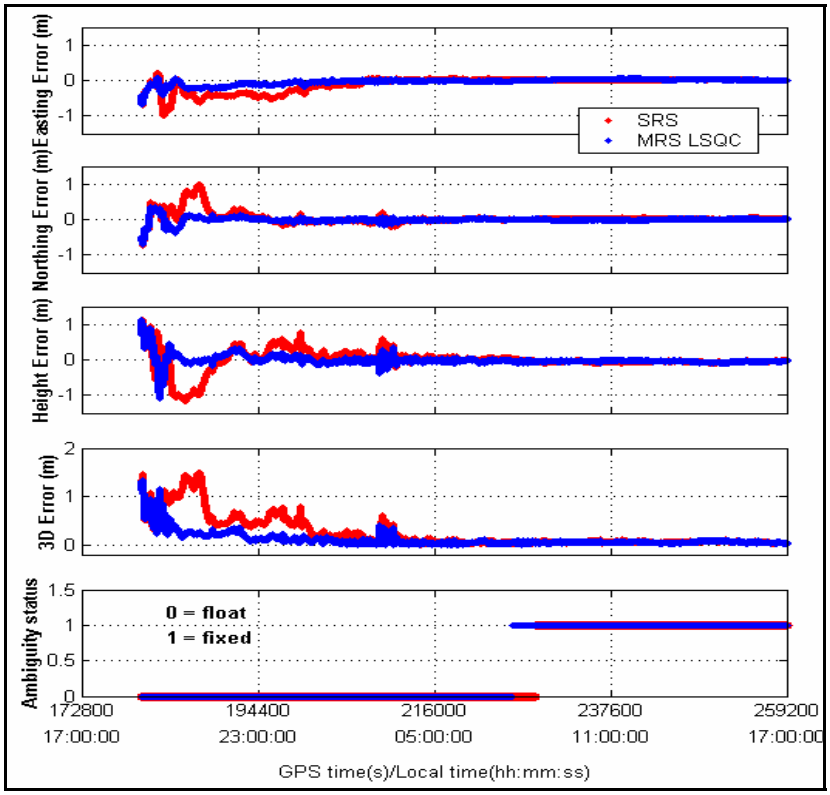

Figure 4.23: Position accuracy and ambiguity status in L1 mode after a two-hour network initialization period - 6 April 2004

Table 4.13: Statistics for position accuracy in L1 mode after a two-hour network initialization period - 6 April 2004

	High ionospheric period – first 12 hours, after 3 hours of network and filter convergence				Low ionospheric period – last 9 hours			
	RMS (cm)				RMS (cm)			
	E	N	H	3D	E	N	H	3D
SRS	26	22	35	49	2	3	5	6
MRS LSQC	9	6	9	14	3	2	5	6
Improvement (%)	65	73	74	71	Not significant			

Figure 4.24 shows the UOFC position errors when using the IF observables of this data set. The ionospheric error is eliminated in this case, resulting in a noticeable improvement in position solution accuracy as compared to the L1 solutions. The associated statistics are given in Table 4.14 for the first 12 hours and the last 9 hours of the day. During the active ionospheric period, the SRS approach yields a 3D position accuracy of 14 cm while that obtained for the MRS LSQC solutions is 4 cm, excluding the converging solutions. This is equivalent to a 70% improvement. Around 23:00, the SRS approach suffers a large degradation in the position accuracy although the ambiguities are reported as fixed. This is because the ambiguities are incorrectly fixed. This problem is occasionally observed in the GrafNav results presented herein. Apart from using a ratio threshold validation as discussed, no further ambiguities checks or indications for whether they are fixed to correct values are provided with the software. This could be done based on the theory that the residuals of estimated positions should be zero-mean. The GrafNav software uses forward and backward ambiguity combination to eliminate incorrectly fixed ambiguities. However, this is not beneficial for the work herein due to the use of only one direction (forward) processing. During the quiet ionospheric period, both approaches produce very accurate position solutions. The MRS LSQC performs slightly worse but only by approximately 1 cm. Both approaches perform very well in resolving the ambiguities; however, the MRS LSQC approach is still slightly superior to the SRS approach with respect to the FTTF.

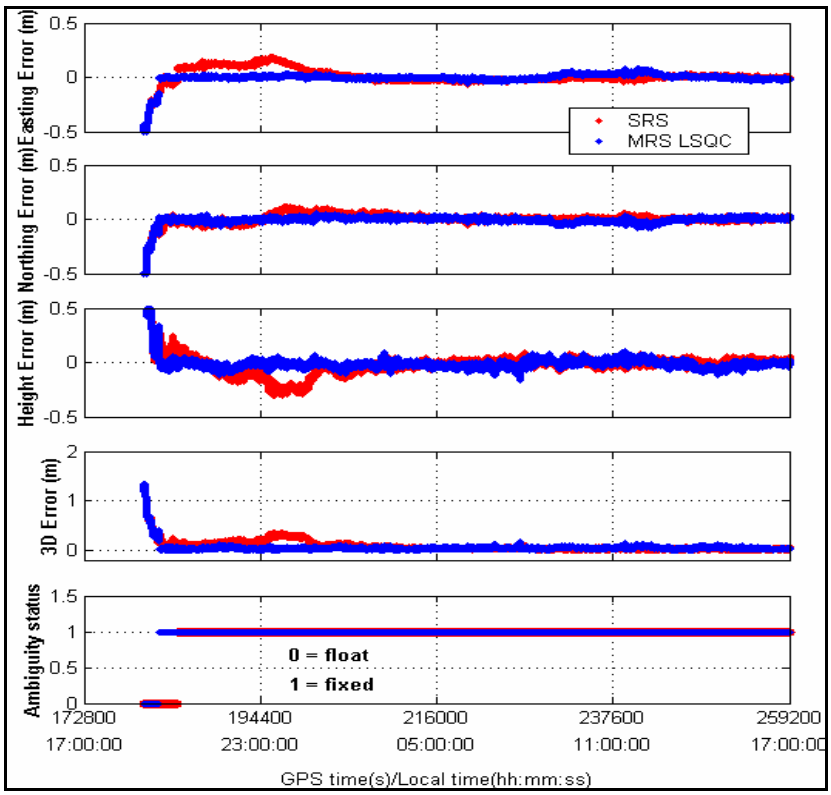

Figure 4.24: Position accuracy and ambiguity status in IF mode after a two-hour network initialization period - 6 April 2004

Table 4.14: Statistics for position accuracy in IF mode after a two-hour network initialization period - 6 April 2004

	High ionosphere period –first 12 hours, after 3 hours of network and filter convergence				Low ionospheric period – last 9 hours			
	RMS (cm)				RMS (cm)			
	E	N	H	3D	E	N	H	3D
SRS	8	4	11	14	1	1	2	3
MRS LSQC	1	1	3	4	3	2	3	5
Improvement (%)	88	75	73	71	Not significant			

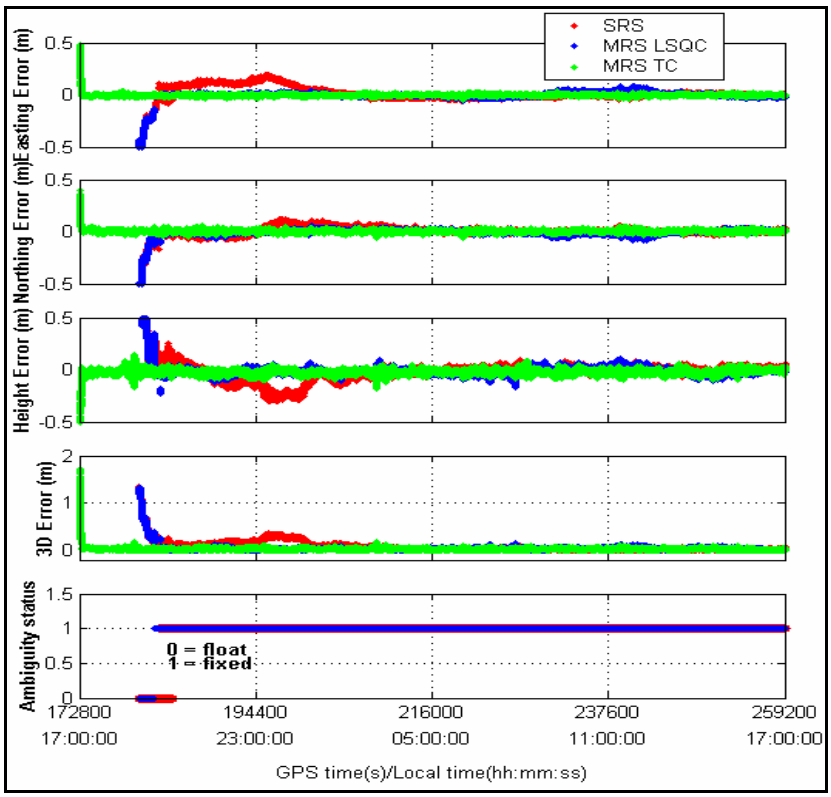

Figure 4.25: Position accuracy and ambiguity status in L1/L2 with stochastic ionosphere modeling after a two-hour network initialization period - 6 April 2004

The MRS TC solutions generated by using L1 and L2 observations along with modeling the ionospheric error are presented in Figure 4.25. The equivalent SRS and MRS LSQC solutions are also estimated for comparison. Statistics are presented in Table 4.15. The L1/L2 position solutions are very similar to the IF solutions using both SRS and MRS LSQC techniques. The MRS TC approach offers some additional improvement to the SRS solutions as compared to the MRS LSQC approach but only by 1 cm in this case. During the quiet hours, the MRS TC also performs better than the MRS LSQC but offers no improvement compared to the SRS.

Table 4.15: Statistics for position accuracy in L1/L2 with stochastic ionosphere modeling after a two-hour network initialization period - 6 April 2004

	High Ionosphere Period – first 12 hours, after 3 hours of network and filter convergence				Low Ionosphere Period – last 9 hours			
	RMS (cm)				RMS (cm)			
	E	N	H	3D	E	N	H	3D
SRS	8	4	10	14	1	1	2	3
MRS LSC	1	1	3	4	3	2	3	5
Improvement (%) relative to SRS	88	75	70	71	Negative improvement			
MRS TC	1	1	3	3	1	1	3	3
Improvement (%) relative to SRS	88	75	70	79	No improvement			

4.1.2.5 Network Ambiguity Performance

The performances in the ambiguity resolution domain of the three approaches in L1/L2 mode are presented in Table 4.16. Among these three, the MRS LSQC approach performs the best, with 98% of ambiguities fixed. The SRS approach offers a level of 92% ambiguities fixed, which is very good with respect to a baseline length of 24 km. This suggests that the stochastic model was effective in modelling the ionospheric error. The MRS TC approach has 85% ambiguities fixed for this baseline. Overall, the MRS LSQC network ambiguities are fixed with a higher percentage compared to the ones resolved by the MRS TC approach.

Table 4.16: Percentage of fixed ambiguities using SRS, MRS LSQC and MRS TC approaches for 6 April 2004 using L1/L2 mode

	AIRD COCH	AIRD STRA	COCH BLDM	COCH UOFC	STRA UOFC	BLDM UOFC	AIRD UOFC
Distance (km)	34	50	59	27	52	45	24
% of fixed							
SRS	n/a	n/a	n/a	n/a	n/a	n/a	92
MRS LSQC	94	91	87	n/a	n/a	n/a	98
MRS TC	n/a	n/a	n/a	93	72	73	85

4.1.2.6 MRS Improvement in Solution Convergence

The results of 3D converging L1 position solutions for SRS (in pink and red) and for MRS LSQC (in light blue and blue) are shown in Figure 4.26. Compared to the previous data set of 24 May 2004, the ionosphere was more active for the first 15 segments. As a result, poorer performance in convergence is obtained from both approaches. For all segments of this data set (with the exception of segment 12), the MRS approach yields not only faster convergence but also more accurate converged solutions, although the magnitude of the improvement depends on the level of ionospheric error.

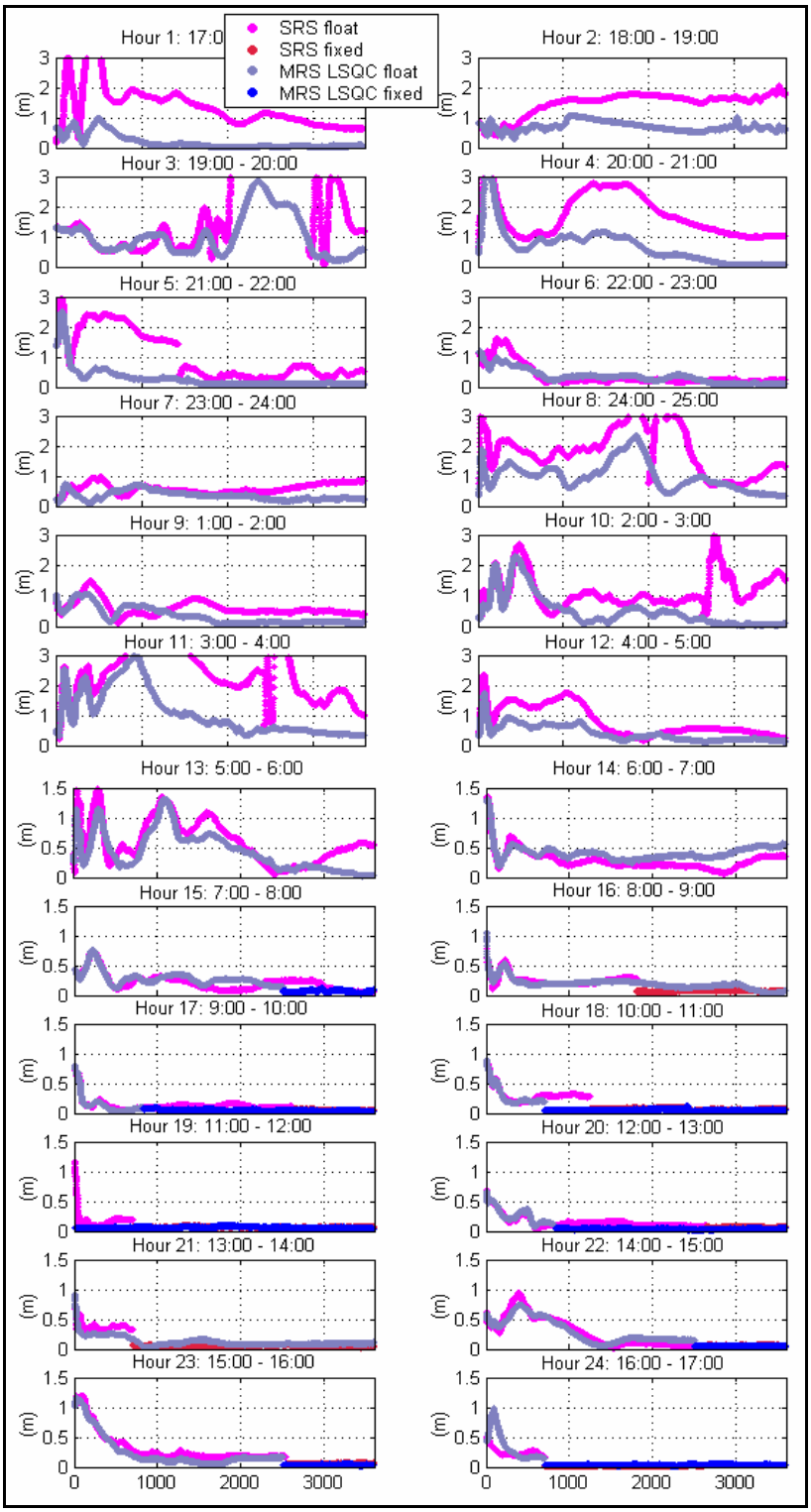

Figure 4.26: Converging 3D position accuracy and ambiguity status in L1 mode for 24 one-hour segments - 6 April 2004

The average and maximum 3D position errors for the segments are presented in Figures 4.27 and 4.28. As shown in Table 4.17, averages of approximately 50% and 10% improvement are realized through the use of the MRS approach for the active ionosphere and quiet ionosphere periods of the day, respectively. The maximum error is also reduced in relative terms using the MRS LSQC approach. For most of the segments, the ambiguities cannot be resolved after one hour for both approaches, as shown in Figure 4.29. Such a result is considered reasonable based on the use of only L1 observations.

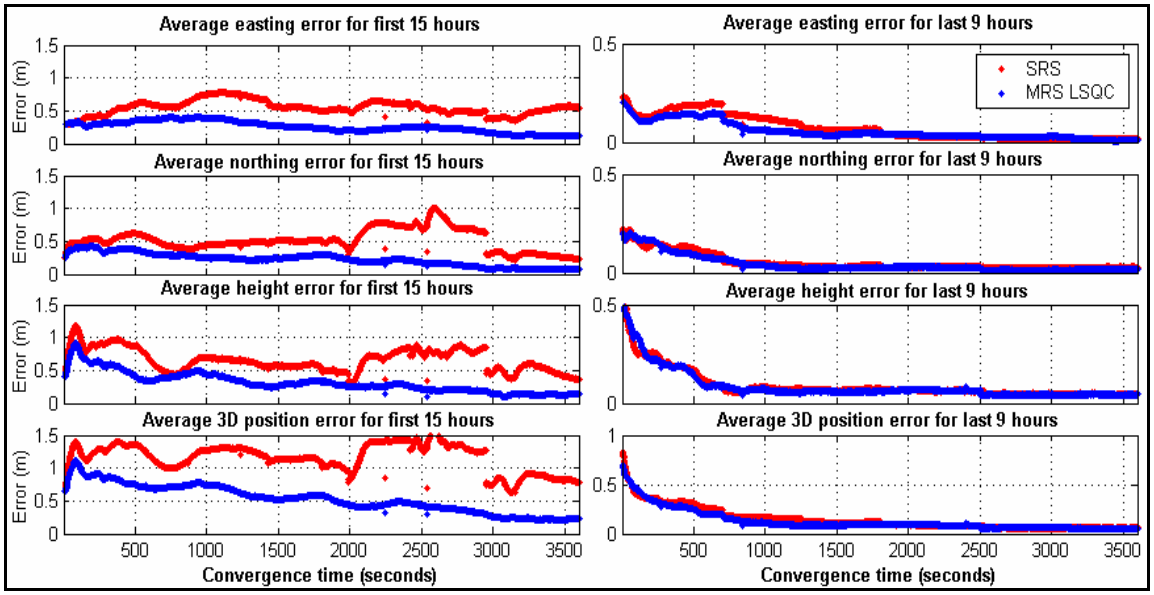

Figure 4.27: Average absolute converging 3D position accuracy in L1 mode for 6 April 2004, separately for the first 15 hours (left) and for the last 9 hours (right)

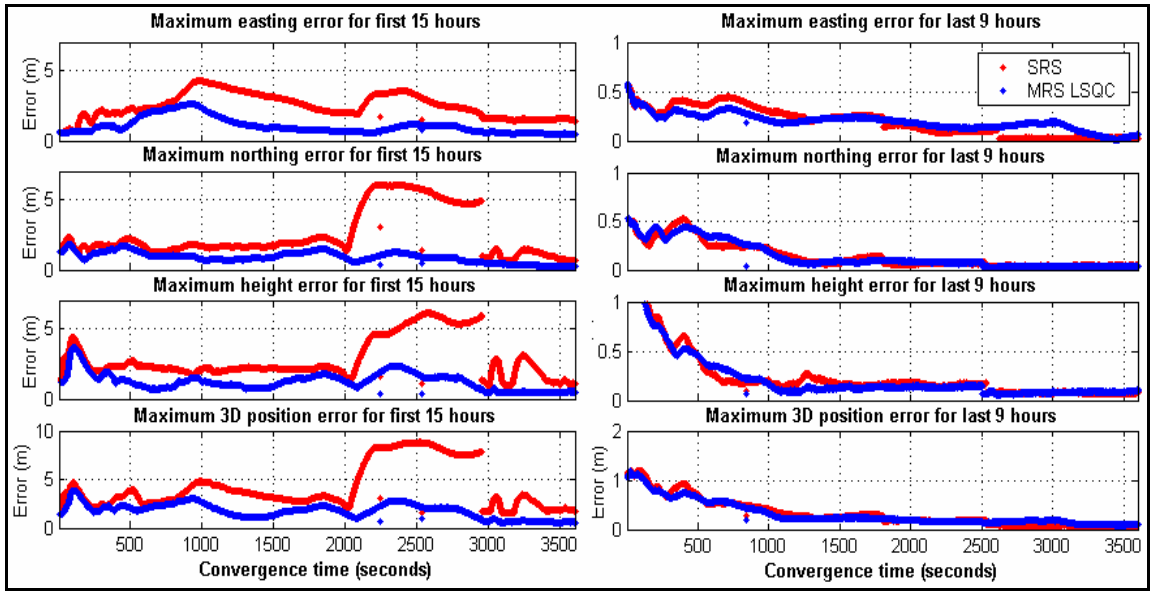

Figure 4.28: Maximum absolute converging 3D position error in L1 mode for 6 April 2004, separately for the first 15 hours (left) and for the last 9 hours (right)

Table 4.17: Statistics for the average and maximum converging 3D position error in L1 mode - 6 April 2004

	Average				Maximum			
	RMS (cm)				RMS (cm)			
	E	N	H	3D	E	N	H	3D
SRS first 15	56	54	68	118	262	815	1013	1765
MRS LSQC first 15	27	24	35	57	407	366	528	860
Improvement (%) first 15	52	56	49	52	-55	55	48	51
SRS last 9	10	7	12	19	24	61	107	168
MRS LSQC last 9	7	6	12	17	64	56	104	151
Improvement (%) last 9	30	14	0	11	-167	8	3	10

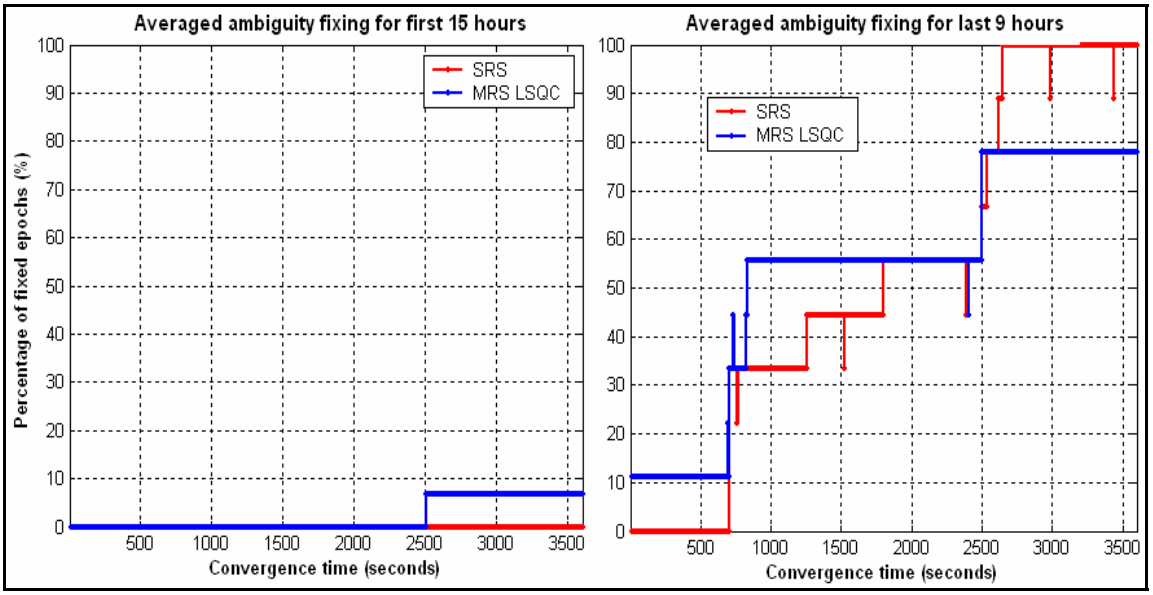

Figure 4.29: Average ambiguity status during convergence in L1 mode for 6 April 2004, separately for the first 15 hours (left) and for the last 9 hours (right)

The IF converging 3D position errors using both SRS and MRS LSQC approaches for 24 segments of this data set are shown in Figure 4.30, while the average and maximum values of the segments are shown in Figure 4.31 and Figure 4.32, respectively. In this case of medium scale ionospheric error, there are some inconstancies in the performance of both SRS and MRS LSQC during the first half of the data set. For example, the SRS approach faces some difficulties in fixing the ambiguities to correct values in segments 2 and 6 as incorrect values are selected. Conversely, the same problem is observed for the MRS LSQC approach during segments 3 and 5.

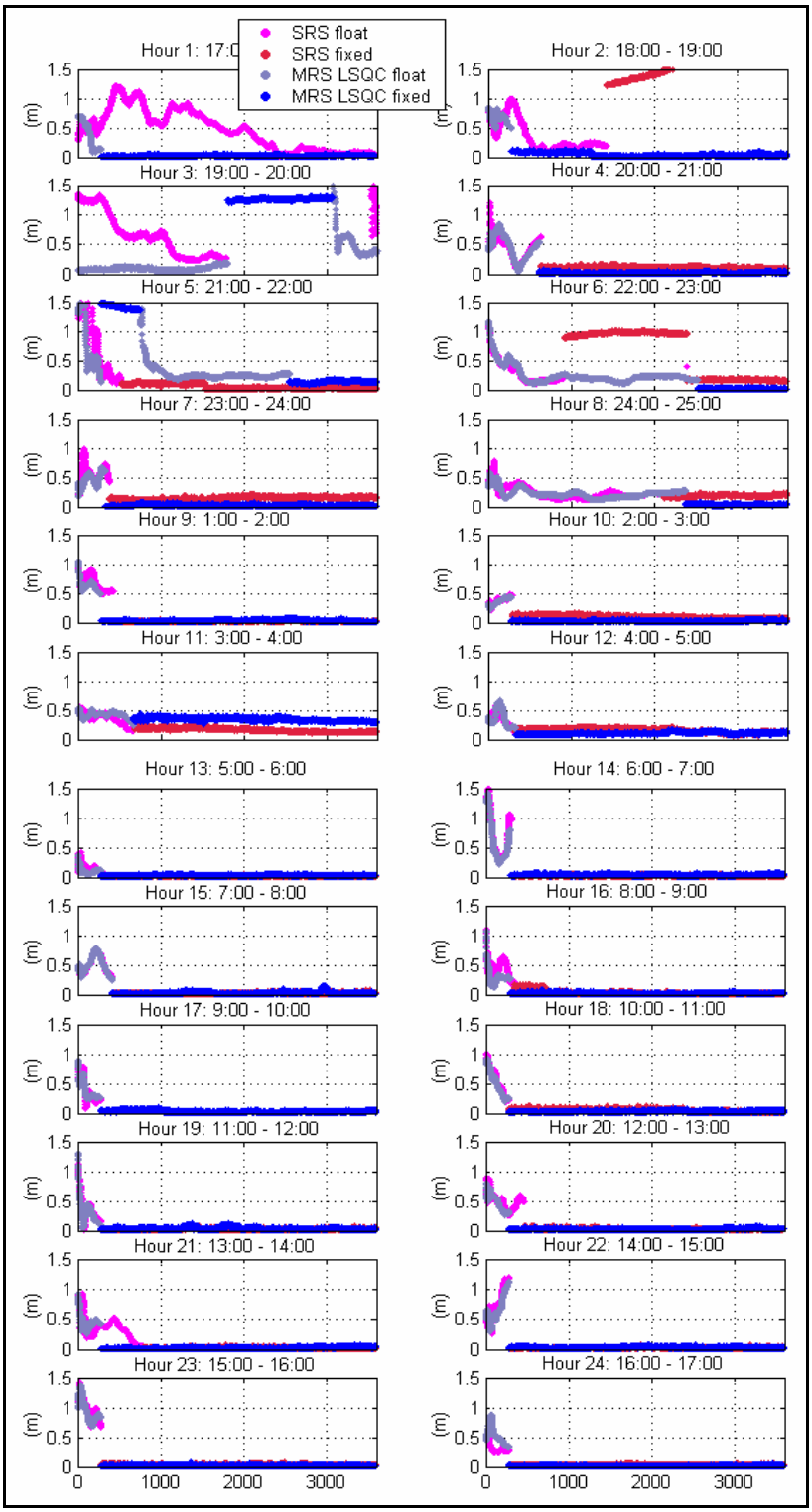

Figure 4.30: Converging 3D position accuracy and ambiguity status in IF mode for 24 one-hour segments - 6 April 2004

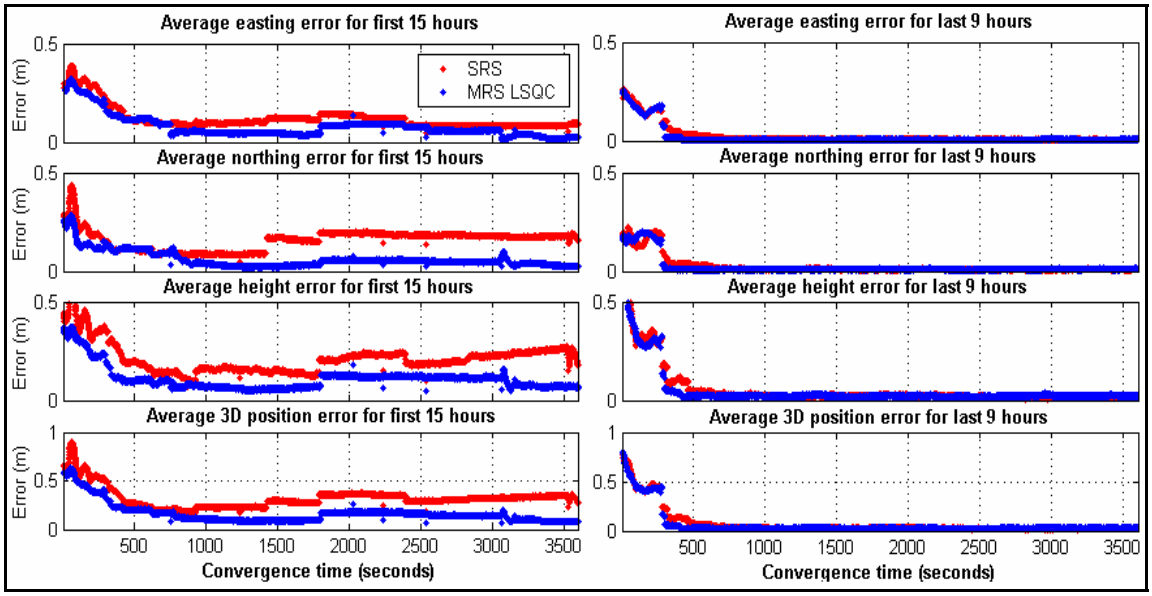

Figure 4.31: Average absolute converging 3D position accuracy in IF mode for 6 April 2004, separately for the first 15 hours (left) and for the last 9 hours (right)

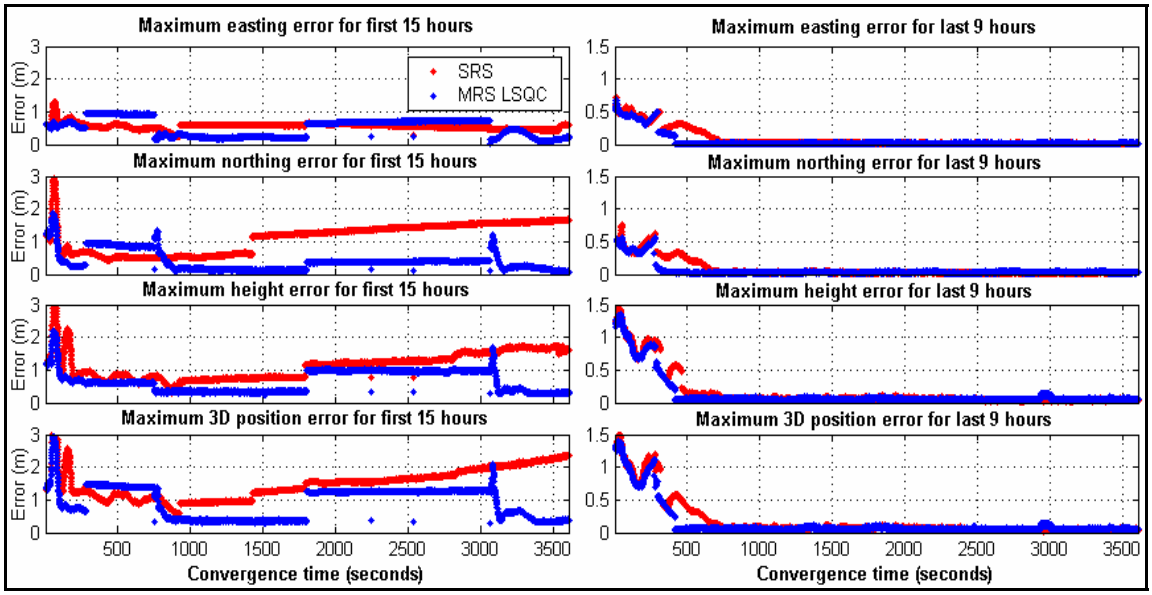

Figure 4.32: Maximum absolute converging 3D position error in IF mode for 6 April 2004, separately for the first 15 hours (left) and for the last 9 hours (right)

However, on average, an MRS approach still offers faster convergence and more accurate converging solutions. During active ionosphere hours, MRS LSQC reduces the average RMS 3D position solution error by 14 cm (equivalent to a 44% reduction), as compared to the SRS approach. The maximum errors are also reduced significantly during this period. However, during the quiet ionosphere hours of the day, the improvement offered by the MRS approach is very small – in the order of a few millimetres. The average performance in ambiguity domain during the convergence is presented in Figure 4.33 separately for the high and low ionosphere periods. It shows that higher percentages of fixed ambiguities are obtained for the MRS approach, especially during the second half of the day.

Table 4.18: Statistics for the average and maximum converging 3D position error in IF mode - 6 April 2004

	Average				Maximum			
	RMS (cm)				RMS (cm)			
	E	N	H	3D	E	N	H	3D
SRS for first 15	13	17	23	34	57	250	338	512
MRS LSQC for first 15	10	8	13	20	148	113	187	292
Improvement (%) for first 15	23	53	48	44	-160	55	45	43
SRS for last 9	5	5	11	15	16	60	137	181
MRS LSQC for last 9	5	5	11	14	60	60	129	170
Improvement (%) for last 9	0	0	0	7	-275	0	6	6

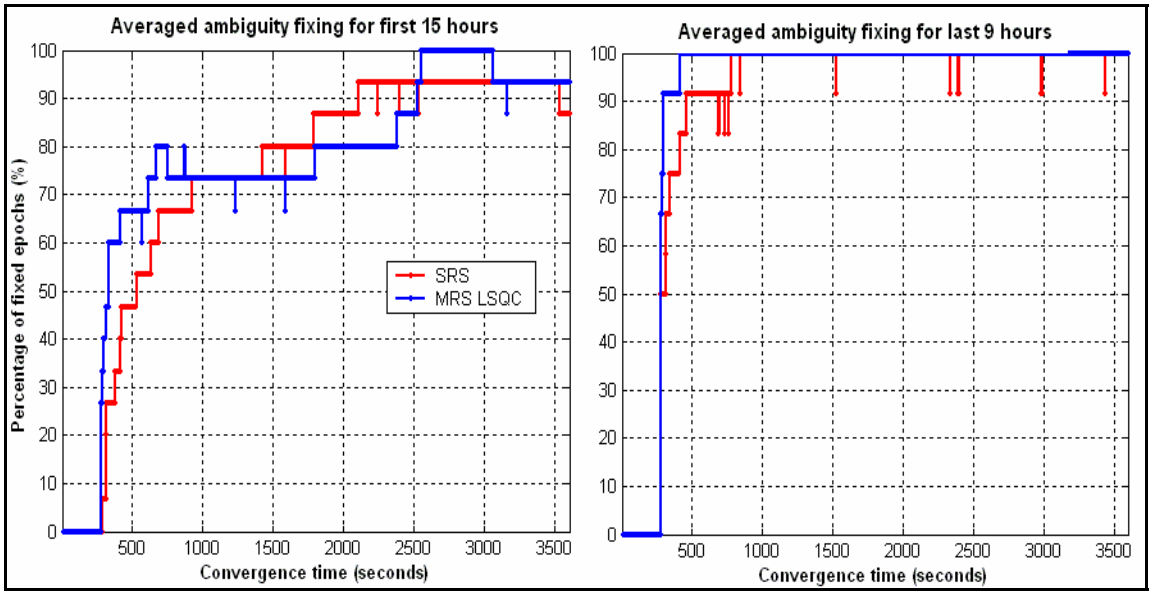

Figure 4.33: Average ambiguity status during convergence in IF mode for 6 April 2004, separately for the first 15 hours (left) and for the last 9 hours (right)

Figure 4.34 depicts the L1/L2 3D position solution errors for all the three methods: SRS, MRS LSQC and MRS TC. Under this medium ionospheric condition, the performance of SRS and MRS LSQC approaches are more or less equal to the case of using IF observables. This suggests that the ionospheric error modeling technique is working very successfully in this case. The results of some segments with wrongly fixed ambiguities, as previously discussed (e.g. SRS segment number 2 and MRS LSQC segment number 3), are improved herein; however, the problem still remains in segments 5 (for MRS LSQC) and 6 (for SRS). Similarly, segment 8 subjected to the MRS TC approach is also problematic. For most of the segments (except 3, 4 and 8), the MRS TC approach shows a noticeable improvement.

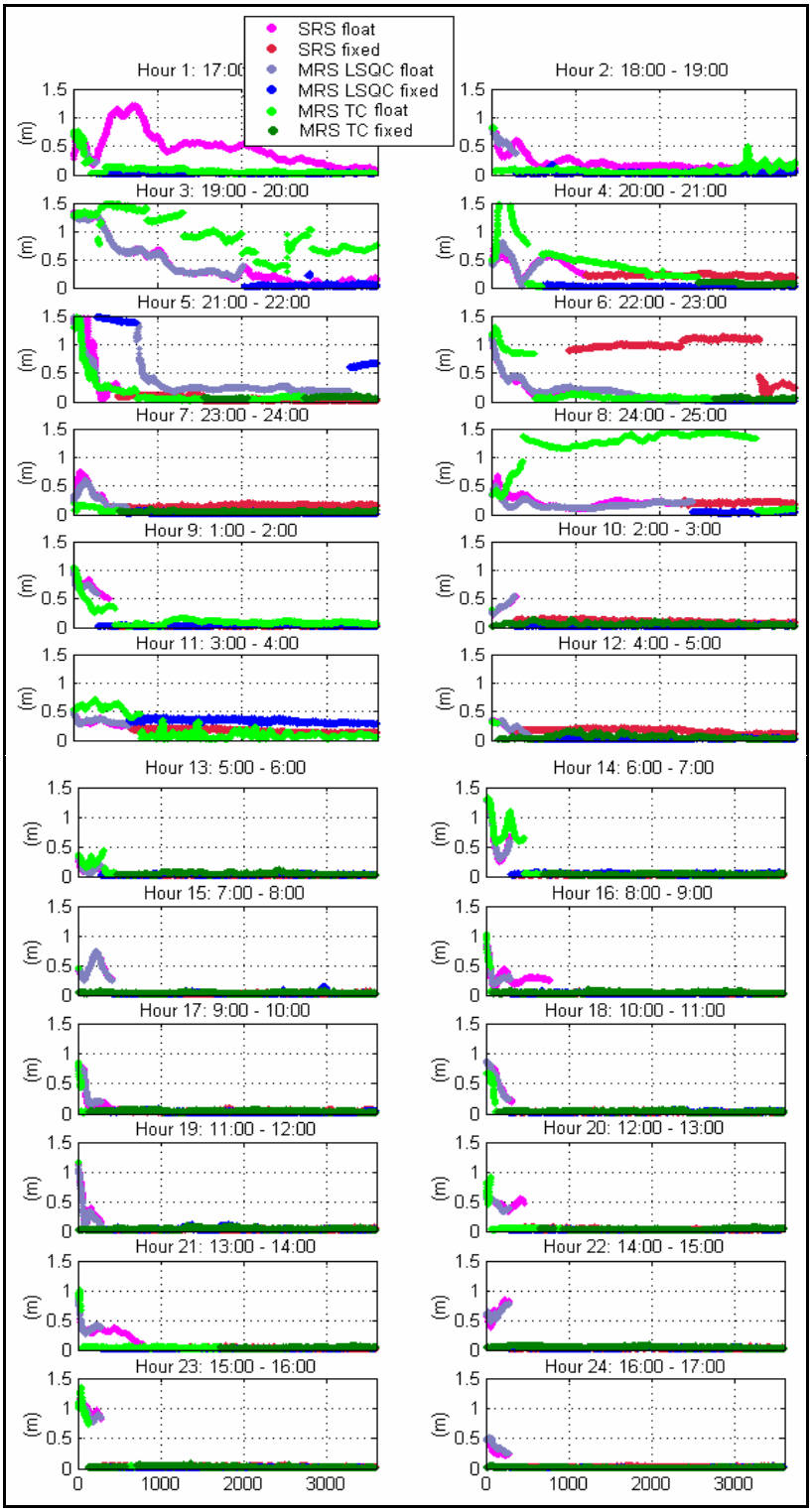

Figure 4.34: Converging 3D position accuracy and ambiguity status in L1/L2 with ionospheric modeling mode for 24 one-hour segments – 6 April 2004

The average 3D position errors of the first 15 segments are presented on the left-hand side of Figure 4.35 while the maximum errors are presented on the left-hand side of Figure 4.36. The average 3D position errors yielded by the MRS TC approach are largest among these three; however, this is due to the small number of segments identified above that dominated the average result. Figure 4.37 shows the same result as Figures 4.35 and 4.36 for the first 15 segments, but excluding segments 6 and 8 where the MRS TC and the SRS perform very poorly; Figure 4.37 shows that, after excluding some of the extreme cases, the MRC TC yields the best performance among the three cases offering a 5 cm (equivalent to 24%) improvement, as compared to the SRS case. The MRS LSQC offers an improvement of 3 cm (equivalent to 14%), as compared to the SRS case. The average and maximum 3D position errors for the last 9 hours of the day are shown on the right-hand side of each of Figure 3.35 and Figure 3.36. Based on these data, it is concluded that, under these quiet ionospheric conditions, the MRC TC approach performs the best and significantly reduces converging time. The average performance of the three approaches in ambiguity resolution domain of both periods of the day are shown in Figure 4.38. Similarly to the previous data set, the MRS TC approach has a very low percentage of fixed ambiguities, compared to the other two but this is not surprising as explained in section 4.1.1.6.

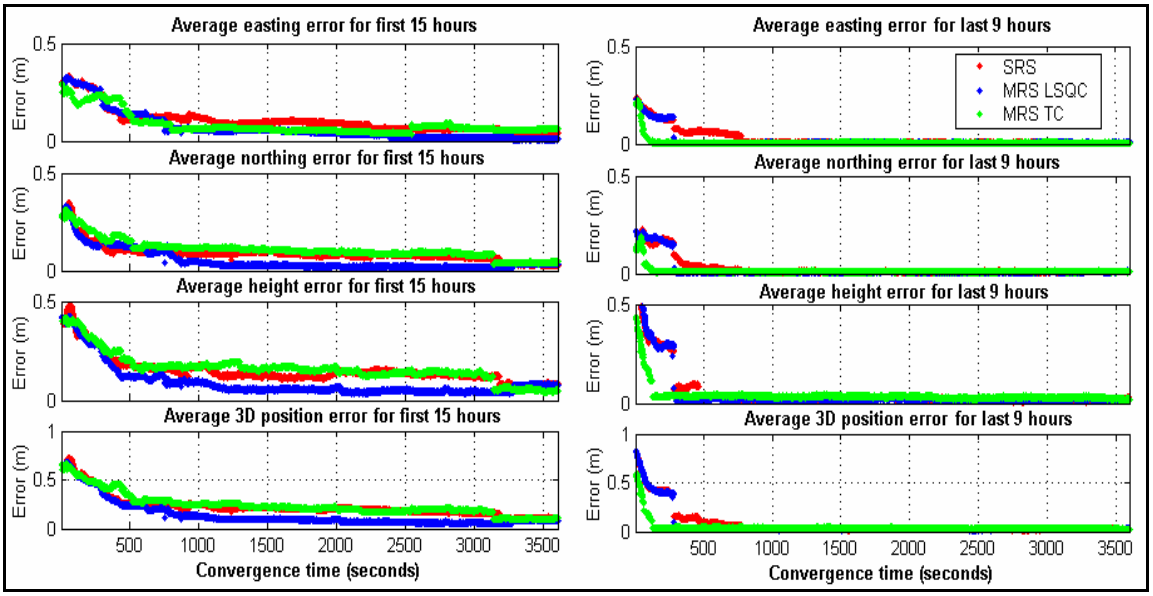

Figure 4.35: Average absolute converging 3D position accuracy in L1/L2 with ionospheric modeling mode for 6 April 2004, separately for the first 15 hours (left) and for the last 9 hours (right)

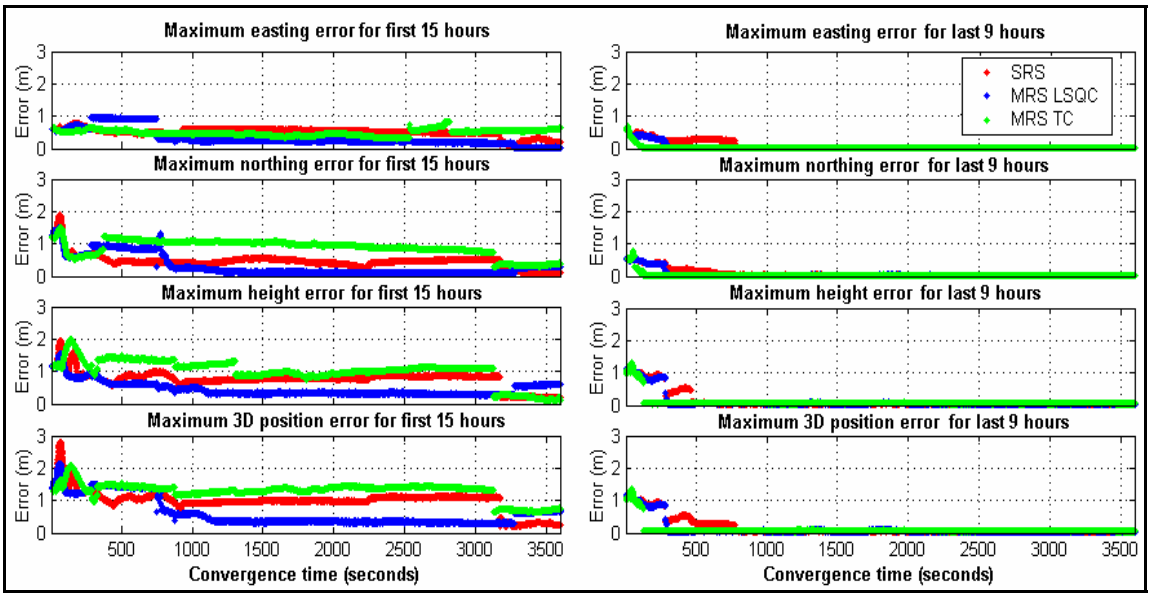

Figure 4.36: Maximum absolute converging 3D position error in L1 and L2 with ionospheric modeling mode for 6 April 2004, separately for the first 15 hours (left) and for the last 9 hours (right)

Table 4.19: Statistics for the average and maximum converging 3D position error in L1/L2 with ionospheric modeling mode – 6 April 2004

	Average				Maximum			
	RMS (cm)				RMS (cm)			
	E	N	H	3D	E	N	H	3D
SRS for first 15	12	10	17	25	52	152	251	380
MRS LSQC for first 15	10	8	12	20	153	118	184	295
Improvement (%) for first 15	17	20	29	20	-194	22	27	23
MRS TC for first 15	10	12	18	27	150	181	269	403
Improvement (%) for first 15	0	-20	-6	-8	-190	-19	-7	-6
SRS for last 9	5	5	11	15	15	47	98	133
MRS LSQC for last 9	4	5	11	14	40	46	100	128
Improvement (%) for last 9	20	0	0	7	-167	4	-2	4
MRS TC for last 9	2	2	6	8	22	20	55	68
Improvement (%) for last 9	60	60	46	47	-47	57	44	49

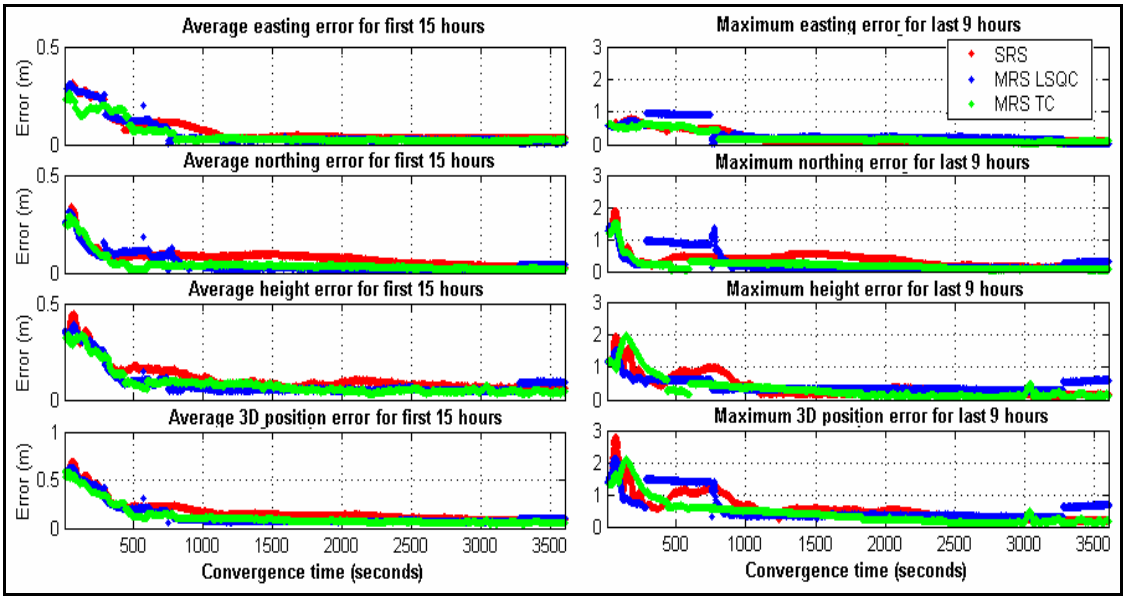

Figure 4.37: Average absolute converging 3D position accuracy in L1/L2 with ionospheric modeling mode for the first 15 segments, excluding segments 6 and 8, - 6 April 2004

Table 4.20: Statistics for the average and maximum converging 3D position error in L1/L2 with ionospheric modeling mode for the first 15 segments, excluding segments 6 and 8, - 6 April 2004

	Average				Maximum			
	RMS (cm)				RMS (cm)			
	E	N	H	3D	E	N	H	3D
SRS for first 15	10	9	13	21	30	106	159	249
MRS LSQC for first 15	9	7	11	18	107	84	132	212
Improvement (%) for first 15	10	20	15	14	-257	21	17	15
MRS TC for first 15	7	7	11	16	89	77	127	195
Improvement (%) for first 15	30	20	15	24	-196	27	20	22

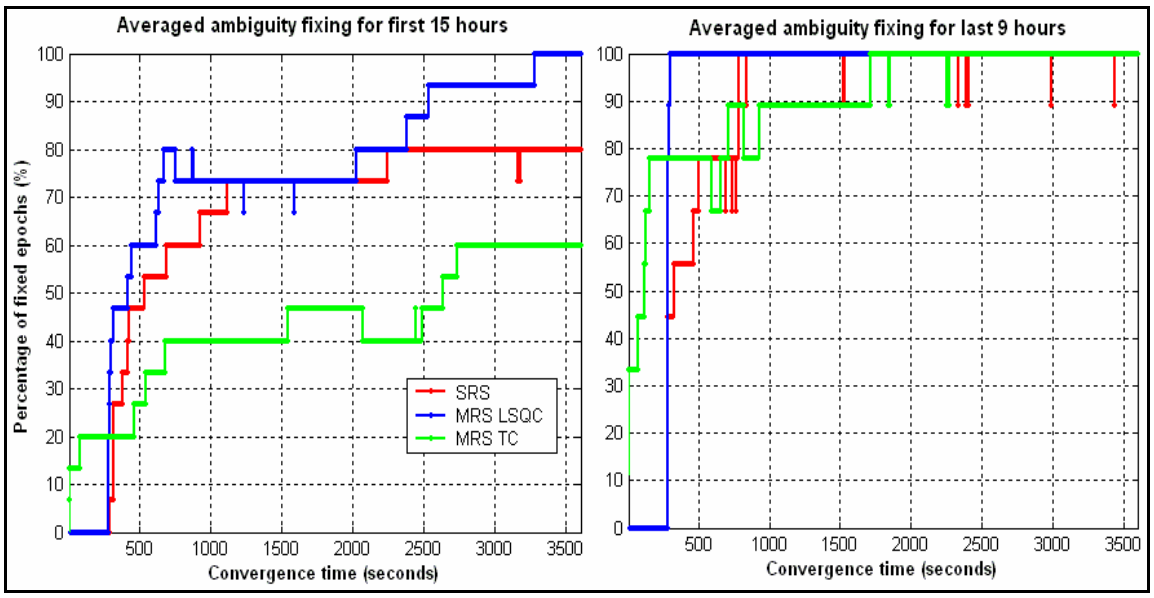

Figure 4.38: Average ambiguity status during convergence in L1/L2 mode for 6 April 2004, separately for the first 15 hours (left) and for the last 9 hours (right)

4.1.3 Ionospheric Storm Condition Results

4.1.3.1 Network Configuration

Because the COCH station was inoperable during the time of interest, the IRRI station is used for the data set obtained on 8 November 2004. Unfortunately, this results in a non-optimal MRS network configuration in which the rover (the UOFC station in this case) is geographically outside the network coverage as shown in Figure 4.39. However, the associated ionospheric activities are very high. The ionospheric error on GPS measurements, in turn, varies significantly in both the temporal and spatial domains.

Therefore, a high improvement yielded by the MRS approaches is not necessarily expected at this particular network scale, even for the case where the rover is situated in the middle of the network region. The improvement could perhaps be obtained only with a very dense network of baselines in the order of several kilometres in size.

The configuration having the shortest baselines was chosen for the tightly-coupled approach in this case, as shown in Figure 4.40. This helps to maximize the ability to resolve the ambiguities and to model the ionospheric error of the tightly-coupled approach. As a result, the UOFC station is not connected in all baselines as the two previous data sets, but only to AIRD and BLDM stations. In this case, the IRRI and STRA stations, without being connected to the rover, are not directly used to estimate the UOFC station position. However, their measurements are still used via their inclusion in the covariance functions.

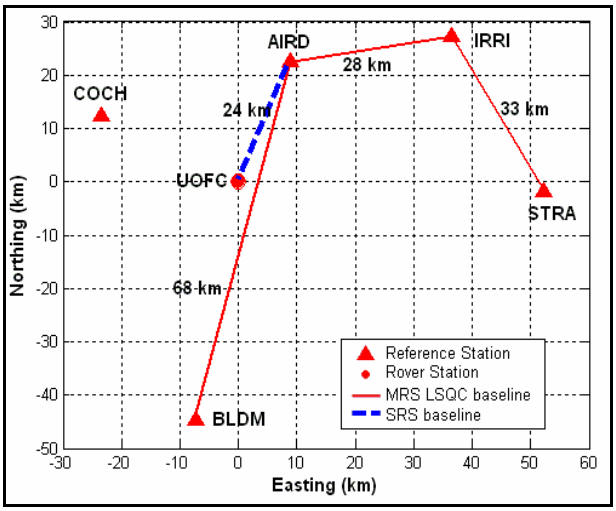

Figure 4.39: Network configuration used with MRS LSQC - 8 November 2004

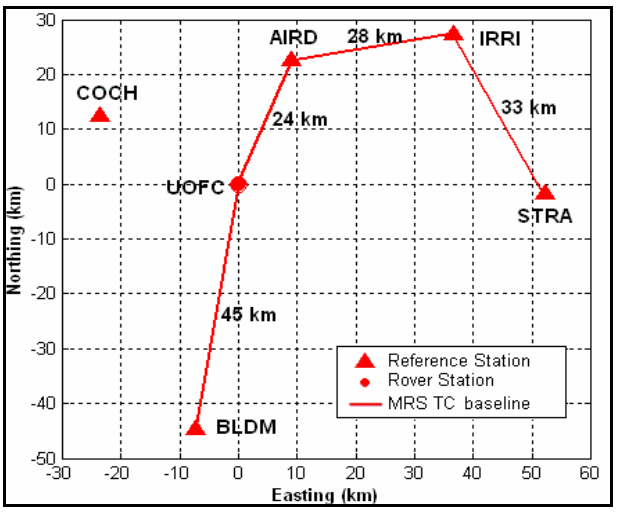

Figure 4.40: Network configuration used with MRS TC - 8 November 2004

4.1.3.2 Network Double-Difference Corrections

The network double-difference corrections generated by the MRS LSQC approach using this data set are presented in Figure 4.41 for different types of observations; namely, C/A code, L1, L2, WL, IF and GF. The corrections obtained in this case are much larger than those resulting from use of the previous data set (6 April 2004) under medium ionospheric error conditions. Further, this difference is more pronounced during night time; for example, the average double-difference of the first 15 hours of the previous day for L1 and GF are 5.7 cm and 3.9 cm, respectively, while the comparable values for this data set are 17.0 cm and 12.3 cm, respectively. These values are equivalent to 7 ppm of the total error on L1, and 5 ppm of ionospheric error. During the day-time, there is generally a few cm difference in corrections between the two data sets. The total error on L1 observations is approximately 4.1 cm (1.7 ppm) and the ionospheric error is 2.8 cm

(1.2 ppm). The variation in correction values correlates very well with the variation in the local K indices. The IF corrections, having a magnitude of approximately 1.6 cm for the entire day, demonstrate that the tropospheric errors were consistent over the region.

In this case, the network ambiguity resolution process performs very poorly as a result of the disturbed ionosphere. In particular, the percentage of fixed ambiguities is only 35% for AIRD-IRRI (at a distance of 28 km), 53% for IRRI-STRA (33 km) and 32% for AIRD-BLDM (68 km). These relative low figures indicate that most of the corrections were generated using float ambiguities and are therefore less accurate.

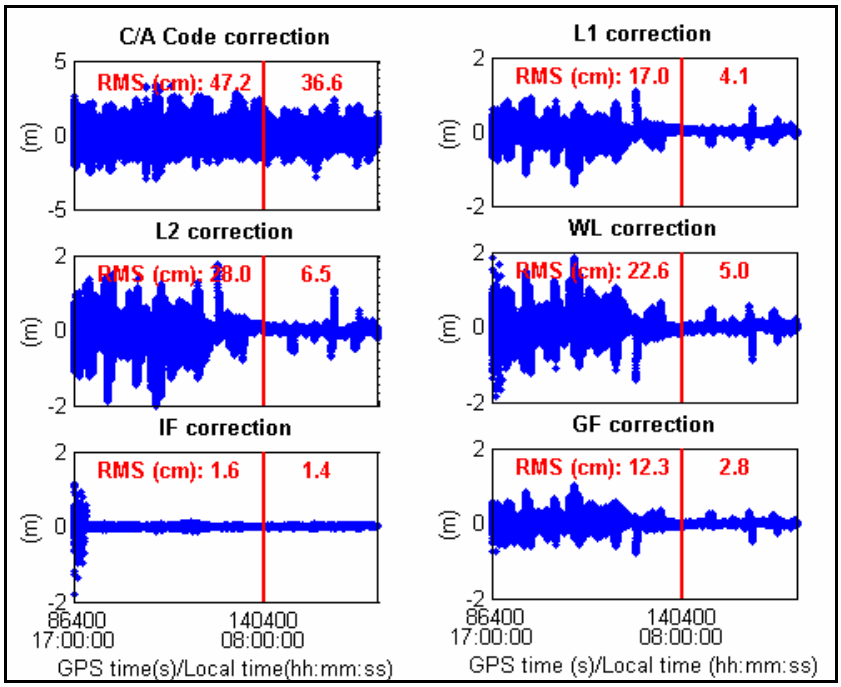

Figure 4.41: Double-difference network corrections generated by MRS LSQC for all satellite pairs - 8 November 2004 (ionospheric storm conditions)

4.1.3.3 MRS Improvement in Observation Domain

In a similar manner to the treatment of the previous two data sets, analysis is carried out in the measurement domain using the estimated misclosures by means of fixing by both the primary reference station and the rover station to their known coordinates. Double-difference misclosures are presented in Figure 4.42 for different types of observables. The statistics are found in Table 4.21. The double-difference misclosures generated using this data set is more than twice the magnitude of those of the previous data sets. This clearly reflects the high level of the ionospheric error. Although the improvement offered by the MRS approach is the most important under this condition, the approach faces difficulties in resolving the ambiguities with a very low percentage of ambiguities fixed, as shown in Section 4.1.3.2. In this case, the MRS LSQC yields a low improvement of only 1 or 2 cm, which is equivalent to an approximately 15% improvement with respect to the SRS case. This means that the MRS approach compensates for only a small part of the errors. This is because of the more rapid spatial decorrelation of the ionospheric errors under the prevailing conditions. Similar to the other two cases, no IF measurement improvement is observed.

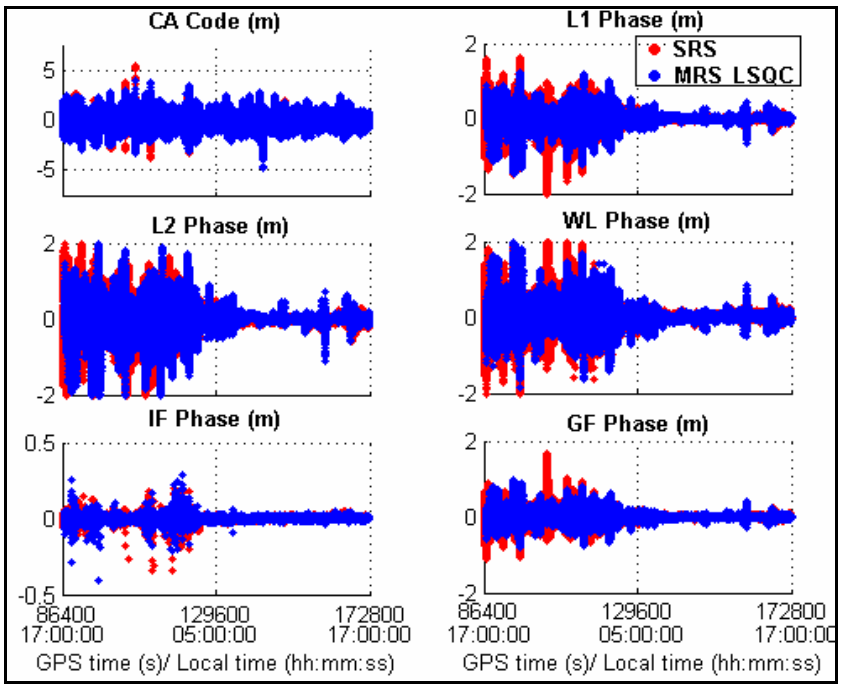

Figure 4.42: Double-difference observable misclosures for all satellite pairs using raw measurements (red) and using MRS LSQC corrected measurements (blue) - 8 November 2004

Table 4.21: Statistics for double-difference observable misclosures for all satellite pairs – 8 November 2004

RMS (cm)	SRS	MRS	Improvement (%)
C/A Code	51.8	52.2	0
L1 Phase	12.0	10.3	14
L2 Phase	19.9	17.0	15
WL	16.2	14.0	14
IF	0.8	0.8	0
GF	7.9	6.8	14

4.1.3.4 Long-term Position Domain Improvement with MRS

Recalling that, for the ionospheric error variations throughout the data set, the local K values were observed at levels of 7 and 8 during the first 15 hours of the data set. During the following six hours, the average local K values were 2 and 3. Although indicative of less active ionospheric activity, as compared to the previous 15-hour period, this lower range of K values is still characterizes unsettled conditions. This is demonstrated by the return of the active phase during the last three hours of the data set with an average local K value of 5.

The highly disturbed ionosphere results in an approximately 2 m RMS 3D L1 position error, as shown in Figure 4.43. The associated ambiguity status and number of available satellites are shown in this figure, and pertinent statistics given in Table 4.22. The ionospheric effect significantly degrades both the SRS and MRS approaches. Overall, during the first 15 hours of the day, SRS provides a RMS of 2.0 m in 3D position solution accuracy. The MRS LSQC position solution accuracy for the MRS LSQC approach is 1.7 m, corresponding to an 18% improvement. This means that the MRS approach is still severely affected by the unusually large ionospheric error. When estimating the corrections using the MRS LSQC approach, some measurements have been rejected using an IF threshold check. This leads to reduced data availability based on a smaller number of satellites between the corrected primary reference station and the raw reference station, particularly between 23:00 and 05:00 local time, and from 07:00 to 12:00 local time. When the total number of remaining satellites is high, this does not have

a significant impact on the MRS LSQC position solutions. However, if there are not many satellites remaining, the effect of any undetected cycle slips will be enhanced, resulting in a degraded MRS LSQC position solution. This effect is observed, in this case, specifically during GPS time of 142600-151000. Due to this problem, the SRS approach also performs better than the MRS LSQC approach in the ambiguity resolution domain in this particular case.

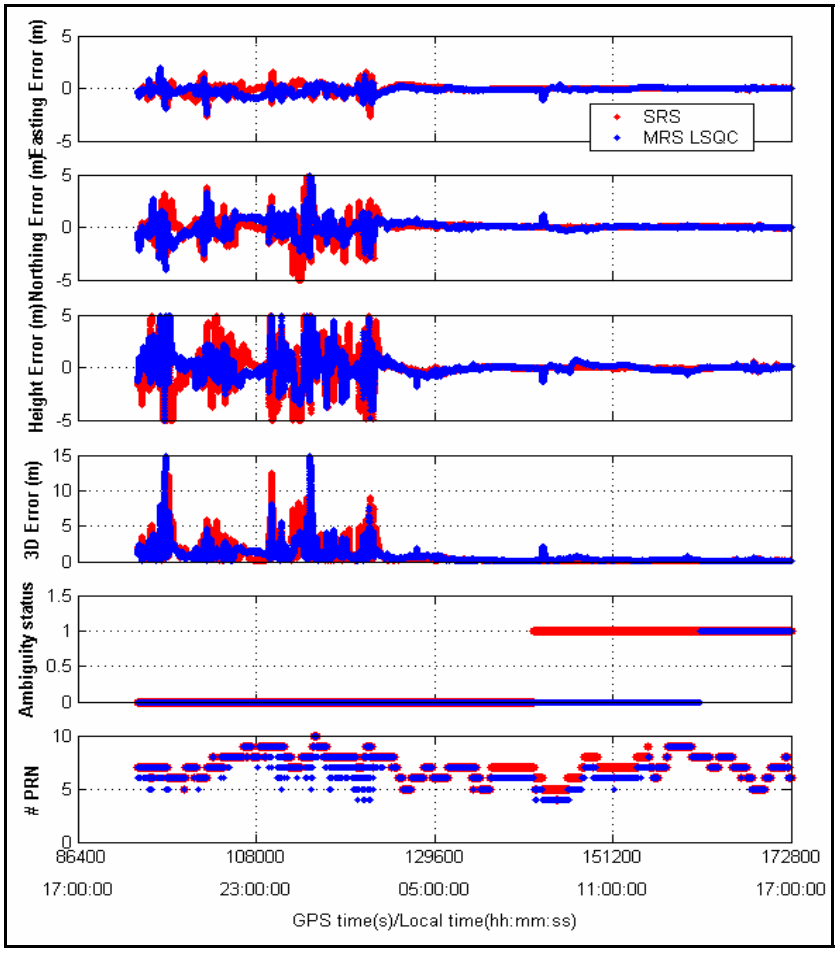

Figure 4.43: Position accuracy and ambiguity status in L1 mode after a two-hour network initialization period - 8 November 2004

Table 4.22: Statistics for position accuracy in L1 mode after a two-hour network initialization period - 8 November 2004

	High ionospheric period – first 13 hours, after 2 hours for network convergence				Low ionospheric period – last 9 hours			
	RMS (cm)				RMS (cm)			
	E	N	H	3D	E	N	H	3D
SRS	42	102	178	209	3	6	9	12
MRS LSQC	41	88	140	171	12	13	24	30
Improvement (%)	2	14	21	18	No improvement			

For further analysis on the correct impact of high ionospheric errors, the least-squares position solutions generated using only C/A code measurements are presented in Figure 4.44. In contrast with carrier phase measurements, the code measurements are not affected by cycle slips or loss of lock. Therefore, the code position solution errors better reflect the impact of differential ionospheric errors, assuming uncorrelated errors such as multipath and noise do not significantly mask the ionospheric effects. In Figure 4.44, the one-second epoch-by-epoch code position solutions are presented in red while the 100-second average code solutions are shown in yellow and the 1800-second average code solutions are shown in black. Overall, the code solutions suffer errors of up to a few metres. Over a baseline length of 24 km, a 2-m error is equivalent to a 80 ppm effect, which is truly exceptionally large. This, however, reflects the impact of not only ionospheric error but also of various other errors on the code measurements such as the tropospheric error, multipath and noise. Figure 4.45 shows the comparison of the 100-second average code solutions (in yellow) and of the 1800-second average code solutions (in black) with the one-second epoch-by-epoch L1 carrier phase-based SRS solutions (in red), the one-second epoch-by-epoch L1 carrier phase-based MRS solutions (in blue) and

the 1800-second average L1 carrier phase-based SRS solutions (in cyan). The results clearly shows that the impact of cycle slips under this active ionospheric condition is very significant on the use of carrier phase measurements, resulting in large position solution error of up to 10 metres, which are not obtained in the code position solutions. These 10-m errors are therefore not solely due directly to the effect of the ionosphere. This shows the danger of using carrier phase measurements under such a highly disturbed ionosphere. As previously discussed, the MRS approach performance in this case is severely affected by the bad data quality, which masks the improvement that the MRS approach could provide if there were not many such cycle slips. However, the rapid decorrelation of the ionospheric error under such active conditions still prevents the MRS approach from effectively performing and providing significant improvement.

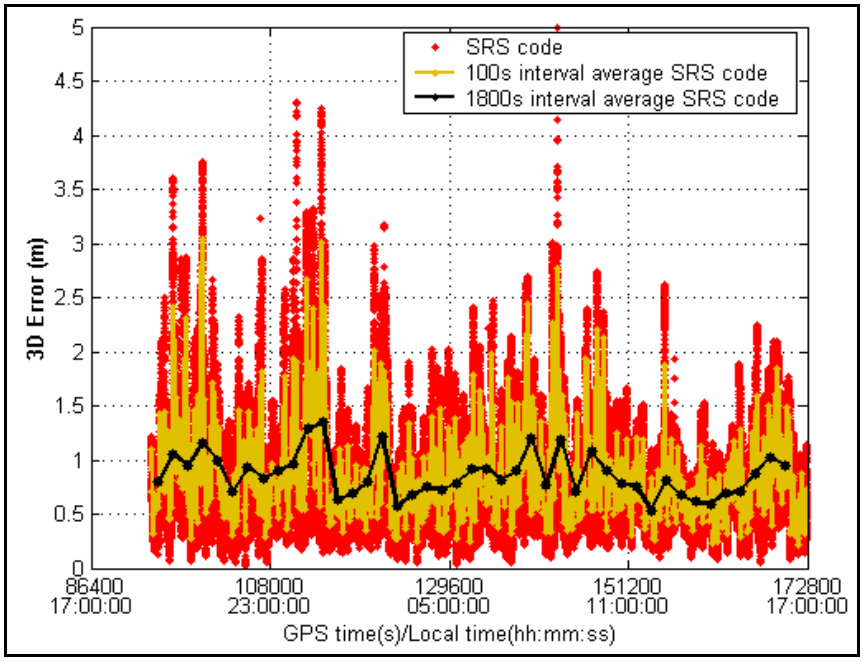

Figure 4.44: One-second C/A code solutions (red), 100-second interval averages of C/A code solutions (yellow) and 1800-second interval averages of C/A code solutions (black) – 8 November 2004

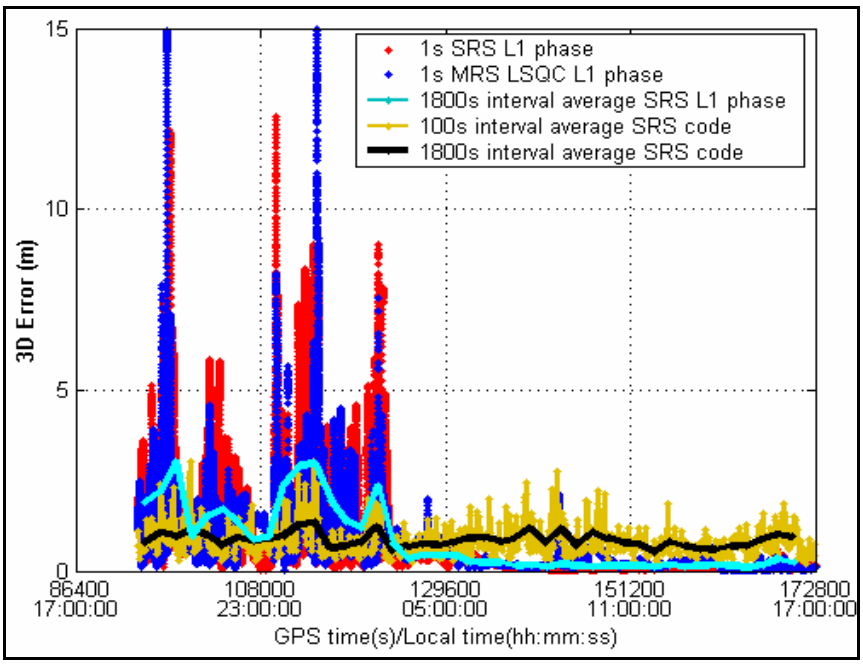

Figure 4.45: One-second L1 carrier phase-based SRS solutions (red), one-second L1 carrier phase-based MRS LSQC solutions (blue) and 1800-second average L1 carrier phase-based SRS solutions (cyan) in comparison with 100-second average of C/A code solutions (yellow) and 1800-second average of C/A code solutions (black) – 8 November 2004

The long-term position solutions - in addition to the ambiguity status and number of satellites available - which were generated using IF observables, are presented in Figure 4.46. SRS solutions are represented by red dots, while blue dots signify MRS LSQC solutions. During the period of 23:00 to 05:00 local time, the solutions offered by both approaches are degraded by cycle slips. The presence of cycle slips on the raw reference station measurements, the corrected reference station measurements, and the raw rover measurements are represented by red crosses in Figures 4.47 to 4.49, respectively. It is notable that a significant number of cycle slips are detected on all L2 observations obtained at both reference and rover during this period. Interestingly, the corrected L1 observations involve significantly more cycle slips than the raw L1 observations obtained

at the primary reference station. This is due to the applications of the corrections, which are invalid for single measurements. During the period 07:00 to 12:00 local time, observations obtained from satellite 13 at reference station AIRD are severely corrupted by cycle slips; the observations are therefore excluded when the MRS LSQC approach generates the corrections. This leads to the problem of low observation availability during this time when applying the MRS LSQC corrected observations. This also affects the use of the L2 raw reference station observations in IF mode. In addition, a cycle slip of a few cycles on satellite 27 was observed at the rover. Thus, with only 4 satellites available, the position solutions are degraded. Overall, in this case, no improvement is obtained by using MRS LSQC throughout the data set.

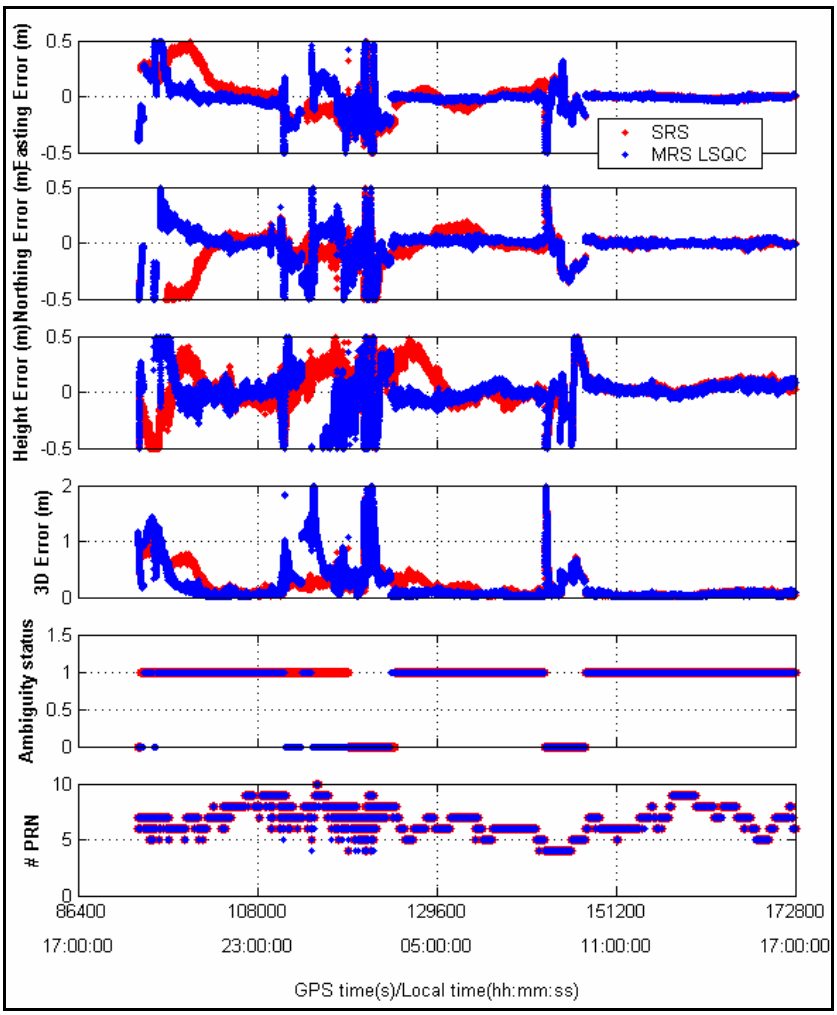

Figure 4.46: Position accuracy and ambiguity status in IF mode after a two-hour network initialization period - 8 November 2004

Table 4.23: Statistics for position accuracy in IF mode after a two-hour network initialization period - 8 November 2004

	High Ionospheric Activity – First 15 hours				Low Ionospheric Activity – Last 9 hours			
	RMS (cm)				RMS (cm)			
	E	N	H	3D	E	N	H	3D
SRS	19	26	22	39	9	12	16	22
MRS	20	22	38	48	9	12	15	21
Improvement (%)	-5	15	-73	-23	0	0	6	5

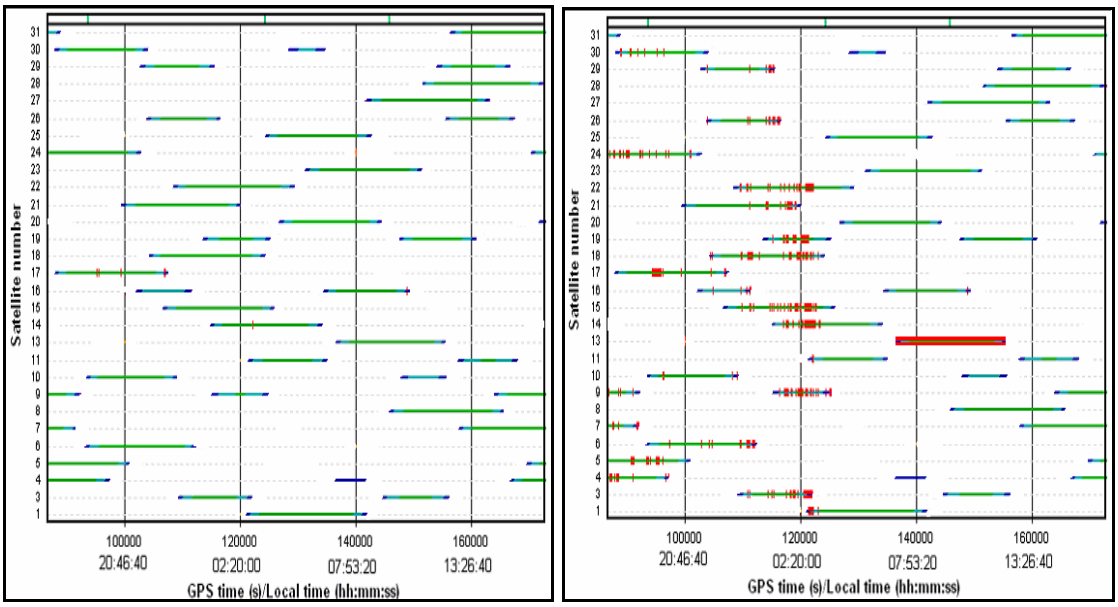

Figure 4.47: Detected cycle slips on raw L1 (left) and L2 (right) reference station AIRD observations – 8 November 2004

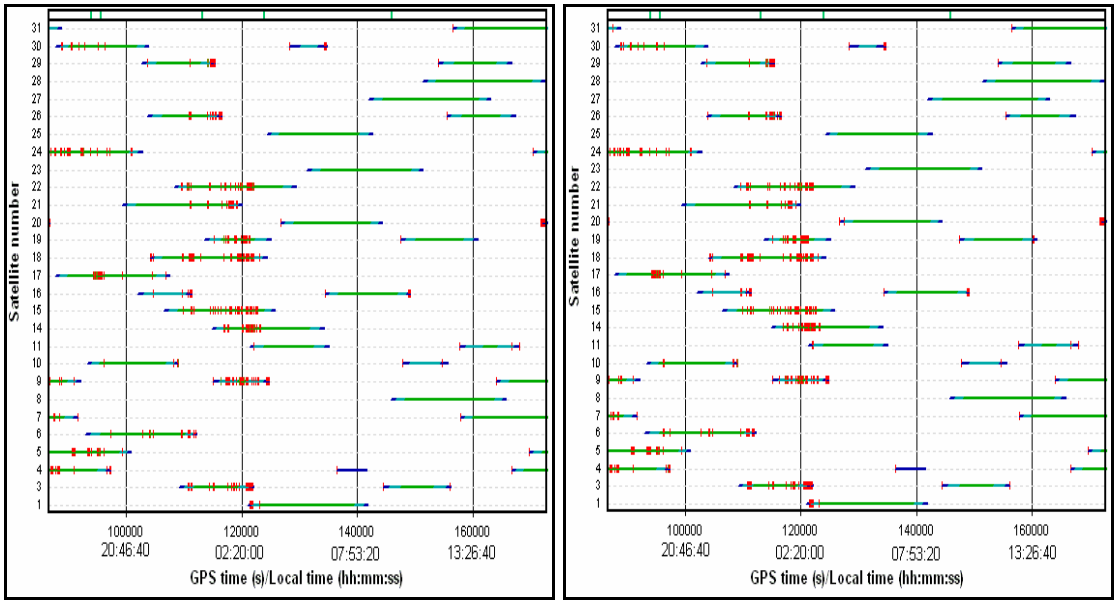

Figure 4.48: Detected cycle slips on corrected L1 (left) and L2 (right) reference station AIRD observations – 8 November 2004

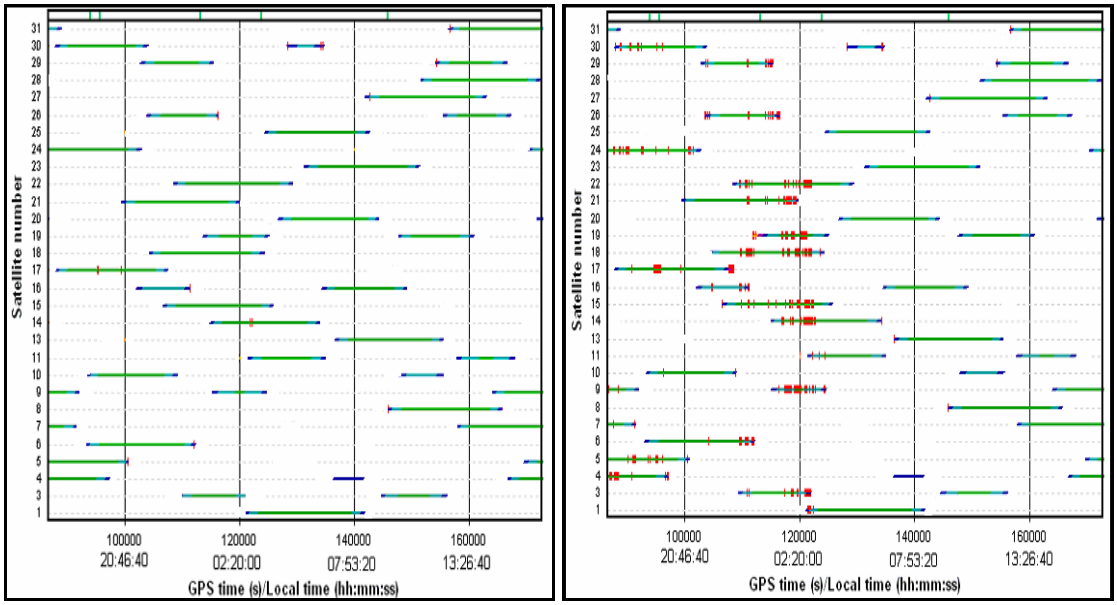

Figure 4.49: Detected cycle slips on raw L1 (left) and L2 (right) UOFC rover observations – 8 November 2004

The position solutions using L1 and L2 observations for all three approaches are presented in Figure 4.50. The numbers of satellites used to generate the MRS TC solutions and SRS solutions are the same. The MRS TC ambiguity performance is shown in Table 4.25. During the first half of the data set, all three approaches suffer a high ionospheric error. As a result, poor solutions are obtained, with RMS 3D position errors of 157 cm, 136 cm and 56 cm for SRS, MRS LSQC and MRS TC approaches. During the second half of the data set, the MRS LSQC approach suffers low observation availability due to the exclusion of satellite 13, as described earlier. This, in addition to cycle slips on satellite 27, results in a position error peak at approximately 07:00 local time. During this period of time, MRS TC affords on average only a 5 cm (equivalent to 29%) improvement over the traditional SRS approach.

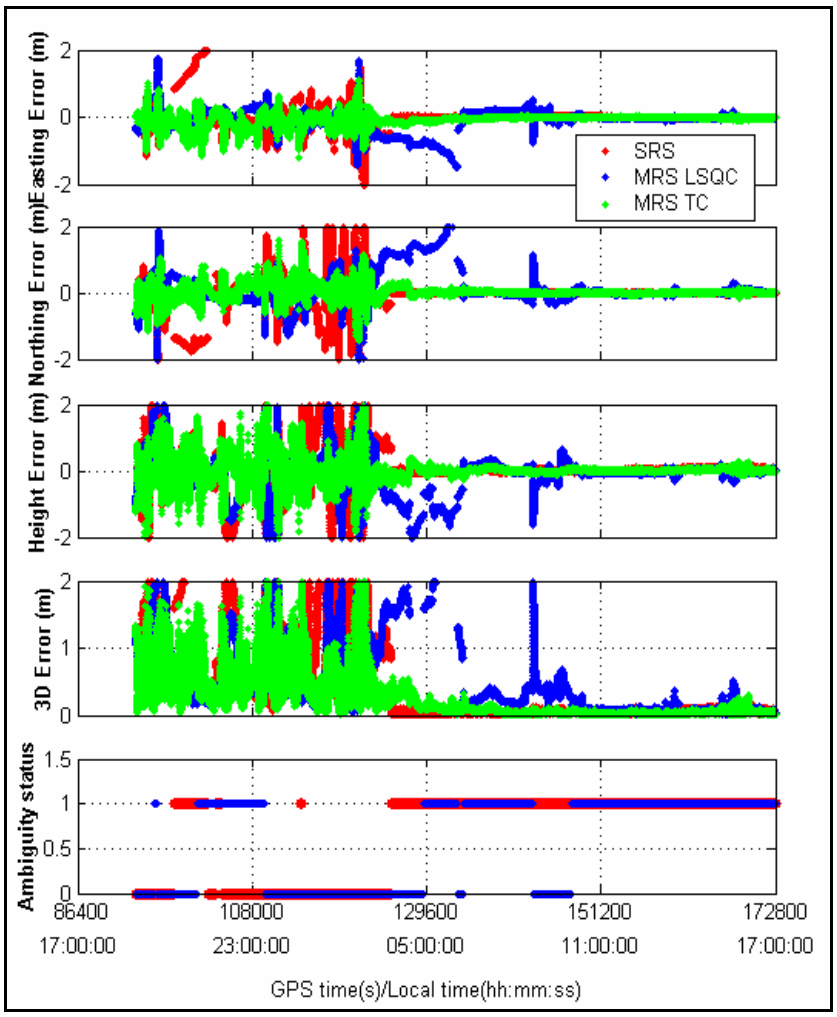

Figure 4.50: Position accuracy in L1/L2 with stochastic ionosphere modeling mode after a two-hour network initialization period - 8 November 2004

Table 4.24: Statistics for position accuracy in L1/L2 with stochastic ionosphere modeling mode after a two-hour network initialization period - 8 November 2004

	High Ionosphere Period – first 12 hours, after 3 hours of network and filter convergence				Low Ionosphere Period – last 9 hours			
	RMS (cm)				RMS (cm)			
	E	N	H	3D	E	N	H	3D
SRS	54	81	123	157	3	1	6	7
MRS LSC	46	75	104	136	11	13	19	25
Improvement (%) relative to SRS	15	7	16	13	-267	-400	-217	-257

MRS TC	23	25	45	56	2	2	4	5
Improvement (%) relative to SRS	57	69	63	64	33	-33	33	29

4.1.3.5 Network Ambiguity Performance

The performances in the ambiguity resolution domain for the three approaches using L1 and L2 observations are shown in Table 4.25. Both MRS approaches perform poorly, with only approximately 10% to 40% of the network ambiguities fixed, depending on the baseline lengths, which range form 28 km to 68 km. For ambiguities of the common baseline among the three approaches (AIRD-UOFC), the SRS approach yields a figure of 67% ambiguities fixed, while the MRS LSQC approach yields only 59%. The MRS TC approach provides very low percentage of ambiguities fixed; however, due to the nature of this method as discussed previously in sections 3.3 and 4.1.1.6, it still yields more accurate position solutions.

Table 4.25: Percentage of fixed ambiguities using SRS, MRS LSQC and MRS TC approaches for 8 November 2004 using L1/L2 mode

	AIRD IRRI	IRRI STRA	AIRD BLDM	BLDM UOFC	AIRD UOFC
Distance (km)	28	33	68	45	24
% of fixed					
SRS	n/a	n/a	n/a	n/a	67
MRS LSQC	35	53	32	n/a	59
MRS TC	19	43	n/a	19	12

4.1.3.6 MRS Improvement in Solution Convergence

The same converging analysis technique presented in the previous sections is carried out for this case. The 24-hour data set is divided into 24 one-hour segments and the position solutions are estimated for each of these segments individually, employing ionospheric error modeling with different observation combinations (e.g. as L1 only, IF and L1/L2). The results for L1 solutions are shown in Figure 4.51, in which the pink color denotes the SRS solutions and the light blue color represents MRS LSQC solutions. Float ambiguities are used in this case. The position solutions during the first 10 segments did not converge, with solution accuracies remaining at the level of a few metres. The MRS LSQC approach offers some improvements, although it is still highly affected by the ionospheric error. The improvement is very noticeable for segments 4 and 5. During the following hours of the day, significantly more accurate converging position solutions are obtained as a consequence of a lower ionospheric error. The SRS approach performs very well in general, and only a small improvement is observed by using the MRS LSQC approach (e.g. segments 13, 14, 22 and 24).

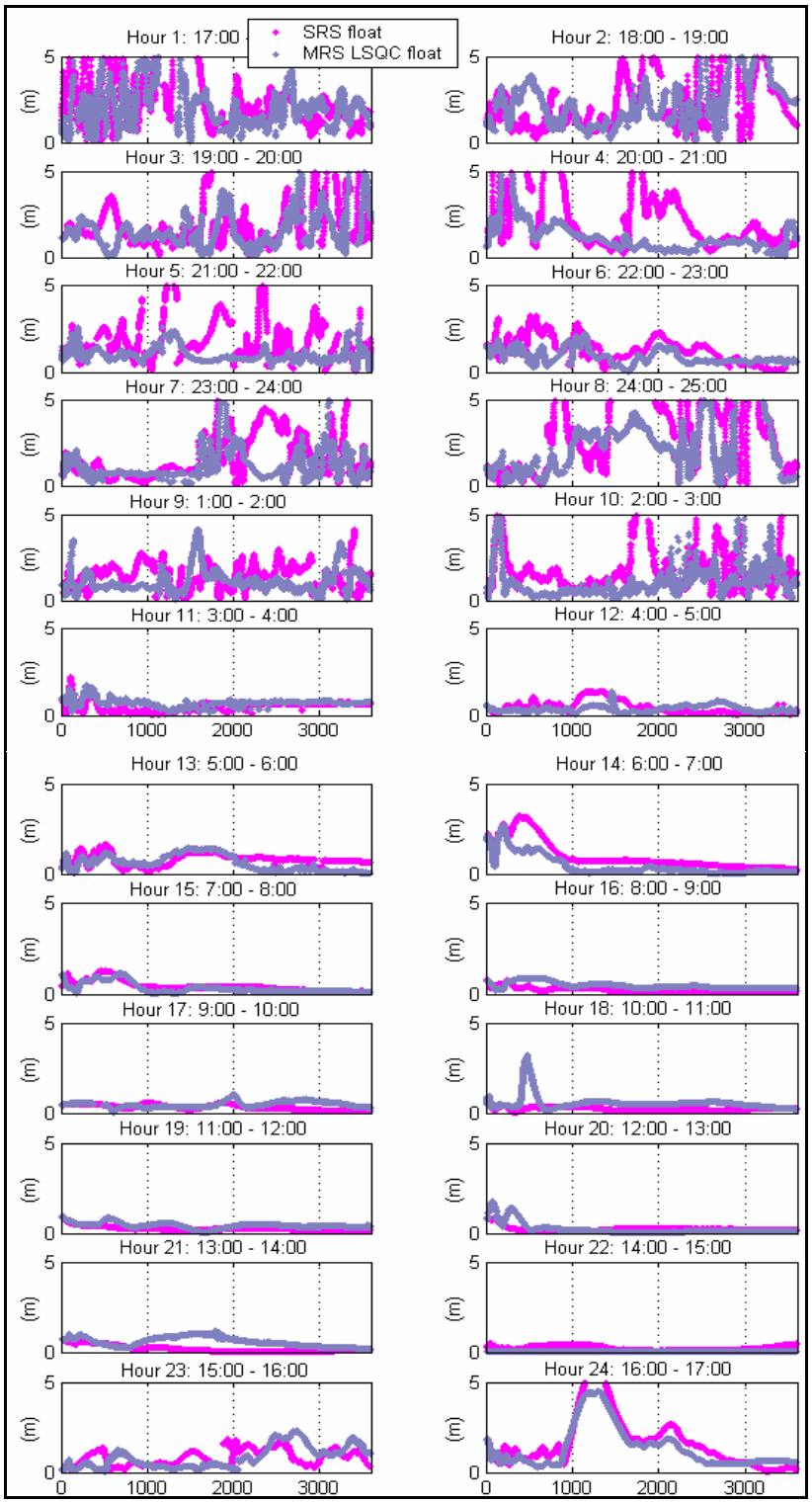

Figure 4.51: Converging 3D position accuracy and ambiguity status in L1 mode for 24 one-hour segments - 8 November 2004

The average and maximum 3D position errors for the first 15 hours are shown on the left-hand side of Figure 4.52 and 4.53. The right-hand side of the figures are for the average and maximum position error of the final 9 hours of each data set. The MRS LSQC approach yields a 22% improvement on average during the first 15 hours of the day but no improvement, on average, during the last 9 hours.

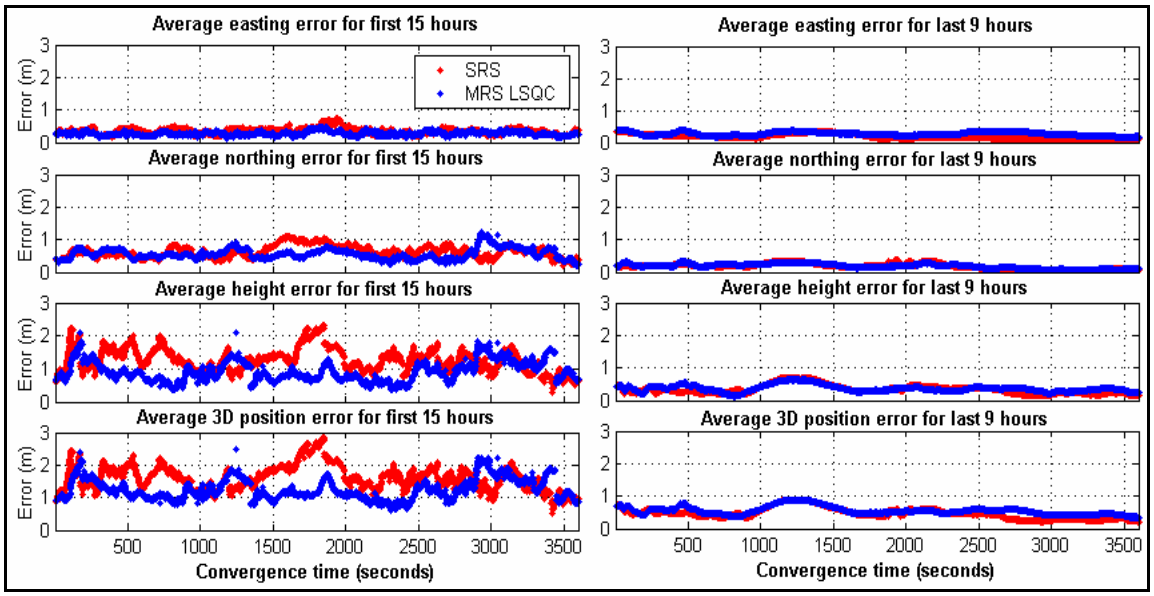

Figure 4.52: Average absolute converging 3D position accuracy in L1 mode for 8 November 2004, separately for the first 15 hours (left) and for the last 9 hours (right)

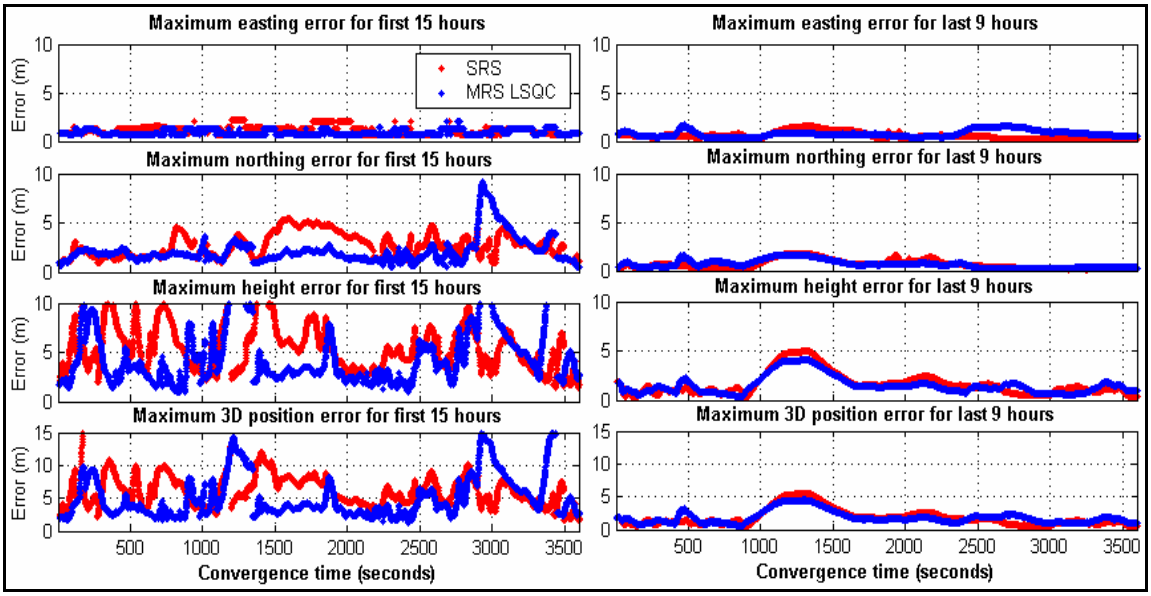

Figure 4.53: Maximum absolute converging 3D position error in L1 mode for 8 November 2004, separately for the first 15 hours (left) and for the last 9 hours (right)

Table 4.26: Statistics for the average and maximum converging 3D position error in L1 mode - 8 November 2004

	Average				Maximum			
	RMS (cm)				RMS (cm)			
	E	N	H	3D	E	N	H	3D
SRS for first 15	37	66	132	166	120	987	1980	2496
MRS LSQC for first 15	29	58	97	129	429	874	1455	1934
Improvement (%) for first 15	19	12	27	22	-258	11	27	23
SRS for last 9	20	20	36	50	67	182	325	447
MRS LSQC for last 9	28	20	38	56	248	178	343	510
Improvement (%) for last 9	-35	0	-6	-14	-269	2	-6	-14

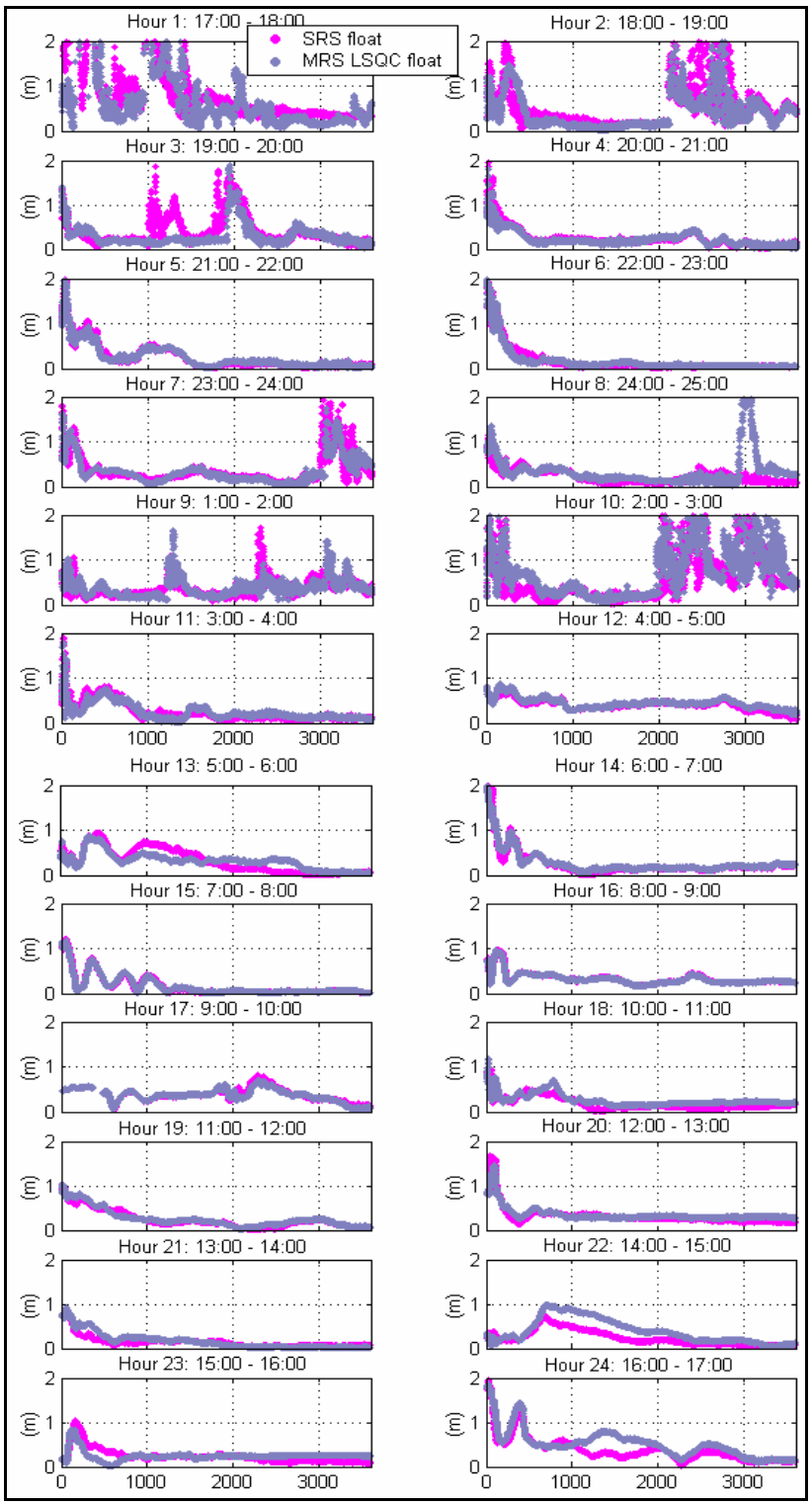

Figure 4.54: Converging 3D position accuracy and ambiguity status in IF mode for 24 one-hour segments - 8 November 2004

The IF converging position solution errors for this data set are presented in Figure 4.54. Ionospheric error is eliminated using IF observables, leading to more accurate converging position solutions. Generally, the position solutions converge to centimetre level accuracy after 1 hour, even during the segments of high ionospheric effects. Although the largest error (ionospheric) is eliminated in this case, the other effects of the active ionosphere on GPS measurements (such as cycle slips or loss of lock) were still evident when using IF observables (e.g. during segments 1, 2, 3, 7, 9 and 10). The MRS LSQC approach offers some improvement during segments 1, 2 and 3. The average and maximum 3D position solution errors for the segments are shown in Figure 4.55 and Figure 4.56, respectively, with associated statistics given in Table 4.27. On average, the SRS and MRS approaches perform similarly during the first 15 hours; however the SRS approach outperforms the MRS approach by a few centimetres during the last 9 hours. This can be explained by the fact that the SRS approach in this case yields, a lower noise level, as compared to the MRS approach, while the effect of the ionosphere is eliminated.

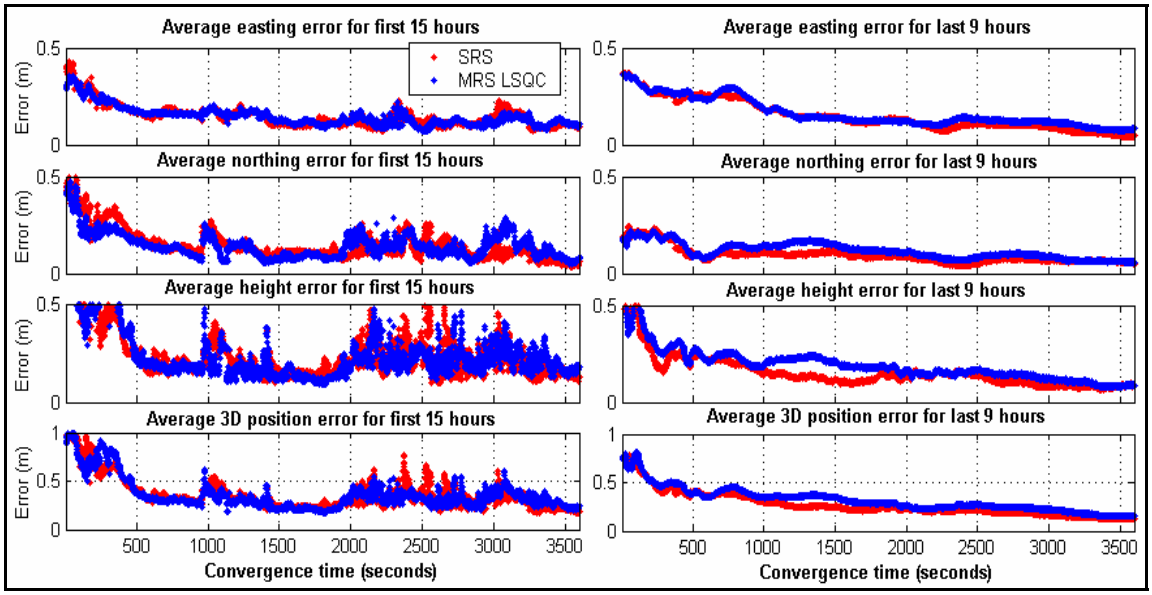

Figure 4.55: Average absolute converging 3D position accuracy in IF mode for 8 November 2004, separately for the first 15 hours (left) and for the last 9 hours (right)

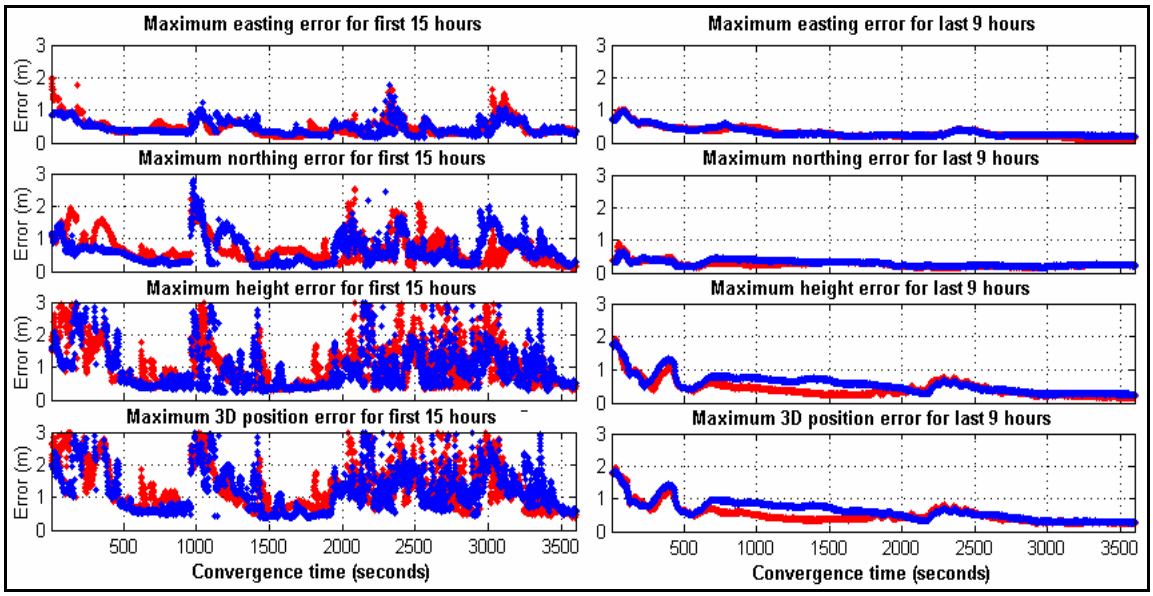

Figure 4.56: Maximum absolute converging 3D position error in IF mode for 8 November 2004, separately for the first 15 hours (left) and for the last 9 hours (right)

Table 4.27: Statistics for average and maximum converging 3D position error in IF mode - 8 November 2004

	Average				Maximum			
	RMS (cm)				RMS (cm)			
	E	N	H	3D	E	N	H	3D
SRS for first 15	16	17	28	41	54	251	426	613
MRS LSQC for first 15	15	16	28	40	231	237	416	595
Improvement (%) for first 15	6	6	0	2	-328	6	2	3
SRS for last 9	17	10	17	30	36	93	157	270
MRS LSQC for last 9	18	12	21	34	161	111	190	309
Improvement (%) for last 9	-6	-20	-24	-12	-347	-19	-21	-14

Figure 4.57 shows the 3D position solution accuracy using L1 and L2 observations with an ionospheric error model and attempts to fix the ambiguities. The pink and red lines are for float and fixed SRS solutions, respectively; the light blue and blue lines symbolize float and fixed MRS LSQC solutions, while the green and dark green are for MRS TC solutions. During the active ionosphere period (e.g. segments 1 to 12), the stochastic model is not effective in modeling the active ionospheric error. This becomes even harder when the quality of the measurements is corrupted by cycle slips and tracking lock is lost. For most of the first 15 segments, the ambiguities remain float. During some segments (such as 4, 7 and 12), they are fixed - but to wrong values - leading to a long-term biased

position solution error of more than one metre. This is observed for both SRS and MRS LSQC approaches during segment 4, but for only MRS LSQC during segments 7 and 12. The MRS TC approach cannot fix the ambiguities during any of these high ionosphere segments. Figures 4.58 and 4.59 depict the average and maximum position solutions of the segments, respectively, while Figure 4.60 shows the average percentages of ambiguity fixing for the segments. On average, the SRS approach performs the worst during the high ionosphere period, providing an average 3D position error of 1.2 m. The MRS LSQC approach yields a 21% improvement with an RMS 3D position error of 98 cm. The MRS TC approach yields a significant improvement of 50% in this case, yielding an RMS 3D position accuracy of 55 cm. The maximum values are also reduced equivalently through the use of MRS approaches. During the low ionosphere period, however, the SRS approach performs very well, resulting in no improvement offered by the MRS LSQC approach. However, the MRS TC approach still yields a small improvement of a few centimetres.

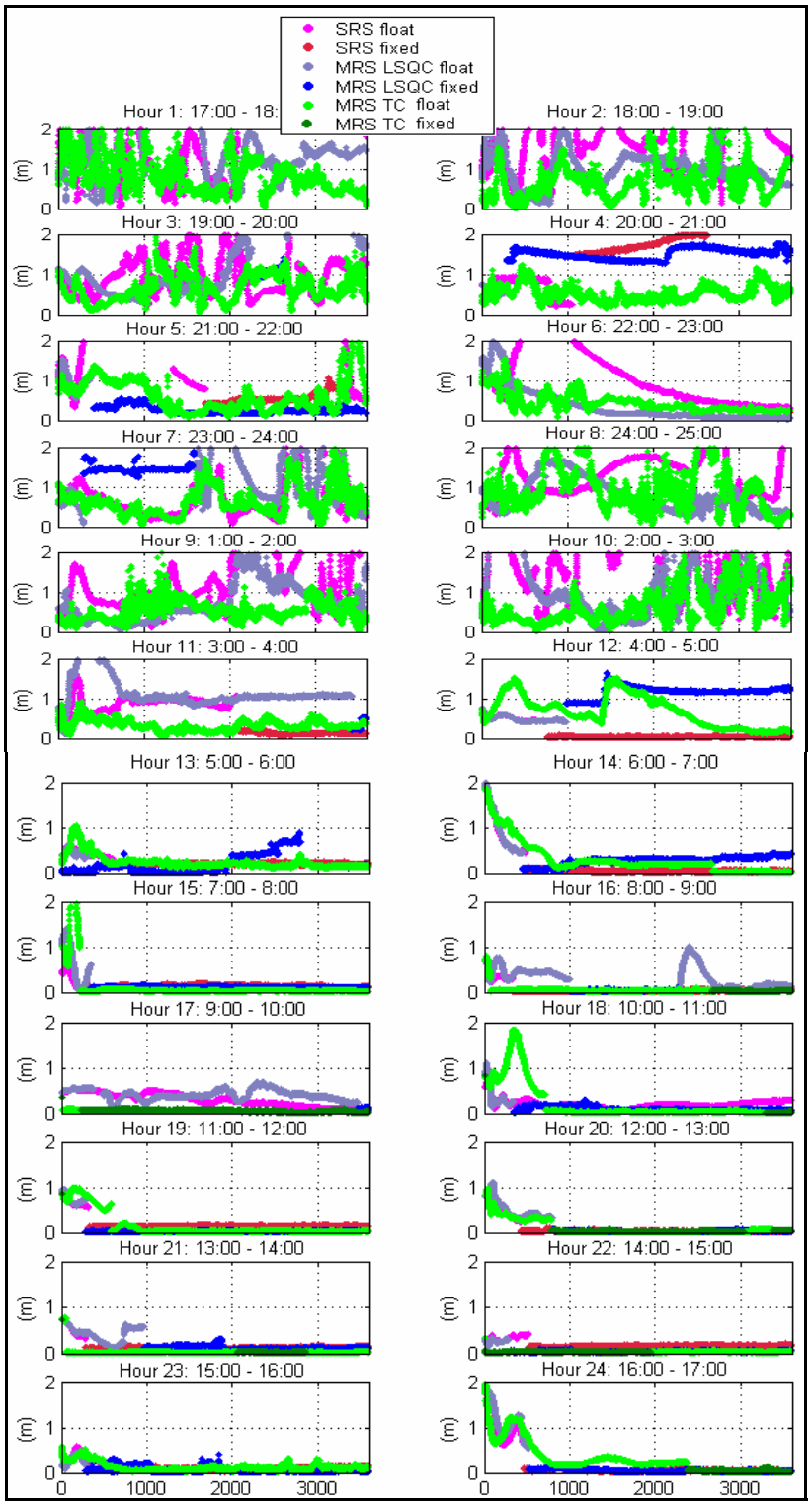

Figure 4.57: Converging 3D position accuracy and ambiguity status in L1/L2 mode for 24 one-hour segments - 8 November 2004

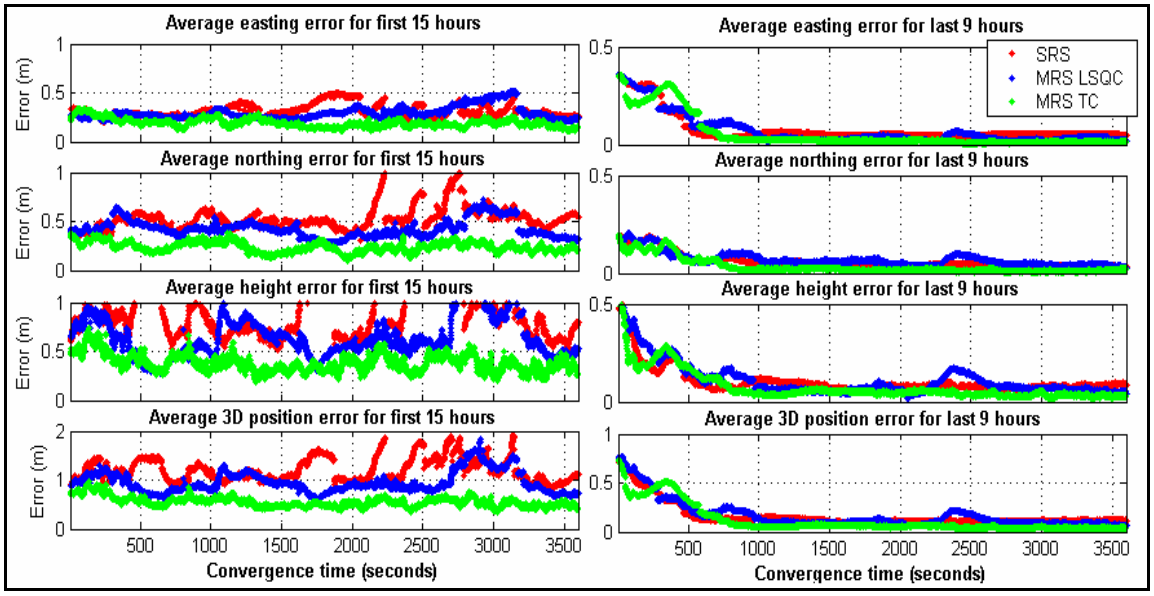

Figure 4.58: Average absolute converging 3D position accuracy in L1/L2 mode for 8 November 2004, separately for the first 15 hours (left) and for the last 9 hours (right)

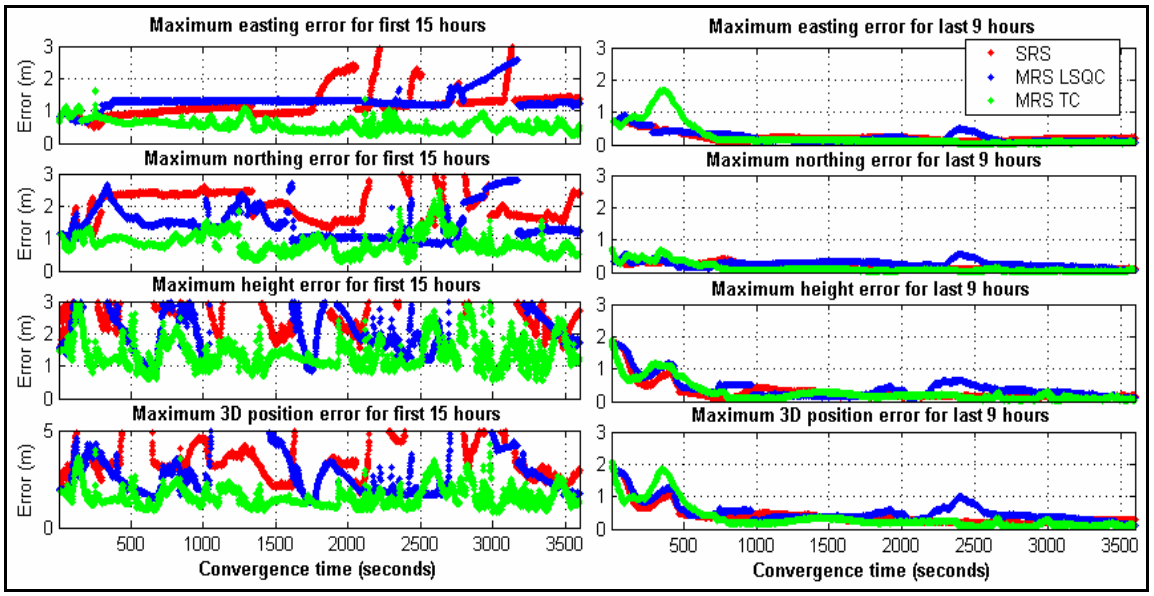

Figure 4.59: Maximum absolute converging 3D position error in L1/L2 mode for 8 November 2004, separately for the first 15 hours (left) and for the last 9 hours (right)

Table 4.28: Statistics for average and maximum converging 3D position error in L1/L2 mode - 8 November 2004

	Average				Maximum			
	RMS (cm)				RMS (cm)			
	E	N	H	3D	E	N	H	3D
SRS for first 15	32	55	92	124	132	818	1379	1853
MRS LSQC for first 15	30	44	68	98	453	652	1019	1473
Improvement (%) for first 15	6	22	26	21	-243	20	26	21
MRS TC for first 15	20	25	39	56	299	369	590	844
Improvement (%) for first 15	38	55	58	55	-127	55	57	54
SRS for last 9	11	7	12	20	28	64	112	183
MRS LSQC for last 9	11	8	14	22	96	71	129	199
Improvement (%) for last	0	-14	-17	-10	-242	-11	-15	-9
MRS TC for last 9	10	5	11	19	93	48	100	168
Improvement (%) for last 9	9	29	8	5	-232	25	11	8

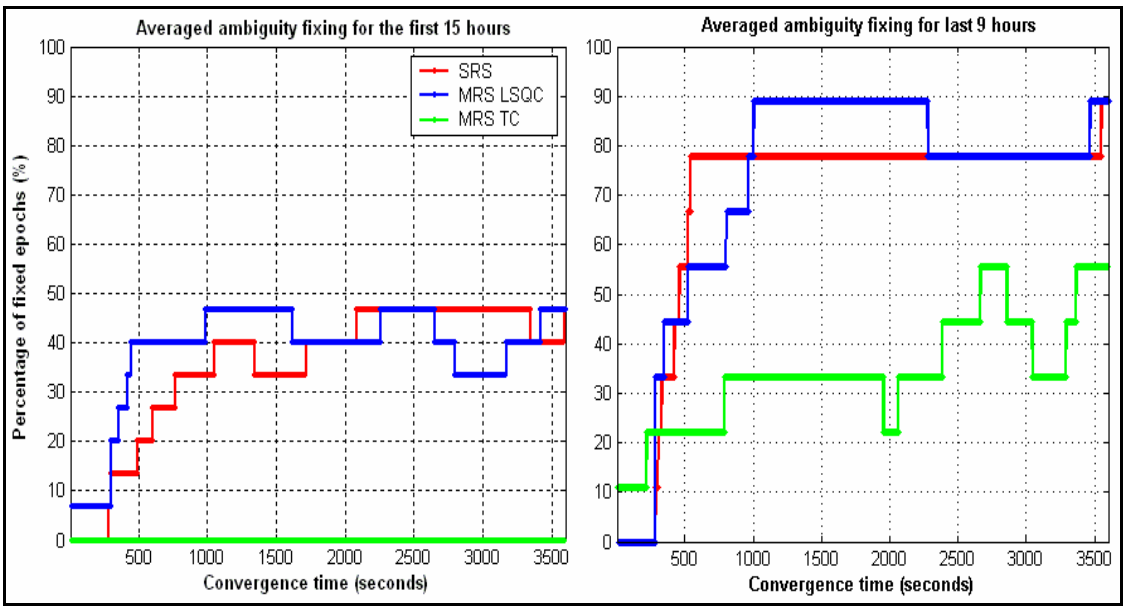

Figure 4.60: Average ambiguity status during convergence in L1/L2 mode for 6 April 2004, separately for the first 15 hours (left) and for the last 9 hours (right)

4.1.4 Impact of MRS LSQC Network Initialization

The MRS LSQC approach makes an assumption of having all ambiguities resolved correctly prior to correction generation. In order to resolve the network ambiguities, a certain amount of time is required and this period is considered as the time for the network to be initialized. The duration of network initialization largely depends on network configuration, baseline lengths and atmospheric conditions. For the data set presented herein, the network initialization last for several minutes under quiet and medium atmospheric conditions. Under active atmospheric conditions, however, it can take a very long time for the network ambiguities to be fixed. Also one has to assume that the data is mostly free of cycle slips or losses of phase lock.

Evaluating the performance of the MRS approach during this period of time is another interesting and challenging aspect. The work presented herein could initially lead to some suggestions based on the case-specific network configuration and atmospheric conditions. In the convergence analysis of the three data sets, the first one-hour segments contain the MRS LSQC corrections generated during the initialization period. For most of the first segments, the MRS approach yields more accurate position solutions than the SRS approach in both single-frequency and dual-frequency modes. Based on these limited results, it would appear that background network ambiguity convergence is not a major issue for missions of this type.

4.2 Kinematic Test Results

A kinematic test was carried out on 22 October 2004 and the obtained data are analysed in post-mission herein using the MRS LSQC and SRS approaches. The network configuration is shown in Figure 4.61. It uses four reference stations, namely AIRD, COCH, STRA and BLDM. The AIRD station was chosen to be the primary reference station in this case and the prediction point placed at the UOFC station position. The UOFC station did not act as a rover in this case but as a single reference station located in the middle of the geographical area covered by the kinematic trajectory to ensure that the rover-UOFC distance was less than 2 km, as shown in Figure 4.62. During the kinematic test, a NovAtel 600 antenna was mounted on the roof of a vehicle moving with an average speed of 60 km/h on the above-described kinematic trajectory. The kinematic

route surrounds the University of Calgary campus and through a sparse residential area. This constitutes a mainly open-sky tracking condition. The kinematic condition is associated with high Doppler effects and multipath. In addition, the number of observed satellites is rapidly changed, dropping to four at several points during the test. Data was collected for analysis when the vehicle completed the circuit four times - the herein so-called four loops of data. The test lasted for approximately 45 minutes, from 19:32 to 20:14 UTC time (corresponding to 12:32 to 13:14 local time). The local K value reported at the MEANOOK magnetometer station was at an average level of 2 during this testing period and this constitutes a quiet ionospheric condition.

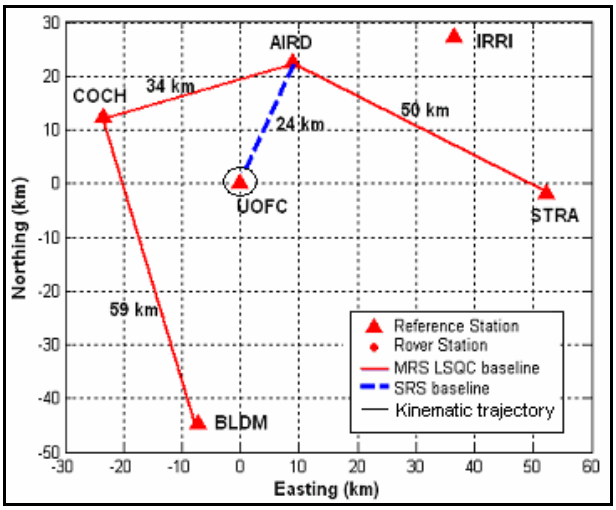

Figure 4.61: Network configuration for kinematic test of the MRS LSQC approach

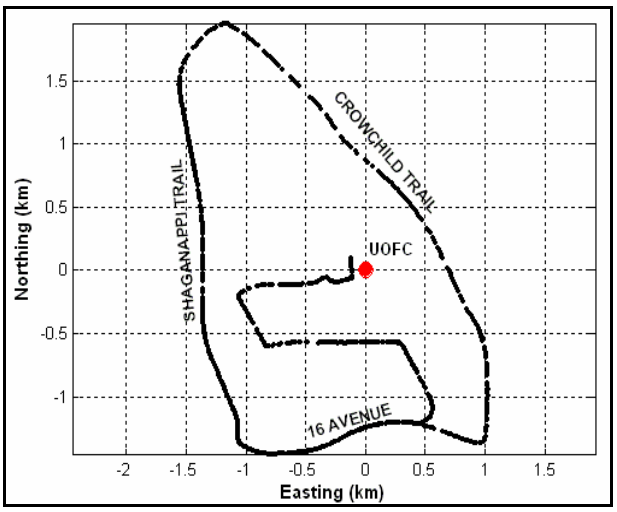

Figure 4.62: Kinematic test trajectory

With a very short distance of less than 2 km to the nearest reference station, the SRS ionospheric-free position solutions estimated using UOFC as the reference station are considered to be the best possible reference one can obtain in this case, assuming that the spatially uncorrelated errors such as multipath and noise are low. The use of a 2 km baseline will obviously yield a reduction in differential tropospheric and satellite orbital errors, as compared to the use of a 24 km baseline. In order to produce the kinematic "reference", forward and backward averaged solutions were estimated in one run using GrafNav^{TM}. They are shown in Figure 4.63, along with the ambiguity status and number of satellites used during solution estimation. The grid lines are used to mark the time separating the loops in this figure. Although the IF observables are used over a very short baseline, kinematic multipath, noise and especially cycle slips have degraded the position solutions to a certain degree, especially at mid-mission during loop 3, from 12:54 to 13:03. The reported cycle slips detected on the kinematic rover L1 and L2 data are represented by the red crosses in Figures 4.64 and 4.65. These cycle slips are due to

signal masking along the trajectory. The actual number of slips will vary between repeated trajectories due to the changing satellite geometry. For further analysis of these solutions, Figure 4.66 presents the separations obtained between the GrafNav™ forward and backward position solutions, which are large during loop 1 and loop 3. This suggests that the solution's so called "reference" herein cannot be treated as error free references but only to compare with the solutions provided later by the MRS approach and its corresponding SRS approach. For further comparisons, only segments of the average trajectory where the forward and backward runs are in agreement within five centimetres will be used in the sequel. These are represented by the green solutions shown in Figure 4.66.

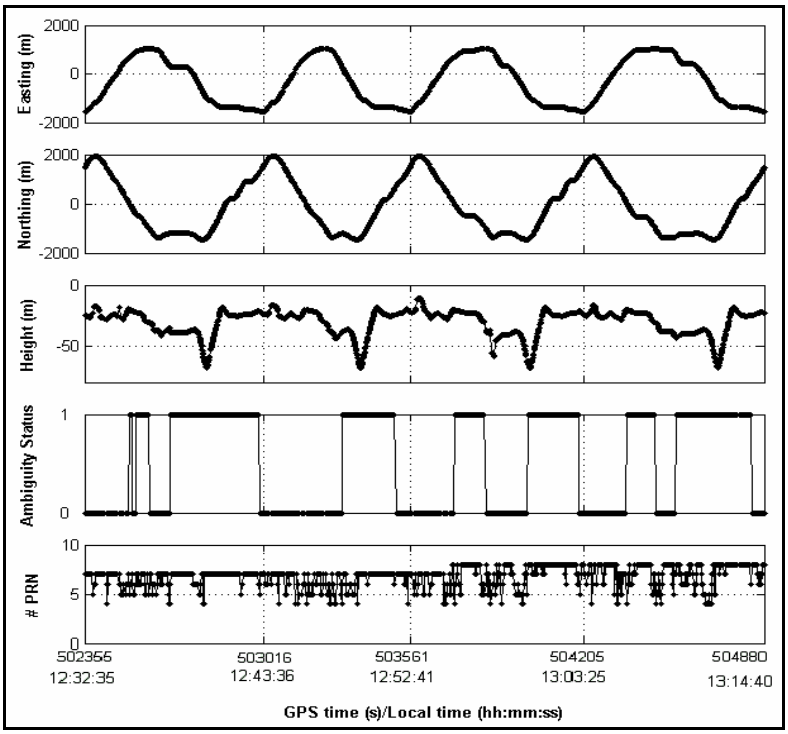

Figure 4.63: Kinematic reference solutions: IF forward-backward averaged using GrafNav with UOFC reference station

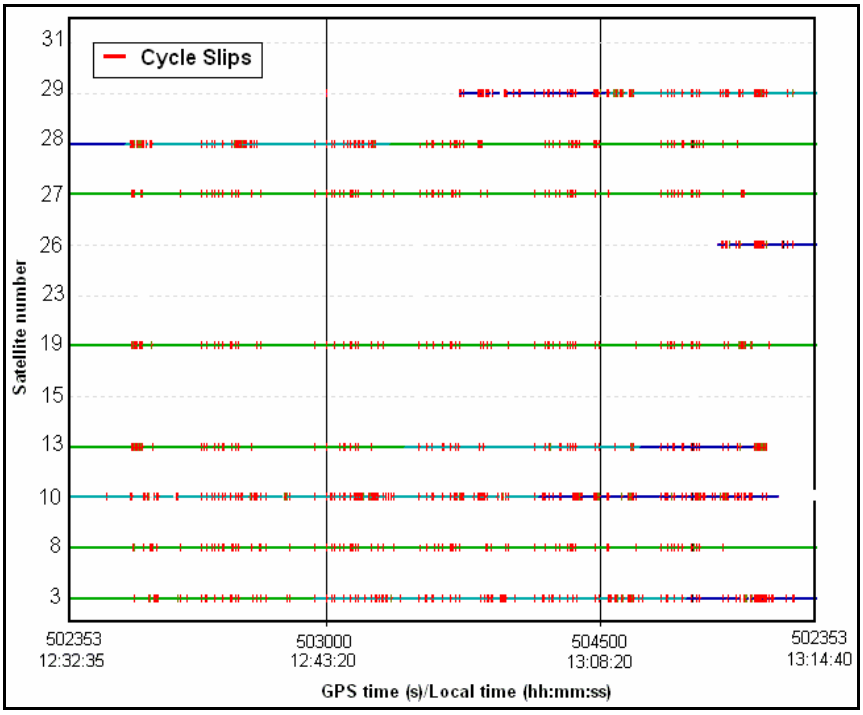

Figure 4.64: Reported cycle slips on L1 measurements obtained at kinematic rover

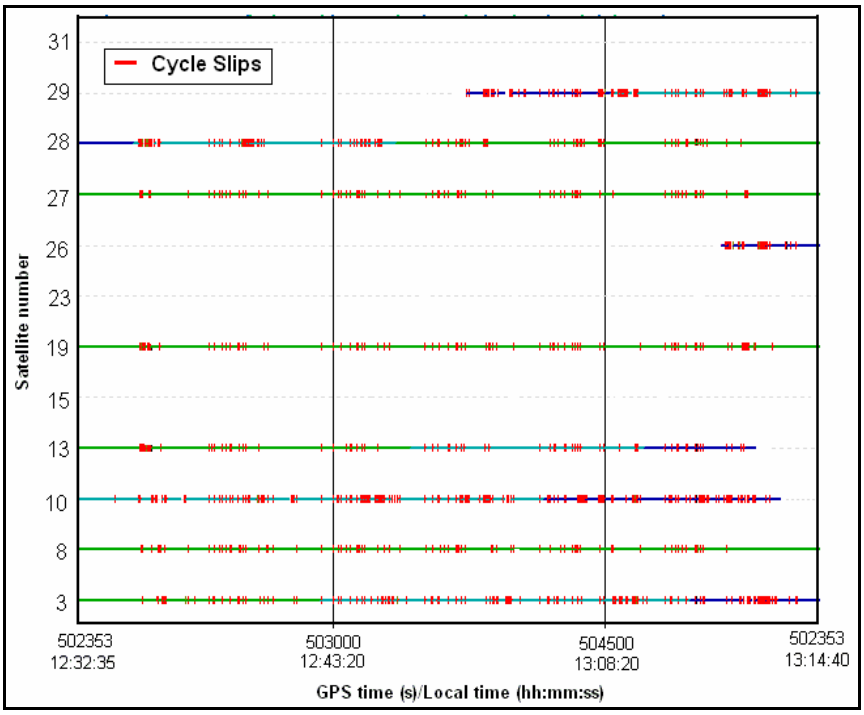

Figure 4.65: Reported cycle slips on L2 measurements obtained at kinematic rover

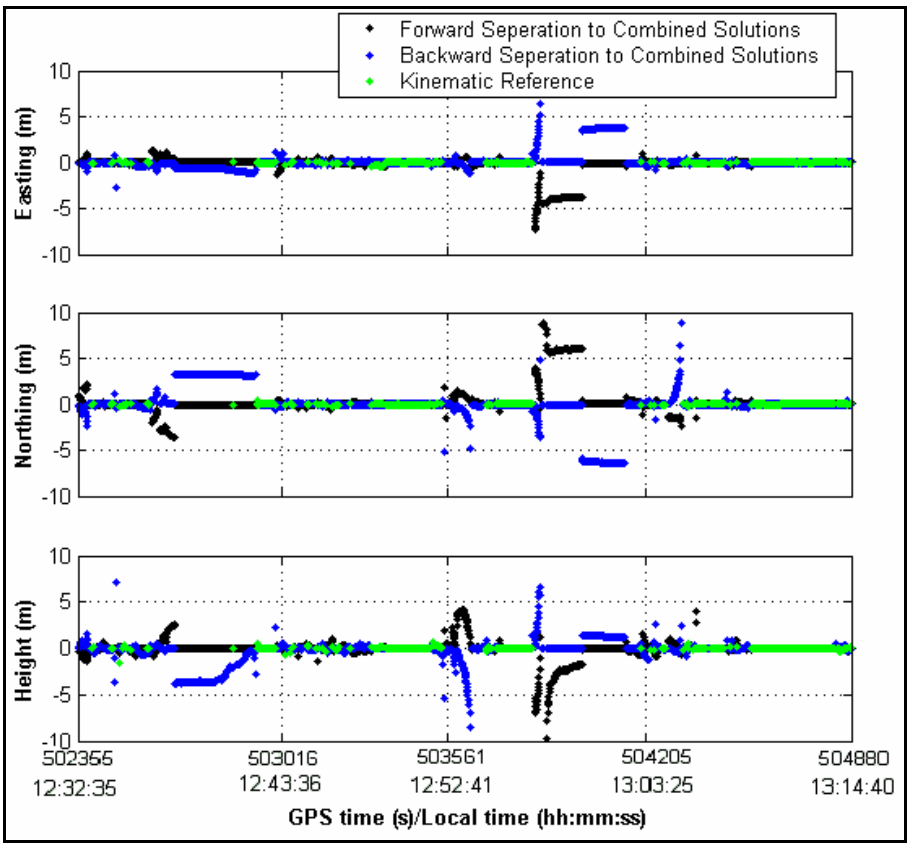

Figure 4.66: Kinematic reference: forward and backward separation from the averaged solutions

The network double-difference corrections generated during testing for AIRD-UOFC are presented in Figure 4.67. The ionospheric condition was quiet and the network performs very well in resolving the ambiguities. The percentages of ambiguities fixed were 99%, 99% and 97%, respectively for baselines AIRD-COCH (34 km), AIRD-STRA (50 km) and COCH-BLDM (59 km). The corrections are therefore reliable; their magnitude is only in the order of a few centimetres, as expected. For example, a RMS of 4.7 cm correction was obtained for L1 observations, 7.5 cm for L2, 1.2 cm for IF and 3.0 cm for

GF. These are equivalent to 2 ppm error on L1 and 1.3 ppm on GF for the ionospheric error.

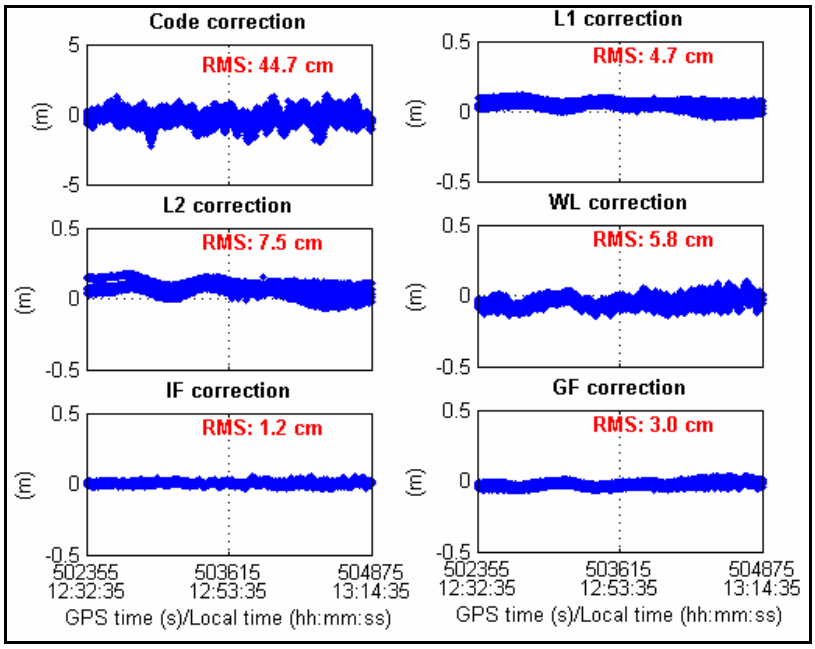

Figure 4.67: Double difference network corrections generated by MRS LSQC for all satellite pairs for 22 October 2004 during the kinematic test

The corrected observations at the primary reference station (AIRD) are used to produce the MRS LSQC position solutions using GrafNav™. In addition, the raw AIRD observations are used to estimate the equivalent SRS solutions. These are compared against the SRS 2-km baseline "reference" described above. Figure 4.68 presents the L1 position solution differences when comparing the SRS and the MRS LSQC solutions to the SRS short baseline "reference". Figure 4.69 shows the same comparison but for SRS and MRS LSQC solutions in IF mode. Statistics are provided in Table 4.29. These differences are not considered as the position errors in this case due to the lack of true

references; however, both SRS and MRS LSCQ approaches yield very similar results in both cases of using IF observables or L1 observations. The IF position solutions are not significantly different from the L1 solutions. This is due to the ionosphere being very quiet over the region leading to a very small ionospheric differential error on L1. Cycle slips and noise herein have a significant impact on the degree of solution degradation.

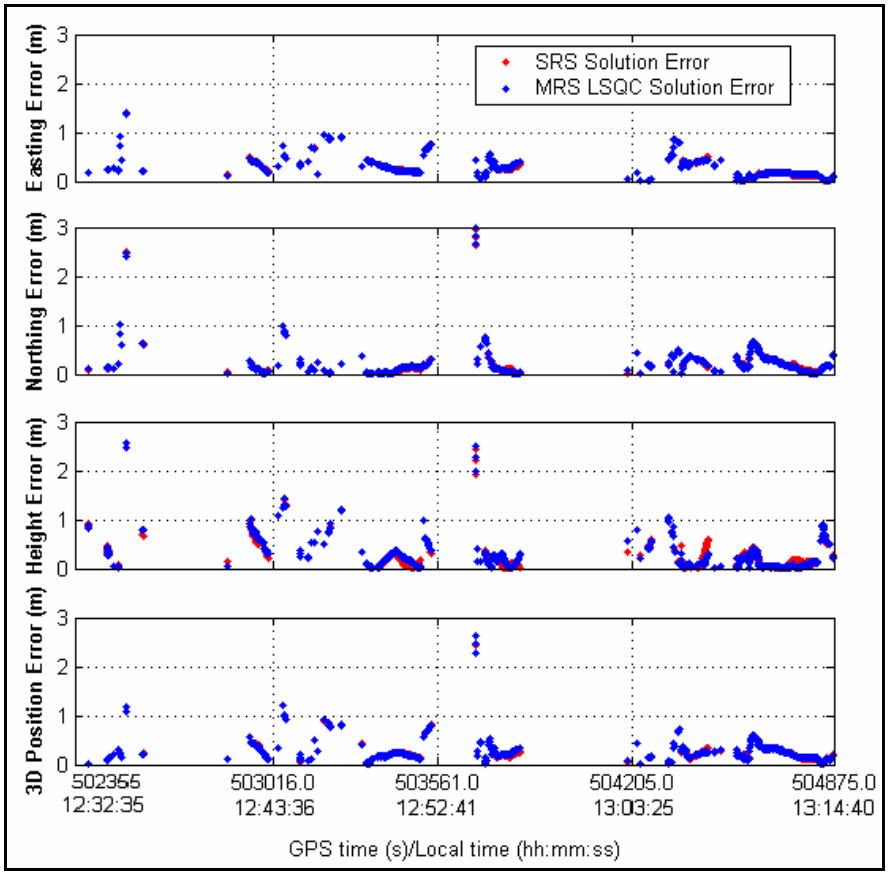

Figure 4.68: Kinematic position solution errors in L1 mode

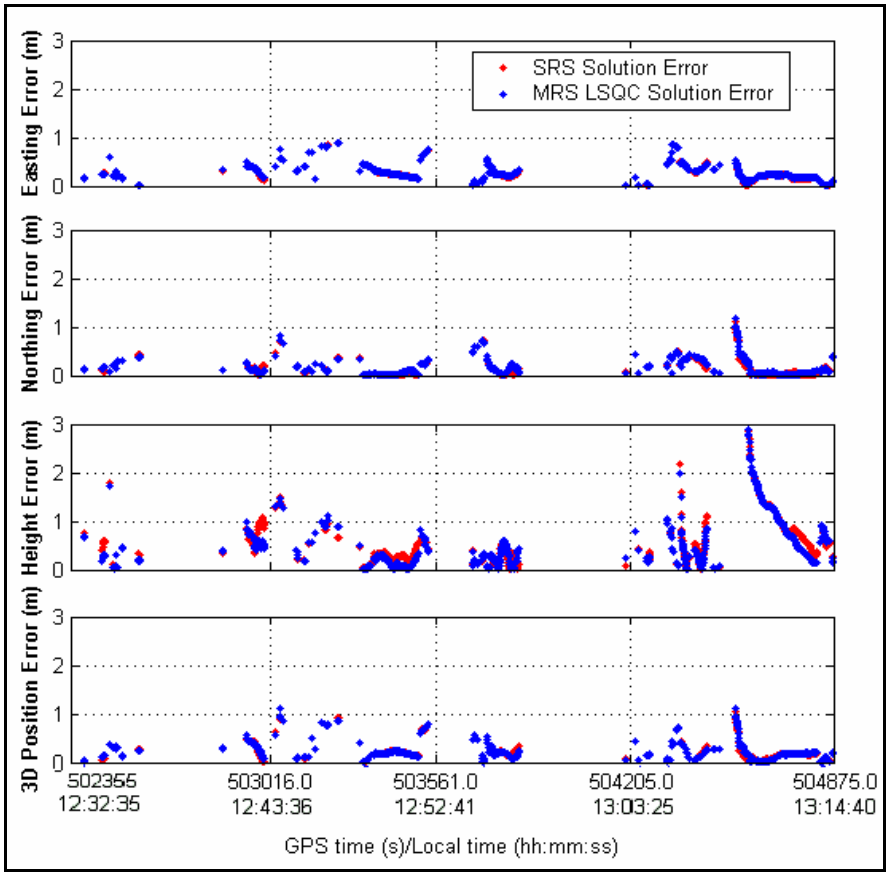

Figure 4.69: Kinematic position solution errors in IF mode

Table 4.29: Statistics for kinematic SRS and MRS position solution error

RMS (cm)	IF solutions error				L1 solutions			
	E	N	H	3D	E	N	H	3D
SRS	31	21	124	28	32	33	49	34
MRS LSQC	31	23	119	28	32	33	49	34
Improvement (%)	0	-9	4	0	No Improvement			

4.3 Real-Time Static Test Results

A real-time test was also carried out to evaluate the performance of the MRS least-squares collocation approach. In contrast to the post-mission test, the real-time test requires the availability of real-time communication links, a real-time single baseline processing software and RTCM encoder and decoder components. The UOFC station acted as the rover in this test. Although the station is in static mode, the obtained data was processed in kinematic mode to evaluate epoch-by-epoch position solutions. Due to the station coordinates being well determined, the "reference trajectory" is known all the time during the evaluation. The test procedure is shown in Figure 4.70. TCP/IP communication links were used to transfer data from the reference stations to the control processing centre located in the PLAN Group lab at University of Calgary. Serial links were used to establish communication among the computers within the processing centre. The single baseline carrier phase-based processing software real-time FLYKINRT+^{TM} was used to estimate the rover's position solution. FLYKINRT+^{TM} was developed by the PLAN Group at the University of Calgary, supporting different reference station data formats such as raw binary OEM4, RINEX and RTCM 2.3 messages; it, therefore, allows both real-time (RT) and post-mission (PM) processing (Liu 2003). The real-time LSQC MultiRef^{TM} software was used herein. Being distinct from the post-mission LSQC MultiRef^{TM}, it allows real-time communication links to receive the reference station's data via a real-time communication link instead of reading from files. After resolving the ambiguities, generating the corrections, and applying the double-difference corrections to the primary reference station observations, a virtual reference station (VRS) is generated,

located one third of the distance from the rover to the closest reference station. The corrected observables obtained at the primary reference station are then geometrically transferred to the VRS location. These VRS observables are then encoded into RTCM 2.3 messages and passed to FLYKINRT+^{TM}. The RTCM 2.3 messages are decoded and used, along with the real-time rover observations, to estimate the rover position solutions. These solutions are referred to as RT MRS LSQC solutions. All necessary data, such as the corrected and raw primary reference station observations and the rover data are saved to produce the equivalent SRS and MRS position solutions in post-mission.

The test lasted 9 hours, from approximately 20:32 of 16 February 2005 to 05:34 of 17 February 2005, UTC time (corresponding to 13:32 to 22:34 local time). The network configuration used in this test is shown in Figure 4.71, employing four reference stations surrounding the rover station UOFC. The double-difference corrections between the PRS AIRD and the rover UOFC are presented in Figure 4.72. The effect of ionospheric condition is expected to be low, based on low reported local K values of 2 and 1 (on average) for every three hours throughout the 9-hour testing duration. In order to generate the corrections, the network ambiguities were resolved. The percentages of ambiguities fixed are 99%, 83% and 94% for baselines AIRD-COCH, AIRD-STRA and COCH-BLDM, respectively.

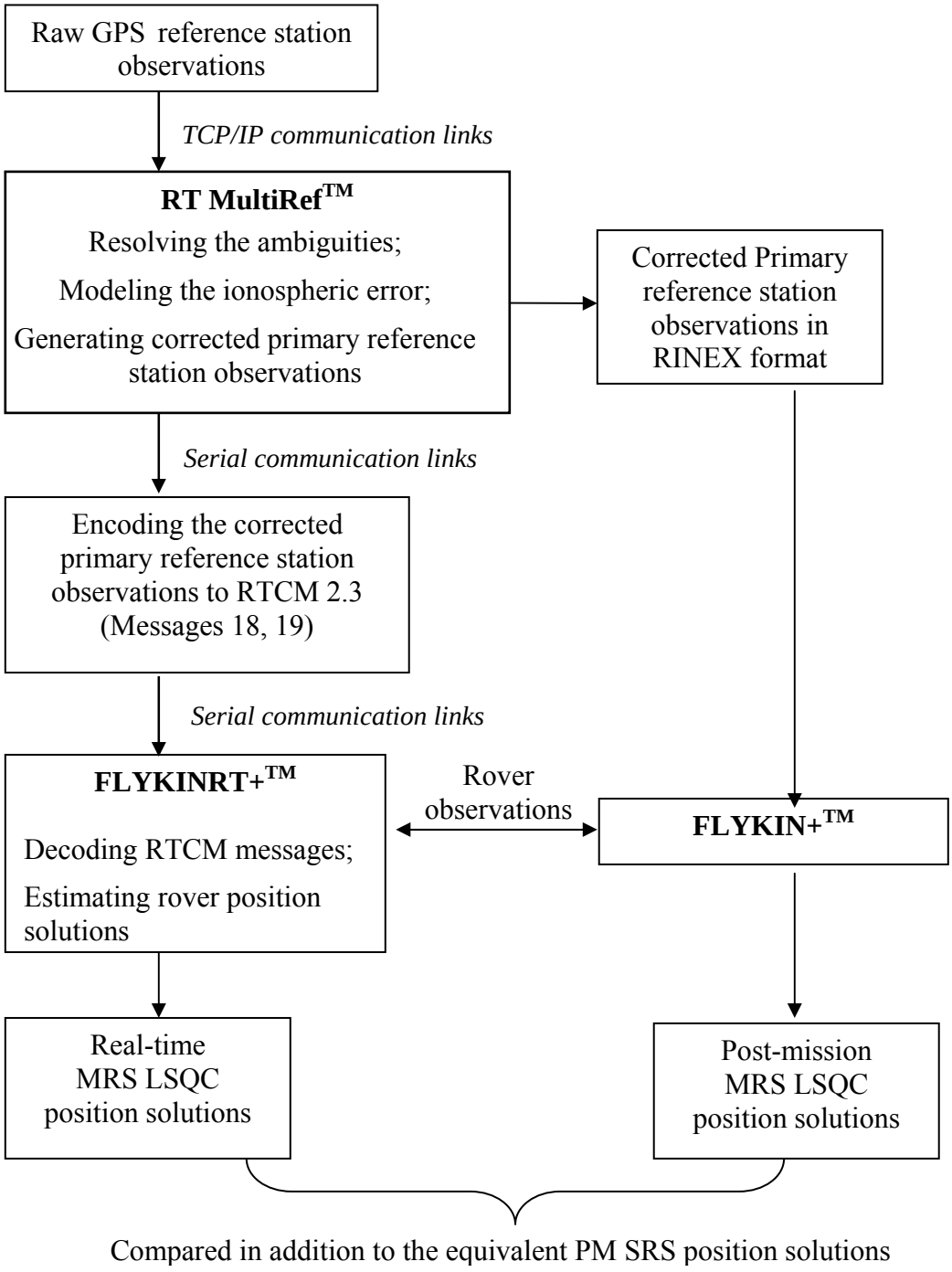

Figure 4.70: Procedure for applying and evaluating the real-time (RT) MRS LSQC approach

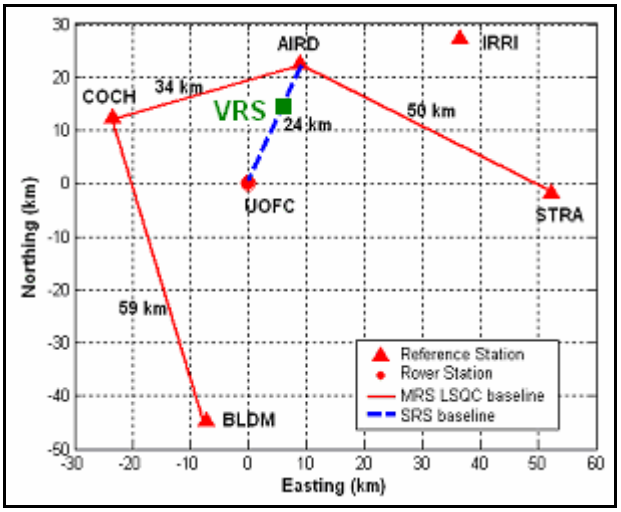

Figure 4.71: Network configuration for real-time test of the MRS LSQC approach

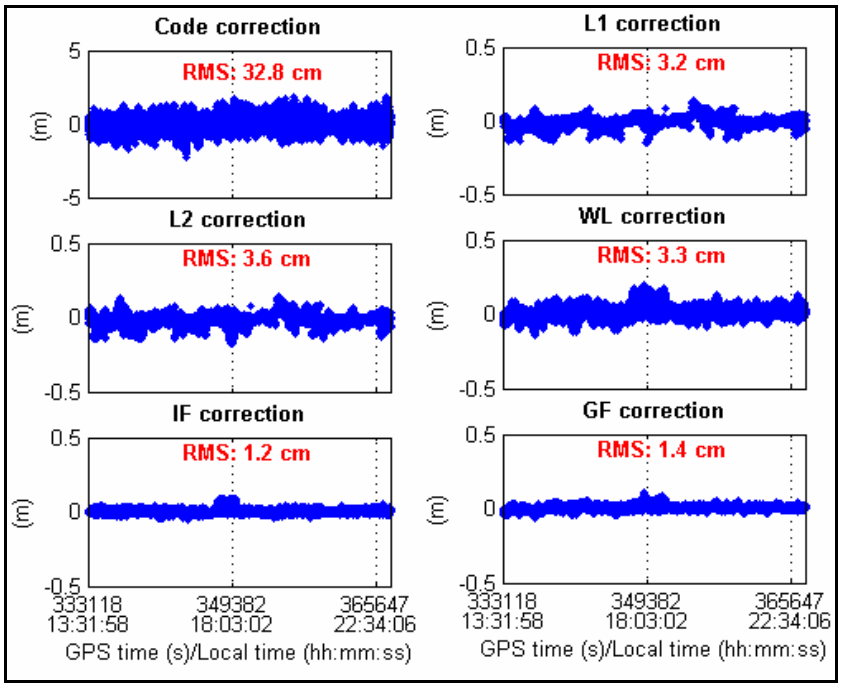

Figure 4.72: Double-difference network corrections during the real-time test

The real-time estimated MRS LSQC position solutions (blue) in comparison with the equivalent post-mission SRS position solutions (red) are shown in Figure 4.73. Unfortunately, FLYKINRT+^{TM} software is not capable of providing IF fixed solutions;

only IF float solutions are estimated herein. The statistics are presented in Table 4.30 for the first two hours of converging position solutions and for the last seven hours of steady position solutions. Overall, the MRS LSQC approach offers results comparable to the SRS approach. During the convergence phase, the MRS LSQC solutions are more accurate than the SRS solutions by only 1 cm. During the steady period, the MRS LSQC approach performs slightly worse than the SRS approach but only by a few millimetres. This result is reasonable, considering that the SRS solutions do not suffer from a significant ionospheric effect, and other differential errors are relatively small. By contrast, the MRS approach is affected by more noise in this case.

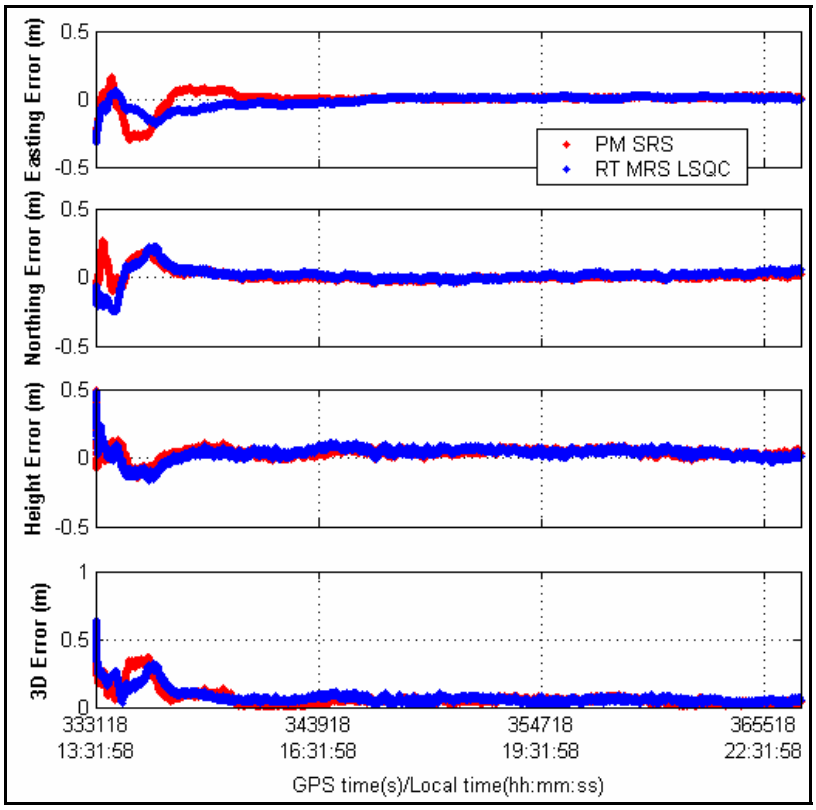

Figure 4.73: Real-time MRS LSQC position solution accuracy in comparison with post-mission SRS solution accuracy using IF observations

Table 4.30: Statistics for real-time position accuracy in IF mode

	First 2 hours of filer convergence				Last 7 hours			
	RMS (cm)				RMS (cm)			
	E	N	H	3D	E	N	H	3D
SRS	13	9	7	18	1	1	4	5
MRS LSQC	9	11	8	17	2	2	5	5
Improvement (%)	31	-22	-14	6	No improvement			

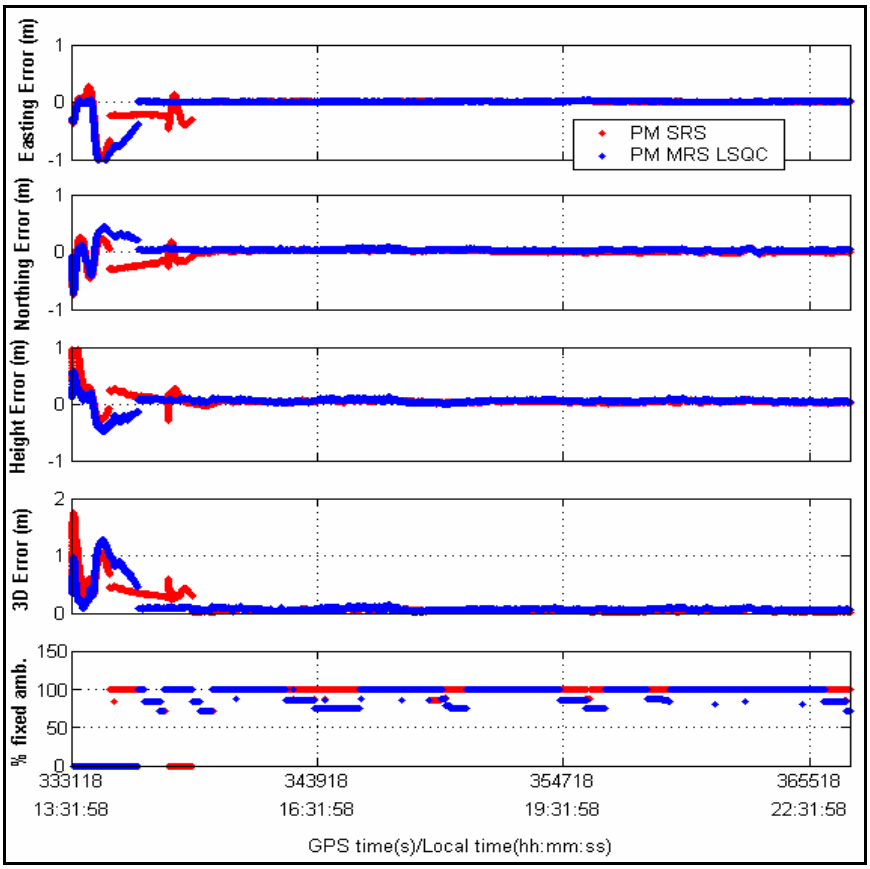

Figure 4.74: MRS LSQC position solution accuracy using real-time corrected L1 observations and FLYKIN+™ (post mission) in comparison with post-mission SRS solution accuracy

Table 4.31: Statistics for real-time position accuracy in L1 mode

	First 2 hours of filer convergence				Last 7 hours			
	RMS (cm)				RMS (cm)			
	E	N	H	3D	E	N	H	3D
SRS	32	20	31	49	1	2	4	5
MRS LSQC	42	20	20	50	1	3	5	6
Improvement (%)	No improvement				No improvement			

The rover position solutions using L1 observations are shown in Figure 4.74 for both the SRS (red) and MRS LSQC (blue) approaches. These MRS solutions are estimated in post-mission but using the saved real-time corrected observables from the primary reference station. The SRS position solutions are estimated in post-mission. The statistics are shown in Table 4.31. The two approaches perform extremely well in this case, yielding an accuracy for position solution of several centimetres after convergence. This is because the ionospheric error is fairly constant over the region, resulting in a small differential ionospheric error. The SRS approach, however, performs better in resolving the L1 ambiguities. During convergence phase, the MRS approach yields faster convergence solutions.

CHAPTER 5

CONCLUSIONS AND RECOMMENDATIONS

The following conclusions are drawn based on the observed results, and are valid for the representative data sets and network configuration used.

The results are consistent with previous studies and confirm that MRS approaches offer improvement relative to the SRS approach on various scales, ranging from unfavourable to significant depending on many parameters. The degree of efficiency of the MRS LSQC approach depends mainly on the ability to estimate the ionospheric error and resolve the ambiguities. The largest improvement in this data set (approaching 70%) was obtained under medium ionospheric conditions with the use of L1 observations. This is due to the MRS LSQC approach's ability to model the spatially correlated errors concurrent with the resolution of network ambiguities. When atmospheric conditions are quiet, the SRS approach performs very well on its own and the gain resulting from the MRS approach is insignificant. High levels of ionospheric activities have a severe impact on both the SRS the MRS approach's means of fixing ambiguities and estimating the ionospheric error. Under these conditions, the MRS LSQC approach yields improvements between (approximately) 0% and 20% using L1 observations. This relatively low level of improvement is disappointing and is caused by a low spatial correlation of ionospheric

effects and also low data quality with cycle slips occurrence under a highly disturbed ionosphere. The advantage produced by the MRS LSQC approaches is also reduced when using ionospheric-free observables under all atmospheric conditions. The MRS LSQC approach however generally provides better performance in convergence, in terms of both faster convergence and more accurate converging position solutions under most of the conditions studied. The accuracy again is however relatively limited.

The MRS tightly-coupled approach, in respect of the range of observed conditions, offers the most accurate position solutions under either quiet or active ionospheric conditions, as compared to the other two approaches; in particular, it yields significantly faster convergence under quiet to medium atmospheric conditions. However, the filter in this case requires greater time to offer fixed ambiguities, although float position solutions are still accurate.

The analysis herein is limited to a medium scale network of four reference stations with baseline lengths ranging from 30 km to 70 km. Ahn (2005) addressed the issue of a larger network scale impact on performance of the MRS approach. A larger scale network with baseline lengths ranging from 50 to 150 km was used therein. Depending on different network configurations, it was found that the MRS approach yields an improvement from 9% to 22% on average in the measurement domain compared to the SRS approach. Overall, there was a marginal improvement of 10% for the IF observables. It remains to be seen as to whether the MRS method would yield significantly better results for a yet

larger scale network, namely with baseline lengths of hundreds of kilometres when using ionospheric-free observables.

In order to extend the research presented herein, the following recommendations are made for prospective future work:

(i) Multiple reference station techniques are still affected by spatially decorrelated high ionospheric errors. In this research, the analysis results are based on only one 24-hour data set under very active ionospheric conditions using a specific network configuration. A possible course of future research may be to confirm this with a larger number of data sets using different network scales.

(ii) As the performance of the MRS LSQC approach heavily depends on the ability to resolve the network ambiguities prior to network correction generation, further investigation on improving the network ambiguity resolution techniques would be beneficial in the future.

(iii) In order to provide a better insight analysis for the algorithm evaluation, the post-mission results produced herein use epoch-by-epoch based measurements and can be used in real time. Further investigations on using batch processing for purely post-mission processing should be carried out. By averaging the

errors over time, this technique would likely provide a significant more accurate solution for cases where real-time results are not needed.

(iv) Within the next few years, new coming GNSS signals, such as the 3rd GPS frequency and GALIEO, obviously offer a significant benefit to users in term of greater signal availability. Various recent studies show the contribution in improving the SRS approach performance when using combined signals (e.g. Julien *et al* 2004, O'Keefe *et al* 2002). The impact of the MRS approach on the new signals should be investigated.

REFERENCES

Ahn Y.W. (2005) Analysis of NGS CORS Network for GPS RTK Performance Using External NOAA Tropospheric Corrections Integrated with a Multiple Reference Station Approach, MSc Thesis, UCGE Reports Number 20211, Department of Geomatics Engineering, The University of Calgary, Canada.

Alves P., Ahn Y.W. and Lachapelle G. (2003) The Effects of Network Geometry on Network RTK Using Simulated GPS Data, CD-ROM Proceedings of ION GPS/GNSS 03, Institute of Navigation, Portland, Oregon, USA, 11 pages.

Alves P., Lachapelle G. and Cannon M.E. (2004) In-Receiver Multiple Reference Station RTK Solution, CD-ROM Proceedings of ION GPS/GNSS 04, Institute of Navigation, Long Beach, California, USA, 9 pages.

Alves P. and Lachapelle G. (2004) A Comparison of Single Reference Station, Correction-Based Multiple Reference Station and Tightly-coupled Methods using Stochastic Ionospheric Modelling. CD-ROM Proceedings of the International Symposium on GPS/GNSS, Sydney, Australia (6-8 December), 14 pages.

Alves P. (2004) Development of two novel carrier phase-based methods for multiple Reference station positioning, PhD Thesis, UCGE Reports Number 20203, Department of Geomatics Engineering, The University of Calgary, Canada. (http://PLAN.geomatics.ucalgary.ca)

Astronomical Institute, University of Bern (2004) Bernese GPS software package, http://www.bernese.unibe.ch/, extract on 4 March 2005.

Brown R.G. and Hwang P.Y.C. (1983) Introduction to Random Signals and Applied Kalman Filtering, 2rd Edition, John Wiley & Sons Inc., New York.

Cannon M.E. (1991) Airborne GPS/INS with an Applications to Aerotriangulations, PhD Thesis, UCGE Reports Number 20040, Department of Surveying Engineering, University of Calgary, Canada.

Dai L., Han S., Wang J. and Rizos C. (2004) Comparison of Interpolation Algorithms in Network-Based GPS Techniques, Navigation, 50(4), pp: 277 – 293.

de Jong C.D., Lachapelle G., Skone S. and Elema I.A. (2002) Hydrography, DUP Blue Print, Delft University Press, The Netherlands.

Environment Canada (2003), Canadian National Climate Data and Information Archive, http://www.climate.weatheroffice.ec.gc.ca/climateData/canada_e.html, extract on 14 Jan 2005

Euler H.J., Keenan C.R., Zebhauser B.E. and Wübbena G. (2001) Study of a Simplified Approach in Utilizing Information from Permanent Reference Station Arrays. Proceedings of the National Technical Meeting of the Satellite Division of the Institute of Navigation, ION GPS/2001, Institute of Navigation, Salt Lake, USA, pp: 379– 391.

Euler H.J., Seeger S., Zelzer O., Takac T. and Zebhauser B.E. (2004a) Improvement of Positioning Performance Using Standardized Network RTK Messages. Proceedings of the National Technical Meeting of the Satellite Division of the Institute of Navigation, ION GPS/2004, Institute of Navigation, San Diego, USA, pp: 453 – 461.

Euler H.J., Seeger S. and Takac F. (2004b) Analysis of biases influencing successful rover positioning with GNSS-Network RTK, CD-ROM Proceedings of the International Symposium on GPS/GNSS, Sydney, Australia (6-8 December), 15 pages.

Fortes L.P.S. (2002) Optimising the Use of GPS Multi-Reference Stations for Kinematic Positioning, PhD Thesis, UCGE Reports Number 20158, Department of Geomatics Engineering, The University of Calgary, Canada.

Gao Y., Li Z. and McLellan J. (1997) Carrier phase based regional area differential GPS for decimeter-level positioning and navigation, Proceedings of ION GPS-97, Institute of Navigation, Kansas City, Missouri, USA, pp: 1305-1313.

Gao Y. and Li Z. (1998) Ionosphere effect and modeling for regional area differential GPS network, Proceedings of ION GPS-98, Institute of Navigation, Nashville, TN, USA, pp: 91-97.

Gao Y. and Sideris M. (2002) Data Analysis in Engineering, ENGO563 Lecture Notes, Department of Geomatics Engineering, University of Calgary.

Georgiadou Y. and Kleusberg A. (1988) On Carrier Signal Multipath Effects in Relative GPS Positioning. Manuscripta Geodaetica, Vol. 13, No. 3, pp: 172-179.

Han S. and Rizos C. (1996a), Integrated Method for Instantaneous Ambiguity Resolution Using New Generation GPS Receivers, IEEE PLANS'96, Atlanta, pp: 254-261.

Han S. and Rizos C. (1996b) GPS Network Design and Error Mitigation for Real-Time Continuous Array Monitoring Systems, Proceedings of ION GPS-96, Institute of Navigation, Kansas City, Missouri, USA, pp: 1827-1836.

IGS (2004) IGS Product Table. International GPS Service, http://igscb.jpl.nasa.gov/components/prods.html, extract on 14 Jan 2005.

Julien O., Cannon M.E., Alves P. and Lachapelle G. (2004) Triple Frequency Ambiguity Resolution Using GPS/GALILEO, European Journal of Navigation, 2(2), 51 – 57.

Kaplan E.D., Leva J.L. and Pavloff M.S. (1996) Understanding GPS: Principles and Applications, Chapter 2: Fundamentals of Satellite Navigation, Artech House, Boston, pp: 15-57.

Klobuchar, J.A., (1996) Global Positioning System: Theory and Applications, Volume I, Chapter 12: Ionospheric Effects on GPS, American Institute of Aeronautics and Astronautics, Inc., Washington D.C., USA, pp: 485-516.

Lachapelle G. (2003) Advanced GPS – Theory and Applications, ENGO625 Lecture Notes, Department of Geomatics Engineering, University of Calgary

Lachapelle G. and Alves P. (2002) Multiple Reference Station Approach: Overview and Current Research, Invited Contribution, Expert Forum. Journal of Global positioning Systems, Vol. 1, No. 2, pp:133-136.

Leva J.L., de Haag M.U. and Dyle K.V. (1996) Understanding GPS: Principles and Applications, Chapter 7: Performance of Standalone GPS, Artech House, Boston, pp:237-320.

Liu J. (2003) Implementation and Analysis of GPS Ambiguity Resolution Strategies in Single and Multiple Reference Station Scenarios, MSc Thesis, UCGE Report Number 20168, Department of Geomatics Engineering, University of Calgary, Canada.

Lui Z. (2004) Ionosphere Tomographic Modeling and Applications Using Global Positioning System (GPS) Measurements, PhD Thesis, UCGE Report Number 20198, Department of Geomatics Engineering, University of Calgary, Canada.

Mikhail E.M. and Ackermann F. (1976) Observations and Least-squares, Thomas Y. Crowell Company, Inc., New York, USA.

Moritz H. (1980) Advanced Physical Geodesy, Herbert Wichmann Verlag, second edition.

O'Keefe K., Ryan S., and Lachapelle G. (2002) Global Availability and Reliability Assessment of the GPS and Galileo Global Navigation Satellite Systems. Canadian Aeronautics and Space Journal, Canadian Aeronautics and Space Institute, 48, 2, 123-132

Parkinson B.W. and Enge P. (1996) Global Positioning System: Theory and Applications Volume II, Chapter 1: Differential GPS, American Institute of Astronautics and Aeronautics, Inc., Washington D.C., USA, pp: 3-49.

Pugliano G. (2002) Tecnica GPS Multi_reference Station: Principi e Applicazione del Sistema MultiRef^{TM}, PhD. Thesis, Università Degl Studi di Napoli, Parthenope, Italy.

Ray J., (2000) Mitigation of GPS Code and carrier Phase multipath Effects Using a Multi-Antenna System PhD Thesis, UCGE Report Number 20136, Department of Geomatics Engineering, University of Calgary, Canada.

Raquet J. (1998) Development of a Method for Kinematic GPS Carrier-Phase Ambiguity Resolution Using Multiple Reference Receivers, PhD Thesis, UCGE Report Number 20116, Department of Geomatics Engineering, University of Calgary, Canada.

Skone S. (1998) Wide Area Ionosphere Grid Modelling in the Auroral Region, PhD Thesis, UCGE Report Number 20123, Department of Geomatics Engineering, University of Calgary, Calgary, Canada.

Skone S. (2003) Atmospheric Effects on Satellite Navigation Systems. ENGO 633 Lecture Notes, Department of Geomatics Engineering, University of Calgary, 2001.

Teunissen, P.J.G. (1993) Least-squares estimation of the integer GPS ambiguities, Paper presented at the General Meeting of the IAG at Beijing, P.R.China, August 8-13.

Wanninger L. (1995) Improved Ambiguity Resolution by Regional Differential Modeling of the Ionosphere, Proceedings of ION GPS-95, Institute of Navigation, Palm Springs, CA, USA, pp: 55-62.

Wells D., Beck N., Delikaraoglou D., Kleusgerg A., Kraviswisky E.J., Lachapelle G., Langley R., Nakiboglu M., Schwarz K.P., Tranquilla J.M., and Vanicek P. (1986) Guide to GPS Positioning, Canadian GPS Associates, Fredericton.

Wübbena C., Bagge A., Seeber G., Volker B. and Hankemmeier P. (1996) Reducing Distance Dependent Errors for Real -time Precise DGPS Applications by Establishing Reference Station Netwroks, Proceedings of ION GPS-96, Institute of Navigation, Kansas City, Missouri, USA, pp: 1845-1852.